

Channel Network Growth and River Basin Morphology

by

Jeffrey D. Niemann

Submitted to the Department of Civil and Environmental Engineering

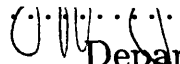
in partial fulfillment of the requirements for the degree of Master of Science in Civil and Environmental Engineering

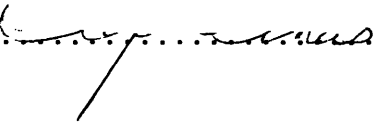
at the

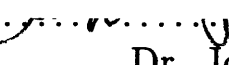
MASSACHUSETTS INSTITUTE OF TECHNOLOGY

January 1997

© Massachusetts Institute of Technology 1997. All rights reserved.

Author 
Department of Civil and Environmental Engineering
January 17, 1997

Certified by 
Rafael L. Bras
Professor
Thesis Supervisor

Accepted by 
Dr. Joseph M. Sussman
Chairman, Departmental Committee on Graduate Students

JAN 29 1997

LIBRARIES

Channel Network Growth and River Basin Morphology

by

Jeffrey D. Niemann

Submitted to the Department of Civil and Environmental Engineering
on January 17, 1997, in partial fulfillment of the
requirements for the degree of
Master of Science in Civil and Environmental Engineering

Abstract

This work examines the influence of the dynamics of basin evolution on the resulting basin form. To achieve this aim, a numerical modeling approach has been adopted which allows the comparison of various evolutionary dynamics in a controlled environment. Resulting basins are compared with one another and with well-known characteristics of natural basins.

First, a relatively broad numerical model is developed which describes erosion as the culmination of discrete events. In this context, the impact of four different descriptions of erosion on the basin form is considered. These variants are shown to have great similarity with other models of erosion and network growth proposed in the literature. Each of these variants is also found to develop differing basin structures. One model variant called Greatest Excess Growth always erodes the point with greatest excess shear stress. Among the variants considered, this one develops the most distinctive and realistic basins.

Second, the roles of uplift and critical shear stress are investigated under varying initial conditions. For flat initial conditions, basins with lower uplift rates and larger critical shear stresses are found to exhibit slightly larger exponents in Hack's Law and less variability in their normalized drainage directions. With initial conditions that slope either toward or away from a line of specified outlets, both the network growth and resulting topography depend on whether there is uplift or critical shear. In addition, the basin evolution model has difficulty developing scale invariant networks when the initial slope is oriented away from the outlets.

Third, the effect of two different storm durations on basin scaling is investigated. The two cases considered are: instantaneous pulses and prolonged storms. When storms are instantaneous, the duration of the related discharge is controlled by the basin structure, but when storms are prolonged, the duration becomes independent of the basin form. These two cases result in different slope-area relationships if the erosion rate depends nonlinearly on contributing area.

Thesis Supervisor: Rafael L. Bras

Title: Professor

Acknowledgments

This work was supported by the U.S. Army Research Office (agreement DAAH04-95-1-0181 and AASERT agreement DAAH04-96-1-0099); this support is gratefully acknowledged.

My sincere thanks to my advisor Rafael Bras for his guidance and support and to Daniele Veneziano for many helpful insights and discussions. I would also like to thank Glenn Moglen for his encouragement during my first year at the Parsons Lab and Greg Tucker for his valuable input during the latter stages of this work.

I would also like to express my profound admiration and appreciation to my parents, Leon and Ann, for their selfless love and enthusiastic support. Finally, I would like to express my deep gratitude to Perrin for her companionship and immeasurable patience.

Contents

1	Introduction	11
2	Literature Review	15
2.1	Channel Network Growth	15
2.2	Landscape Evolution	19
2.3	Summary	22
3	The Discrete Event Model	23
3.1	Conceptual Basis	24
3.2	Summary of Model Algorithm	28
3.3	Comparison with the Slope-Area Model	31
3.4	Self-Organized Criticality	36
3.4.1	Characteristics of Self-Organized Criticality	38
3.4.2	Does the Threshold Model Exhibit SOC?	41
3.4.3	SOC and Cluster Growth	43
3.4.4	Summary	44
4	Sequencing of Erosion Events	47
4.1	Sequencing Variants	49
4.1.1	Headward Growth	49
4.1.2	Simultaneous Growth	52
4.1.3	Random Growth	55
4.1.4	Greatest Excess Growth	57

4.2	Basin Morphology Implications	59
4.3	Conclusions	71
5	A Comparison of Stability and Dynamic Equilibrium	73
5.1	Uplift in the Discrete Event Model	74
5.2	Flat Initial Conditions	76
5.3	Escarpment Retreat and Sloping Antecedent Conditions	83
5.3.1	Modes of Escarpment Retreat and Network Growth	84
5.3.2	Stationary Basin Forms	88
5.4	Summary	95
6	Influences of Storm Duration	97
6.1	General Framework	98
6.2	Prolonged Precipitation	102
6.3	Instantaneous Precipitation	102
6.4	Application Through the Discrete Event and Slope-Area Models . . .	106
6.5	Implications for Basin Form	109
6.6	Conclusions	115
7	Conclusions	117
7.1	Summary of Results	117
7.2	Avenues for Further Study	119

List of Figures

2-1	Schematic diagram showing three proposed modes of drainage network growth from Schumm et al. [37]	17
3-1	The development of topography by the Discrete Event model with an outlet specified in the corner	32
3-2	Topography and river networks as developed by (a) the Discrete Event model and (b) the Slope-Area model	35
3-3	Comparison of slope-area relationships for (a) the Discrete Event model and (b) the Slope-Area model	37
3-4	Distribution of avalanche sizes and lifetimes from Bak et al. [4] for (a) a 50x50 array, averaged over 200 samples, and (b) a 20x20x20 array, averaged over 200 samples	40
3-5	Distribution of avalanche (a) sizes and (b) lifetimes in the Slope-Area model (from Ijjasz-Vasquez et al. [18])	45
4-1	Schematic diagram of three different erosion algorithms at work on two example slopes. Solid lines indicate slope profiles in between model iterations, whereas dashed lines indicate the changing profile shape during a single iteration. The bold line shows the profile when point 6 is captured	51
4-2	Snapshots during the erosion of a basin using (a) Headward Growth, (b) Simultaneous Growth, (c) Random Growth, and (d) Greatest Excess Growth	53
4-3	A basin developed by the Headward Growth variant	59

4-4	A basin developed by the Simultaneous Growth variant	60
4-5	A basin developed by the Random Growth variant	60
4-6	A basin developed by the Greatest Excess Growth variant	61
4-7	Networks developed by the Discrete Event model variants	62
4-8	Distribution of drainage directions normalized by the outlet direction for a collection of runs of the four model variants	64
4-9	Distributions of contributing area for basins developed by the Discrete Event model variants	65
4-10	Width functions for basins developed by the Discrete Event model variants	67
4-11	Slope-area relationships for basins developed by the Discrete Event model variants	69
4-12	Hypsometry for basins developed by variants of the Discrete Event model	70
5-1	Topography generated by the Discrete Event model with (a) $\tau_{cr} = 0.01$, $U = 0$, and $K = 0.01$, (b) $\tau_{cr} = 0.005$, $U = 0.005$, and $K = 0.01$, and (c) $\tau_{cr} = 0$, $U = 0.01$, and $K = 0.01$	79
5-2	Slope Area relations for stationary topographies generated with (a) $\tau_{cr} =$ 0.01 , $U = 0$, and $K = 0.01$, (b) $\tau_{cr} = 0.005$, $U = 0.005$, and $K = 0.01$, and (c) $\tau_{cr} = 0$, $U = 0.01$, and $K = 0.01$	80
5-3	Hack's Law for stationary topographies generated with (a) $\tau_{cr} = 0.01$, $U = 0$, and $K = 0.01$, (b) $\tau_{cr} = 0.005$, $U = 0.005$, and $K = 0.01$, and (c) $\tau_{cr} = 0$, $U = 0.01$, and $K = 0.01$. Solid line shows regressions, and dashed lines show slope of $1/2$	81
5-4	Distribution of drainage directions for basins generated with (a) $\tau_{cr} =$ 0.01 , $U = 0$, and $K = 0.01$, (b) $\tau_{cr} = 0.005$, $U = 0.005$, and $K = 0.01$, and (c) $\tau_{cr} = 0$, $U = 0.01$, and $K = 0.01$	82

5-5	Snapshots during the evolution for the four cases where (a) and (b) include a non-zero critical shear and (c) and (d) include a positive uplift. (a) and (c) have initial surfaces sloping towards the baselevel whereas (b) and (d) have initial surfaces sloping away from the baselevel	86
5-6	Snapshots during the growth of the channels networks for Case 3 . . .	87
5-7	Snapshots during the growth of the channels networks for Case 4 . . .	89
5-8	Networks developed by the Discrete Event model where (a) and (b) include a non-zero critical shear and (c) and (d) include a positive uplift. (a) and (c) have initial surfaces sloping towards the baselevel whereas (b) and (d) have initial surfaces sloping away from the baselevel	91
5-9	Distribution of contributing areas for the four cases	92
5-10	Hack's Law for the four cases	93
5-11	Distribution of drainage directions for the four cases	94
5-12	Slope-area relationships for the four cases	95
6-1	Diagram of the discharge during a period of simulation	100
6-2	Diagram of the relationship between peak flow and contributing area for the long storm case	103
6-3	Diagram showing two basins with the same contributing area but different peak flows after an instantaneous pulse of precipitation	104
6-4	Diagram showing peak flows for the instantaneous storm case	105
6-5	Correlation between contributing area and flow duration (or main stream length) using (a) a constant ruler length and (b) a ruler length that varies according to contributing area (solid lines show regressions) . .	111
6-6	Simulated basins where (a)-(c) have instantaneous precipitation and (d) has prolonged precipitation. Parameters are: (a) $m = 1/2$, $n = 1$, (b) $m = 1$, $n = 2$, (c) $m = 2$, $n = 4$, (d) $m/n = 1/2$	112
6-7	The dependence of m on $\alpha \equiv \phi/\theta$	114

Chapter 1

Introduction

One of the fundamental principles of geomorphology is that the forms exhibited by topography reflect the processes that have been active in shaping that topography. This implies that river basin forms reflect climatic and tectonic forcing, the internal mechanics of erosion and other process, and to some extent previous basin forms and historical changes in the relevant processes.

Especially over the past ten years, a much greater understanding of the structure of river basins and channel networks has been achieved. This has in part been due to the widespread availability of digital elevation data. Such data has allowed the detailed analysis of many basins throughout the world. Another impetus was the introduction of fractals and scale invariance which has helped enrich the interpretation this data. The consistency of scale invariance between varied climatological and geological circumstances has hinted at new underlying aspects of basin evolution. Now, in addition to traditional geomorphological measures, fractal measures can be used to quantify natural topography and validate numerical models.

With the growing availability of data and interpretation techniques, quantitative modeling of river basins and topography in general has also expanded. Geomorphic modellers use the field data and simple conceptual arguments to construct their best quantitative understanding of the dynamics of basin evolution. In these models, we hope to capture the interplay between the internal dynamics, external forcing, and initial conditions that leads to the commonly observed forms of topography.

An expansive array of modeling approaches exist in geomorphology. Such numerical models include finite difference expressions of differential equations, cellular automata, and stochastic models based on fractals. The reasons for this diversity are the different interests and applications associated with many of these models. Another cause is the stochastic nature of basin development and topography which limits validation techniques to statistical measures alone. However, it is often unclear how various models relate to one another and what each implies about the fundamental links between basin dynamics and form.

This work has one overarching goal. That is to investigate how various quantitative descriptions of basin development affect the resulting basin geomorphology. This goal involves a comparison between the statistics of model simulations with well known characteristics of natural basins, and it includes a comparison between the model behavior with other published insights on the dynamics of basin evolution.

The first several chapters are dedicated to an introduction of the history of geomorphological modeling and the general framework used in the analysis. Chapter 2 presents a literature review which attempts to summarize several of the main conceptual and numerical models of basin evolution and channel network growth. Chapter 3 develops the model framework used throughout the rest of the analysis. This model is based on a description of shear stress and includes variants that encompass both a finite difference modeling approach and a discrete event approach. The model is quite similar to the one proposed by Rinaldo et al. [30] and to a lesser extent the one proposed by Ijjasz-Vasquez et al. [17]. Chapter 3 also makes some model comparisons and discusses the relevance of the principle of Self-Organized Criticality (SOC) to geomorphological models.

The second set of chapters describe several experiments performed with the model developed in Chapter 3. Chapter 4 presents different possible dynamics of basin evolution which focus particularly on the mode of network growth and its affect on the resulting basin form. Four variants of the model are presented which are shown to approximate some of the classical conceptual models of channel network growth. Similar numerical models from the literature are also discussed.

The models in Chapter 4 approach a stationary condition termed *stability* which differs from *dynamic equilibrium*, another stationary condition reached by some geomorphological models. Either state may be achieved by some basins in nature. Chapter 5 investigates how these conditions differ, and the effects of the initial conditions on topography approaching either state. This chapter has some relevance to escarpment retreat since the initial conditions that are considered include an overall slope towards or away from an specified or growing escarpment crest.

Chapter 6 examines the role that precipitation events play in basin evolution. It analytically develops the commonly used substitution of precipitation intensity times the contributing area for discharge. However, the case is derived under the condition of prolonged precipitation events. The chapter shows that an alternative case may also be derived in which precipitation arrives in instantaneous pulses. The implications of this theoretical change in climatic forcing on basin geomorphology is considered.

Chapter 2

Literature Review

It is the purpose of this chapter to provide some context for the analysis in the following chapters. The work to be presented draws from a wide variety of previous modeling studies as well as field and laboratory investigations. For the sake of brevity, only a few previous modeling efforts will be outlined here, and further discussion of relevant work will be included throughout the other chapters as applicable. The first section of this chapter considers some important conceptual and numerical models of channel networks. The second section considers some conceptual and numerical models of landscape evolution.

2.1 Channel Network Growth

Horton [14] was among the first to consider in detail how channel networks develop. A schematic diagram of his model is shown in part (a) of Figure 2-1 which is based on a similar diagram by Schumm et al. [37]. Horton suggested that parallel rills form quickly to drain an initially undissected slope. By chance, a certain rill which he termed the *master rill* carries more flow than the others, and with a higher discharge rate, this rill also has a greater incision rate. As the master rill incises, it exerts an influence on the surrounding rills. New areas are captured through a process of *micropiracy*, and the low relative elevation of the master rill causes flow in nearby territory to *cross-grade* and drain towards the master rill. Smaller side rills therefore

change their orientation to connect to the master rill and begin to form an organized network structure. According to Horton, such network growth can be seen on the slopes along the sides of highways.

Based on observations of channel network growth including those of Schumm [36] in the badlands at Perth Amboy, New Jersey, Howard [15] proposed that networks grow in a headward fashion. In his view, a channel network grows as an intense “wave of dissection” progresses headward from an outlet to capture new territory. Once this wave has passed, a virtually complete channel network is left behind (see part (b) of Figure 2-1). This view differs from Horton’s which regards the organization of channel networks as a product of readjustment of the initial pattern. Howard also proposed a set of related numerical models that describe this type of growth. Some of these models are simply topological, but others are simulated on a grid to include geometric limitations on channel growth. In one grid-based model, he first specifies some initial seeds or outlets. Then, at each iteration, one adjacent point on the grid is randomly selected for addition to the existing network. Several variants are also included in which the probabilities of branching and inactivity are explicitly controlled.

Glock [10] proposed a more complex conceptual model of growth than the ones considered by either Horton or Howard. Unlike Howard’s model, Glock envisaged that channels of different sizes would progress headward at different rates during an *extension* phase of network growth. He expected the main channels to grow first in a stage he called *elongation* followed by the *elaboration* of the minor tributaries (see part (c) in Figure 2-1). Glock, however, also expected a reduction or *integration* of the network form. One case where this might occur (called *abstraction*) is when a smaller tributary disappears due to the lateral movement of a main stream. Glock allowed the possibility that the extension phase may coincide with the integration phase. His model is based on the interpretation of various mapped channel network forms.

Leopold and Langbein [24] and Shenck [19] suggested a model where channel networks grow by random walks. At the beginning of each iteration, a channel source is randomly placed somewhere on a grid. Then, the channel grows as the water flows

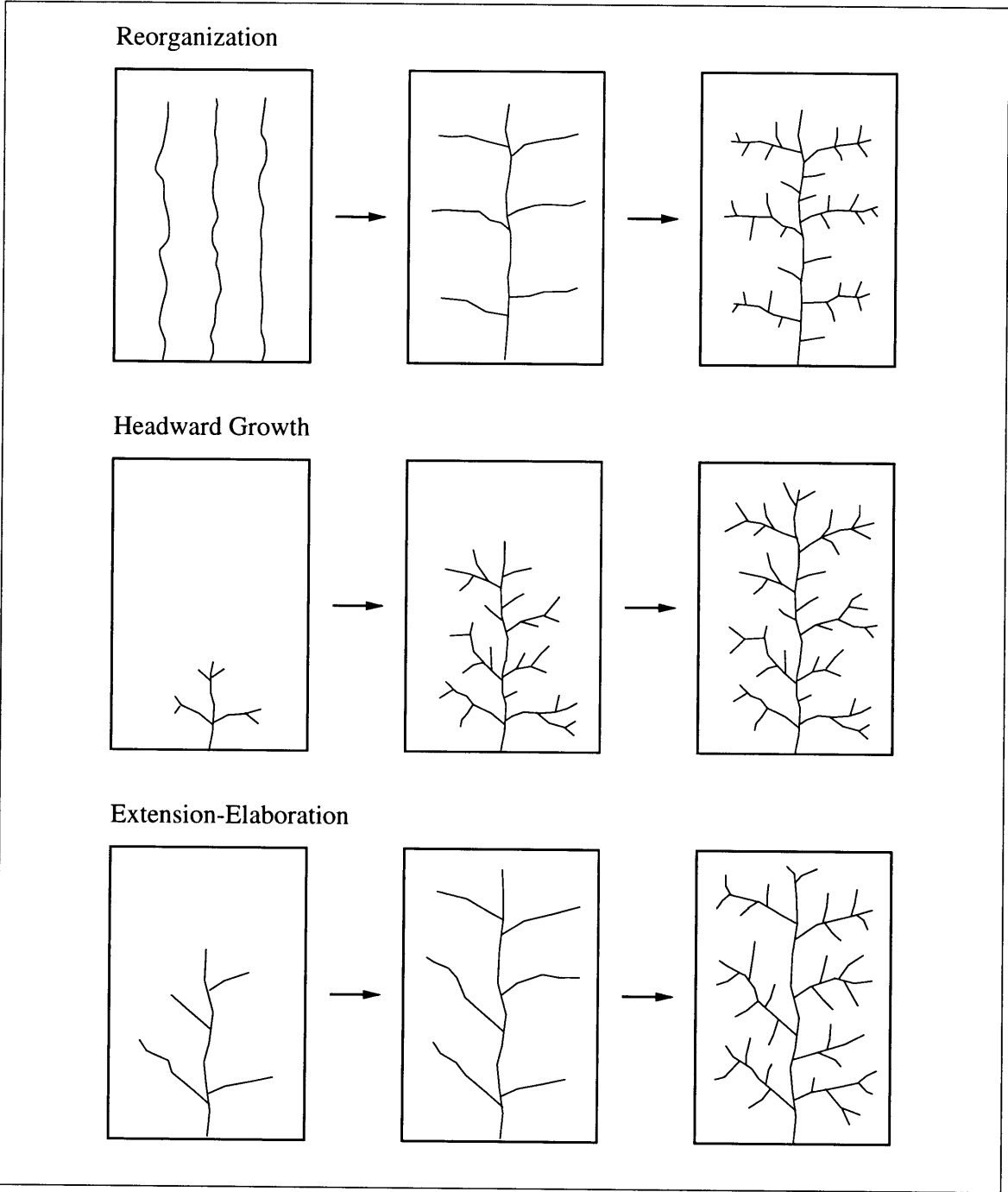


Figure 2-1: Schematic diagram showing three proposed modes of drainage network growth from Schumm et al. [37]

downstream from this point. At any point, it has equal probability of growing in each direction. The channel continues to develop until meeting an existing stream or region boundary, and loops are forbidden. While such a model develops fairly reasonable networks, its description of the dynamics of growth is probably now out-dated.

More recent network growth models have focused on the adaptation and testing of various cluster growth models. Stark [41] suggested that Invasion Percolation with self-avoidance may be an accurate method of simulating channel networks. In this model, a random strength is initially assigned to every link in a rectangular lattice. A single seed is specified which corresponds to the basin outlet. Then, at each iteration, the adjacent bond with the weakest strength is added to the growing network. Stark compares Invasion Percolation to the model of Howard [15] and determines that only Invasion Percolation obeys Hack's law.

Masek and Turcotte [26] propose Diffusion Limited Aggregation (DLA) as a model of channel network growth. In this model, first a seed is specified for the basin outlet, and then random walkers are introduced throughout the grid. These walkers move about until they either reach the edge of the simulation domain or meet the existing tree. When they meet the existing tree, the current location erodes to expand the network in that location. Masek and Turcotte suggest that the random walkers are similar to water parcels moving over an initially flat surface and eventually draining into the network.

In addition to the above models of channel network growth, two models of channel network structure are worth mentioning. First is the classic idea of topologically random networks proposed by Shreve [39]. He first considered the population of *topologically distinct* networks all having the same number of links. *Topologically distinct* implies that no amount of stretching and rotating will transform one network shape into another. Shreve showed that the most probable configurations of these networks when their magnitude goes to infinity are those that give Horton's bifurcation ratio [14] near 4 (which lies well within the observed range). In addition, if link lengths are randomly distributed then Horton's law of stream lengths [14] is also upheld with $R_L \approx 2$ (again well within the observed range). Thus this theory explains the network

structure as the most probable configuration from a random population.

Rodriguez-Iturbe et al. [32] suggested an alternative view: “We believe that in an evolutionary system like the drainage network both chance and necessity should be operating; and, moreover, that the influence of necessity is felt through a tendency to minimize the total rate of energy expenditure in the network and the rate of energy per unit area of channel anywhere in the network.” Along these lines, they proposed three principles of energy dissipation. The first principle states that energy is minimized in every link of the network. The second principle says that energy expenditure per unit area of channel is equal throughout the network. The third principle states that the energy in the network as a whole is minimized. Through a derivation described in detail in their paper, these principles amount to the minimization of energy expenditure E where:

$$E = \sum_i Q_i^{1/2} L_i. \quad (2.1)$$

In this expression Q is discharge and L is the length of link i . Networks developed by minimizing energy expenditure have been shown to obey many statistical properties of real networks.

2.2 Landscape Evolution

In addition to the topological and two-dimensional modeling efforts described above, many authors have studied the three-dimensional dynamic form of rivers basins. In this section, a few of the classical perspectives and some of the most recent quantitative modeling approaches are described.

Davis [7] anticipated that topography progresses through a series of stages from youth, through maturity, to old age. At the beginning of his cycle of erosion, a brief period of rapid uplift raises the region above the baselevel. Over time, denudational processes wear down the landforms resulting in lower relief and a decline in slope angles. Without an interruption of renewed uplift, the landforms continue their decay until reaching a *penplain*. A *penplain* is defined as topography very near baselevel with subdued relief.

An alternative view has grown out of the work of Hack [12]. He proposed that after some time of denudation, topography reaches a state of *dynamic equilibrium* where the slopes are adjusted according to their lithological conditions and stream gradients are sufficient to carry their sediment loads. In this condition, he suggested, topography is uniformly lowered. Over time, this idea has been transformed to express an equilibrium where the addition of material to the system through tectonic uplift is balanced by the removal of material through denudational processes. Clearly this view differs from that of Davis since it implies a stationary state, and in the modern incarnation, suggests that uplift occurs over the same time scales as erosion. While both the models proposed by Hack and Davis are quite old, they still remain relevant interpretations of the geomorphological dynamics.

More recently, several numerical models have been developed which incorporate some of the ideas of Davis and/or Hack [21]. Here, only a few three dimensional models which include channel network growth are reviewed.

Willgoose et al. [49] and Tucker and Slingerland [45] analyzed *transport-limited* models. In transport-limited or *alluvial* channels, erosion is restricted by the capacity of the flow to carry weathered material. Therefore, the numerical simulations are controlled by the Exner continuity equation which states that the addition of elevation at a point is the uplift minus the increase in the carrying capacity in the downstream direction. The carrying capacity has the form $Q^m S^n$ where Q is discharge, S is slope, and m and n are parameters. These models usually include diffusion to represent a suite of hillslope processes including tree throw, rheologic creep, and rainsplash.

An alternative set of landscape evolution models are *detachment-limited* models. In such models, erosion is assumed to be restricted by the detachment of material rather than its transport through the channels. These models apply to *bedrock channels* and coarse-bed rivers. Now the change in elevation of a point is the uplift minus the erosion where the erosion rate has a similar form to the capacity above: $Q^m S^n$. Models of this type have been studied by Moglen and Bras [27], Tucker and Slingerland [45], and Howard and Kerby [16]. Here again, diffusion is often used to simulate the relevant collection of hillslope processes.

A hybrid model which includes both detachment-limited and transport-limited conditions as special cases was developed by Kooi and Beaumont [20, 21]. In this model, it is assumed that the transport rate is not always at capacity. Instead, it takes some work to reach the transport capacity, or equivalently there is some erosion length scale. Detachment-limited conditions arise when the carrying capacity is much larger than the material erodability, and transport-limited conditions arise when the erosion length scale goes to zero.

All of the above detachment-limited and transport-limited models involve the description of erosion using differential equations. However, alternative approaches have also been suggested. Chase [6] used cellular automata to describe the erosion process. In his model, *precipitons* are dropped at random locations on the simulation domain. When the precipiton lands, it causes some local erosion in the form of diffusion. Then the precipiton travels in the downslope direction, eroding at a rate proportional to the slope until reaching a carrying capacity which is proportional to the stream power. When carrying capacity is exceeded by a reduction in the surface slope, material is deposited according to specified rules.

A similar lattice model was proposed by Kramer and Marder [22]. In their numerical model (which differs from their analytical model), precipitation falls on the grid points at random intervals. At each site, both the water depth and the surface elevation are explicitly treated. If the water elevation differs between neighboring sites, water moves to reduce the difference, and for each unit of water that shifts, a corresponding unit of sediment is eroded if the neighbor's surface elevation is also lower.

Another lattice model was proposed by Leheny and Nagel [23]. In this model, precipitation again enters the model at a random site. The water then flows to a randomly selected downslope neighbor where the probability of selection is dependent on the elevation difference. All sites visited by a parcel of water are eroded by the same amount. Landsliding also occurs on the surface when the elevation difference between adjacent points exceeds a critical value.

Other approaches that cannot be reduced to differential equations are those pro-

posed by Ijjasz-Vasquez et al. [17] and Rinaldo et al. [30]. The model proposed by Ijjasz-Vasquez et al. [17] is called the *Slope-Area model* and involves determining the basin configuration at dynamic equilibrium by enforcing the slope-area relationship [9, 11] at all points. The model developed by Rinaldo et al. [30] describes erosion as the culmination of discrete or episodic events. Both of these models will be considered in greater detail in the following chapter.

2.3 Summary

As this review has shown, a great diversity of models has been used to simulate the development of channel networks and river basins. These models differ in the processes that are included (e.g. soil creep or landsliding) as well as their descriptions of the various processes. The main result found from an overview of these analyses is that aggregation patterns similar to those of natural river networks can be developed from a variety of approaches and that each of these approaches is able to match some of the observed characteristics. However, the link between the specified dynamics of the evolution and the resulting basin and network characteristics remains somewhat unclear. The next chapter develops a relatively broad framework through which some of the above models can be compared, and the following three chapters investigate the role that the erosional dynamics, initial conditions, and climatic and tectonic forcing play in determining the basin form.

Chapter 3

The Discrete Event Model

A wide variety of approaches has been utilized to model the evolution of river basins. One evolution model is the Threshold model of Rinaldo et al. [30] and Rigon et al. [29]. This model attempts to describe the evolution of river basins from the perspective of self-organization principles. It differs from many process-based evolution models because it includes a threshold below which erosion is ineffective and because it describes erosion as the culmination of discrete events rather than the continual movement of sediment.

This chapter describes a variant of the Threshold model which for clarity will be called the *Discrete Event* model. The next section develops the conceptual basis for the model which relies on a consideration of shear stress and highlights the differences between the model of Rinaldo et al. and the Discrete Event model. The second section discusses the algorithm through which the model is implemented. A comparison is made in the third section between the Discrete Event model and its cousin the Slope-Area model [17]. Finally, some comments are made regarding the self-organizing characteristics of these geomorphological models. In particular, can any of these models be considered a self-organized critical system as originally defined by Bak et al. [5]?

3.1 Conceptual Basis

Unfortunately, the mechanics of bedrock erosion remain poorly understood. However, three main processes are thought to drive the downwearing of bedrock beds: abrasion, plucking, and solution. Abrasion describes the affect of water and its sediment load as they flow or saltate across the bed surface. Over time, the impacts of the sediment load and the shear created by the flow wear down the bedrock. Plucking involves the removal of pieces of bedrock either by hydraulic lifting or the wedging of smaller material into the bedrock joints. Finally, solution describes chemical reactions that occur between the bedrock and the flow which break down the rock into new compounds that can be removed in the flow. The effectiveness of each of these processes will depend on the rock type, jointing characteristics, and climate. Additionally, in channels where the capacity to carry eroded material is small relative to the erosion rates (transport limited or alluvial channels), the material already in transport may limit the local erosion.

Considering only detachment limited channels, two of these processes, abrasion and plucking, depend in some way on the shear stress created by the flow over the rock surface. In addition, these two processes are expected to dominate under most combinations of rock type and climate. Thus, a reasonable model for bedrock channels is:

$$\frac{\partial z}{\partial t} = \begin{cases} -k_1(\tau - \tau_{cr}^*)^\alpha & \text{if } \tau > \tau_{cr}^* \\ 0 & \text{otherwise} \end{cases} \quad (3.1)$$

where z is the bed elevation, t is time, τ is shear stress on the bed, τ_{cr}^* is a critical shear stress, and k_1 and α are parameters. According to this equation, the elevation of the river bed is reduced only when the shear stress exceeds some critical value. This critical shear reflects the inherent strength of the bedrock and the degree of jointing. Once the shear exceeds this critical value, erosion occurs at a rate proportional to some power of the excess shear. The parameters controlling this rate, K_1 and α , will probably depend both on the material and the type of erosion.

A similar equation was first suggested by Howard and Kerby [16]. In their evalua-

tion of the processes, τ_{cr}^* could be neglected and $\alpha \approx 1$. By these assumptions, erosion is considered to be a smoothly operating process in time which depends nearly linearly on the excess shear, and Equation 3.1 reduces to:

$$\frac{\partial z}{\partial t} = -k_1 \tau \quad (3.2)$$

since $\tau \geq 0$ by definition.

An alternate view was proposed by Rinaldo et al. [30]. They considered the threshold to be a critical component of erosion and the degree of nonlinearity to be severe. In this extreme, $\alpha \rightarrow \infty$, indicating that, when the critical stress is exceeded, erosion occurs to abruptly reduce the shear stress directly to a critical value τ_{cr} . Thus, erosion is not considered to be a smoothly acting process. Rather, it is a collection of discrete events, and Equation 3.1 reduces to a condition of stability:

$$\begin{cases} \tau \longrightarrow \tau_{cr} & \text{if } \tau > \tau_{cr} \\ \frac{\partial z}{\partial t} = 0 & \text{otherwise} \end{cases} \quad (3.3)$$

where $\tau_{cr} = \tau_{cr}^* + 1$. The different critical shear stresses, τ_{cr} and τ_{cr}^* , arise because as $\alpha \rightarrow \infty$, $(\tau - \tau_{cr}^*)^\alpha$ goes to zero in Equation 3.1 when $\tau - \tau_{cr}^* < 1$.

To evaluate this condition of stability at all locations and times, one requires some additional information to determine the dependence of shear stress on the existing topography. The boundary shear stress created by steady uniform flow can be written:

$$\tau = \rho g R S \quad (3.4)$$

where ρ is density of water, g is the acceleration of gravity, R is hydraulic radius, and S is the slope. Notice that under the condition of steady uniform flow, the bed slope, friction slope, and water surface slope are equivalent.

The hydraulic radius will vary systematically throughout any given channel network. This dependence can be understood by considering three additional relations.

First, for a wide channel, hydraulic radius can be related to the discharge Q as:

$$R = \frac{Q}{vb} \quad (3.5)$$

where v is the cross-sectionally averaged flow speed and b is the channel width. Second, the Darcy-Weisbach Equation describes the average flow speed as a function of the geometry and a friction factor f :

$$v = \sqrt{\frac{8gRS}{f}}. \quad (3.6)$$

Third, observations by Leopold and Maddock [25] show a dependence of channel width on discharge rate as one moves along a channel network. The resulting empirical relation is:

$$b = k_2 Q^\delta \quad (3.7)$$

where k_2 is a coefficient, and $\delta \approx 1/2$. Given these three relations, the hydraulic radius can be written in terms of discharge and slope:

$$R = \left(\frac{f}{8gk_2^2} \right)^{1/3} Q^{2(1-\delta)/3} S^{-1/3} \quad (3.8)$$

Substituting this relationship for the hydraulic radius into the expression for shear stress, one finds that:

$$\tau = kQ^m S^n \quad (3.9)$$

where $k = \rho g [f / (8gk_2^2)]^{1/3}$, $m \equiv 2(1 - \delta)/3 \approx 1/3$, and $n = 2/3$.

It should be noted that Rinaldo et al. [30] use a different methodology to derive the dependence of hydraulic radius on slope and discharge. They assume directly that:

$$R = k_3 Q^m \quad (3.10)$$

where k_3 is a coefficient and $m \approx 1/2$. As will be shown below, slope depends on discharge *at the stability threshold*, and a similar relation between hydraulic radius

and discharge results from the approach using the Darcy-Weisbach equation above. Using the Rinaldo et al. [30] derivation, Equation 3.9 still holds, however, $k = \rho g k_3$, $m \approx 1/2$, and $n = 1$. Because the exact values of the coefficient and exponents depend on the assumptions, the general form of Equation 3.9 will be used in the following discussion, but no specific parameter values will be endorsed.

In order to complete the model, it remains necessary to describe the variation of discharge in terms of the topography. The simplest approach is to assume that discharge increases linearly with increasing upstream area or:

$$Q = PA \tag{3.11}$$

where P is the characteristic effective precipitation intensity (where effective precipitation indicates the precipitation that becomes runoff) and A is contributing area. Obviously, this parameterization is extremely simple, and further analysis regarding this point is performed in Chapter 6 where an alternative (simple) hydrologic model is developed and compared with this approach.

Substituting for discharge in the description of hydraulic radius, and then substituting this into the relationship for shear stress, one finds:

$$\tau = KA^m S^n \tag{3.12}$$

where $K \equiv kP^m$. Now the condition for stability, previously written in terms of shear, can also be written in terms of slope. Given an existing channel configuration and the associated contributing areas:

$$S_{cr} = \left(\frac{\tau_{cr}}{K} \right)^{1/n} A^{-m/n}. \tag{3.13}$$

Notice that the two approaches described above supply differing m and n values but the same m/n value. The numerical evaluation of Equation 3.13 is at the heart of the Threshold and Discrete Event models.

It should be noted that in Rinaldo et al. [30], the topography developed by the

effects of erosion is also perturbed by adding elevation to randomly selected locations. The justification of this approach relies on the notion of energy minimization. Rodriguez-Iturbe et al. [32] have proposed that river networks develop under three principles of energy minimization, and networks simulated according to these rules have been shown to strongly resemble existing networks. Rinaldo et al. [30] have shown that by perturbing a network developed by the above erosion model, lower states of energy expenditure are achieved. However, their analysis has also shown that the reduction in energy due to such perturbations is strongly dependent on the selected initial conditions.

In this analysis, the use of perturbations will be avoided because their physical meaning is unclear. It is known that the perturbations help the model achieve lower states of energy expenditure, but the efficiency with which real river networks are able to minimize energy and the relationship of the efficiency to the perturbations is an unresolved question. Therefore, this analysis will not employ perturbations and will avoid using the particular initial conditions where the effects of these perturbations are significant (i.e. conditions which begin with many stable points and an unrealistically developed river network).

In addition, Rigon et al. [29] have extended the Threshold model to include the effects of diffusive hillslope processes. Because hillslopes are not the focus of this analysis, this aspect of the extended model will also be neglected here. It should be noted, however, that the spatial discretization used for numerical simulations introduces some numerical diffusion which plays an important role (see below). The next section describes the numerical application of the model derived above.

3.2 Summary of Model Algorithm

Before applying the Discrete Event model, the domain of simulation must be specified along with boundary and initial conditions. The model is applied on a rectangular grid and the domain can be any selected shape. The boundaries are fixed in location and elevation and do not allow flow to pass in or out of the domain. For initial conditions,

the model only requires that the flow directions are well defined at all locations. This implies that adjacent elevations must not have identical elevations. Published initial conditions [30, 29] include antecedent river networks (realistic and unrealistic) and nearly constant elevations with some superimposed, uncorrelated noise.

Additionally, any number of outlets can be specified. An outlet is simply a point with significantly lower elevation than the rest of the region. Physically, a single outlet may correspond to the head of a pre-existing, deeply incised channel at the region's edge; lines of outlets roughly represent an escarpment edge. Because outlets are much lower than the rest of the domain, they will tend to capture the flow from a large portion or all of the region depending upon their number, locations, and elevations. However, in all other respects, outlets behave the same as any pit on the topography.

Once the initial and boundary conditions are defined, simulation may begin. As described above, the model is rule-based rather than rate-based, and can therefore be most easily described algorithmically:

1. *Determine drainage directions.* Water and sediment are assumed to flow from a given point deterministically in the direction of steepest decent. However, because the model operates on a grid, this vector must be mapped towards one of the point's neighbors. In this analysis, the eight nearest neighbors will be consider valid flow directions, but four or even sixteen neighbors may also be used. The simplest procedure to assign a flow direction is to route the flow towards the neighbor which forms the steepest slope with respect to the current point. Thus the drainage direction for a node i, j on the lattice is assigned towards $z_{i,j}^{down}$ where $z_{i,j}^{down}$ satisfies:

$$z_{i,j}^{down} = \text{Max}_{ii,jj} \left(\frac{z_{i,j} - z_{i+ii,j+jj}}{\Delta l_{ii,jj}} \right) \quad ii = -1, 0, 1 \quad jj = -1, 0, 1 \quad (3.14)$$

where the indices ii, jj indicate relative locations of the nearest eight neighbors and Δl is the horizontal distance between i, j and $i+ii, j+jj$. Rinaldo et al. [30] use $\Delta l = \text{constant}$ in all directions. In this case, the above maximization reduces to the selection of the neighbor with the lowest elevation. Here, we

instead maintain lattice geometry, and the distances of the diagonal directions will be $\sqrt{2}$ times the principal directions. Since, by definition of the grid, all neighbors are not equally distant from the point, anisotropy will be introduced no matter which approach is taken. Conditions for isotropy have recently been studied in the context of cellular automata models of lattice gases by Rothman and Zaleski [33].

2. *Determine contributing areas.* Because unique flow directions are known at all locations, the area contributing to the flow at any grid point is also known. A given point is assumed to drain its own grid cell and all of those draining through it.
3. *Select sites for adjustment.* Now that the configuration of the existing networks are known, any locations where the shear stress exceeds the critical value can be identified. At any given iteration of the simulation, some proportion or all of these points must be selected for elevation adjustment due to erosion. Rigon et al. [29] select only the point with the greatest excess shear for adjustment. Alternatives to this approach will be considered in detail in the next chapter.
4. *Erode the selected unstable points.* When a point is eroded, its elevation is immediately reduced to a value which brings about minimal stability, where minimal stability means $\tau = \tau_{cr}$ or $S = S_{cr}$. The slope at a grid point i, j is calculated by the elevation change in the downstream direction:

$$S_{i,j} = \frac{(z_{i,j} - z_{i,j}^{down})}{\Delta l_{i,j}}. \quad (3.15)$$

Because Δl is finite, some numerical diffusion is introduced into the simulations. This diffusion plays an important role since it causes the attenuation of baselevel changes as they propagate upstream.

The elevation at the point after erosion ($z_{i,j}^{new}$) can be set from Equation 3.13:

$$z_{i,j}^{new} = z_{i,j}^{down} + \Delta l_{i,j} \left(\frac{\tau_{cr}}{K} \right)^{1/n} A_{i,j}^{-m/n}. \quad (3.16)$$

Note that there are effectively two parameters in this model: a coefficient and an exponent on A . The coefficient controls the vertical scale of the topography, and the exponent controls the overall concavity (and affects the network structure). Elevations are always decreased by the adjustments so that this equation forms an upper bound on the elevation of a point with a given contributing area. The sequencing and number of adjustments may be important since z^{down} and A will potentially change due to the erosion of points in the vicinity of i, j .

5. *Repeat the process.* The process of characterizing the existing basin and adjusting elevations is repeated until no point in the basin is unstable. The growth occurs because of two main feedback mechanisms in the model. First, as a point is reduced in elevation, points upstream may now find themselves with much higher relative elevations (or steeper slopes) than stability allows. This new instability will require a reduction in their elevations as well. Second, if a point is reduced in elevation, it may become the downstream neighbor for new points and capture additional contributing area. If the point drains a greater area, it will find itself unstable again since larger contributing areas require flatter slopes for stability. Thus, by either mechanism, the erosion of one point may propagate to affect larger regions of the domain.

An example of the growth of a river basin by this model is shown in Figure 3-1. In this application, an outlet is specified in the lower left corner of the basin and is sufficiently low to eventually capture the entire domain. Growth occurs principally but not exclusively headward from this location.

3.3 Comparison with the Slope-Area Model

The description of landscape evolution presented above is also quite similar to the Slope-Area model proposed by Ijjasz-Vasquez et al. [17]. This section compares the two models.

Conceptually, the Slope-Area model begins with an equation of the form proposed

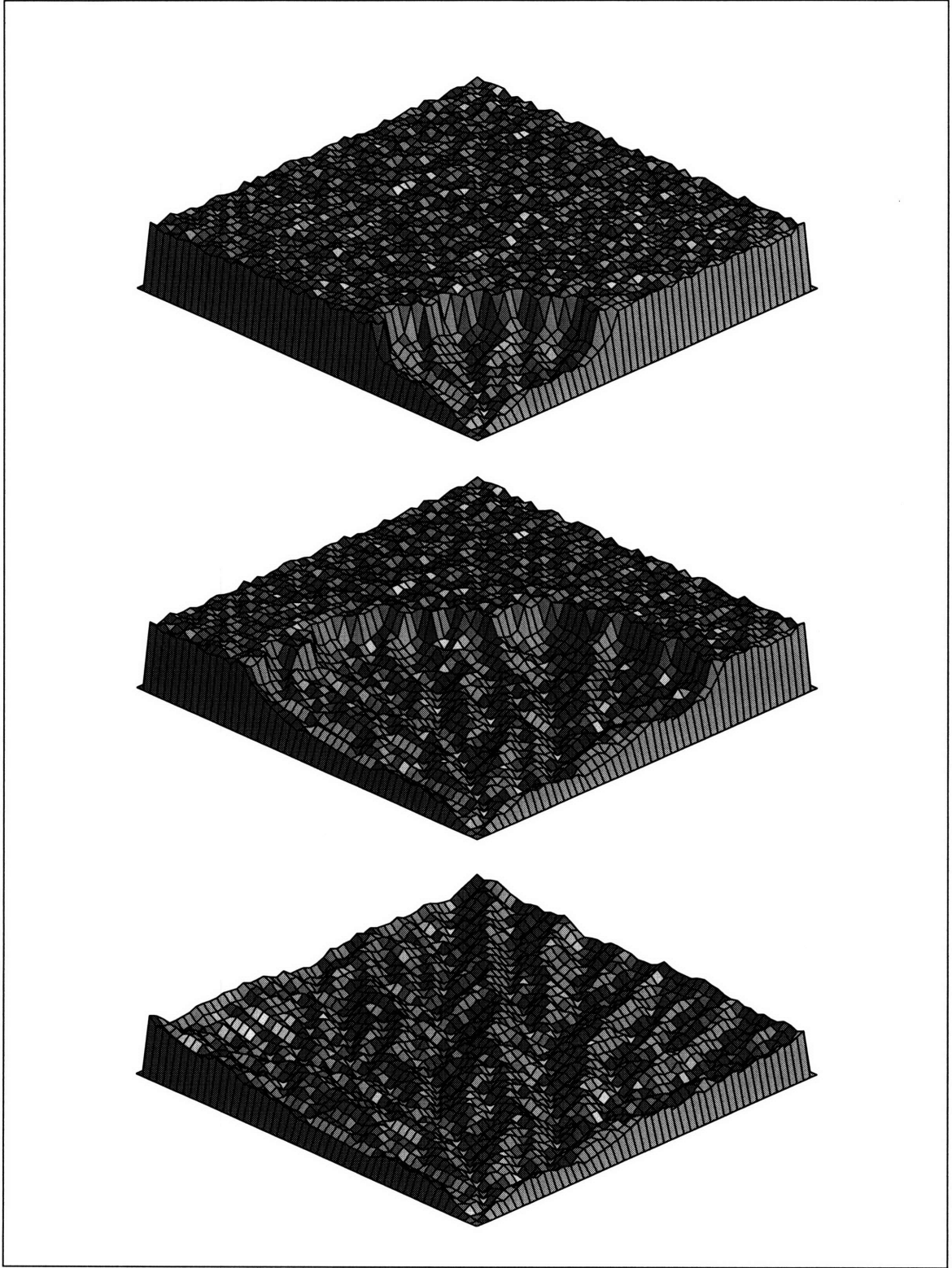


Figure 3-1: The development of topography by the Discrete Event model with an outlet specified in the corner

by Moglen and Bras [27] and Tucker and Slingerland [45]. They consider landscapes which develop under the competition between uplift and erosion by bedrock channels. Erosion in this approach is assumed to depend on slope and area each to some power, a form which can be derived from a consideration of shear stress as shown above with $\tau_{cr} = 0$. Neglecting any term reflecting diffusive processes, their model can be written:

$$\frac{\partial z}{\partial t} = U - \beta A^m S^n \quad (3.17)$$

where U is uplift, β , m , and n are parameters. At equilibrium $\partial z/\partial t = 0$, so the slope can be found in terms of the contributing area:

$$S_{eq} = \left(\frac{U}{\beta}\right)^{1/n} A^{-m/n}. \quad (3.18)$$

Note that a similar relationship also arises from transport limited models. On a discrete grid as described above, one can solve for the elevation at a point i, j :

$$z_{i,j}^{new} = z_{i,j}^{down} + \Delta l_{i,j} \left(\frac{U}{\beta}\right)^{1/n} A_{i,j}^{-m/n}. \quad (3.19)$$

The Slope-Area model employs Equation 3.19 to develop the landscape. Like the Discrete Event model described above, the Slope-Area model has essentially two parameters: a coefficient of A which controls the vertical scale of the topography and an exponent on A which affects the concavity and network structure. At every iteration, drainage directions and contributing areas are determined at all locations on the network, and elevations of all points are adjusted according to Equation 3.19 to enforce a slope-area relationship. Again, the order in which the adjustments are made plays a significant role in the model (see Chapter 4). Any initial conditions that provide well defined drainage directions can be selected.

Clearly similarity is expected in the resulting topographies because of the similarity between Equation 3.19 and Equation 3.16. Both equations essentially enforce the slope-area relationship throughout the basin development, but they do so for different reasons and in a slightly different manner. The Slope-Area model can either raise or

lower points to enforce this relationship because it describes the competition between uplift and erosional processes. Thus, its final state is an equilibrium where the effects of these processes exactly balance. The Discrete Event model can only lower the elevation of points since it describes only the effects of erosion on bedrock without uplift or deposition. Thus, its final state is one characterized by the stability of all points rather than dynamic equilibrium, and the vertical dimension of the topography is determined by $\tau_{cr} \neq 0$. The addition of uplift to the Discrete Event model is considered in Chapter 5.

Another important conceptual difference exists between the two models. The Discrete Event model is proposed as a physical description of the process of bedrock erosion without uplift. Thus, transient states which occur during the evolution are interpreted as phases of physical evolution to the extent that this model represents reality. In contrast, the Slope-Area model, only has physical meaning for the final state where the system reaches equilibrium. Before this state, the series of intermediate topographies must be considered as merely trial solutions.

Figure 3-2 shows a visual comparison between basins developed by the Discrete Event model and the Slope-Area model (top and bottom of the figure, respectively). Both basins began with the same initial and boundary conditions so that these two topographies differ only because the lower one allows the increase of elevations to enforce the Slope-Area relationship. This figure shows that these two topographies are different. One would expect that the networks will differ some in appearance because some small differences in elevations that occur during the growth may reroute channels and slightly alter the network structure. However, some systematic differences are visible. In particular, confluences tend to occur further upstream for basins developed by the Slope-Area model than for those from the Discrete Event model. This observation is confirmed by an examination of energy expenditure for the two types of basins. In general, Slope-Area basins on a 100x100 pixel grid have about 5 percent less energy expenditure than their corresponding Discrete Event basins.

Figure 3-3 shows the Slope-Area relationships for both basins. At small contributing areas, the Discrete Event model leaves some points below their critical slopes.

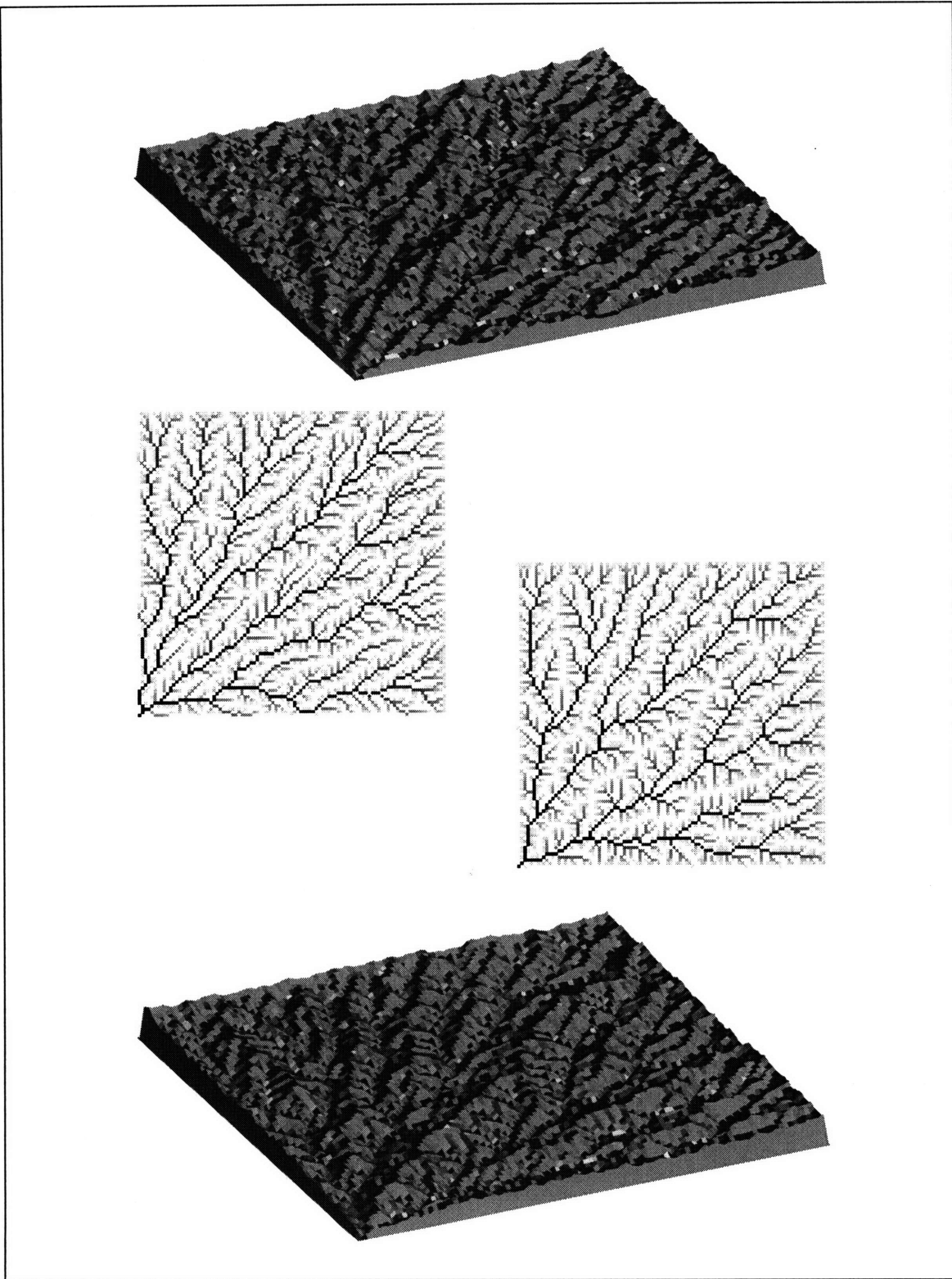


Figure 3-2: Topography and river networks as developed by (a) the Discrete Event model and (b) the Slope-Area model

Because the elevations of all points were reduced during evolution, these points were once at their critical slopes. However, reduction in their contributing areas by alterations in the channel network left these points well below their critical values. In other geomorphic characteristics such as exceedance probability distribution of contributing areas, hypsometry, and width functions these two basins appear quite similar.

3.4 Self-Organized Criticality

Fractal structures and power law scaling have been recognized in a large number of natural systems. The commonality of such characteristics indicates that power laws inherently result from the dynamics of many complex systems without detailed specification of the conditions. However, a physical understanding of how such properties arise remains an important question in the study of fractal phenomena. As Bak et al. [3] write, “The grand and general question is how the laws of physics—which describe processes on the microscopic scale—can lead to a world organized on all scales.”

One step in the investigation of this question has been the notion of Self-Organized Criticality (SOC) as proposed by Bak et al. [4, 5]. They suggest that fractal characteristics occur so commonly in natural systems because these systems are *attracted* under a broad range of initial and boundary conditions to critical states. As observed previously in the literature [5], critical states such as phase transitions imply that small perturbations can have influence over a wide range of spatial and temporal scales.

This section investigates the idea of SOC and its relevance to geomorphology where power laws are extremely common. In the first subsection, the characteristics that are observed at the self-organized critical state are summarized. Then, in the following subsection, an overview of the current debate on the self-organized critical nature of geomorphic models is presented. The position of Sapozhnikov and Foufoula-Georgiou [34] is summarized first. In their view, the current set of geomorphic models does not display SOC. A counter argument by Ijjasz-Vasquez et al. [18] is then pre-

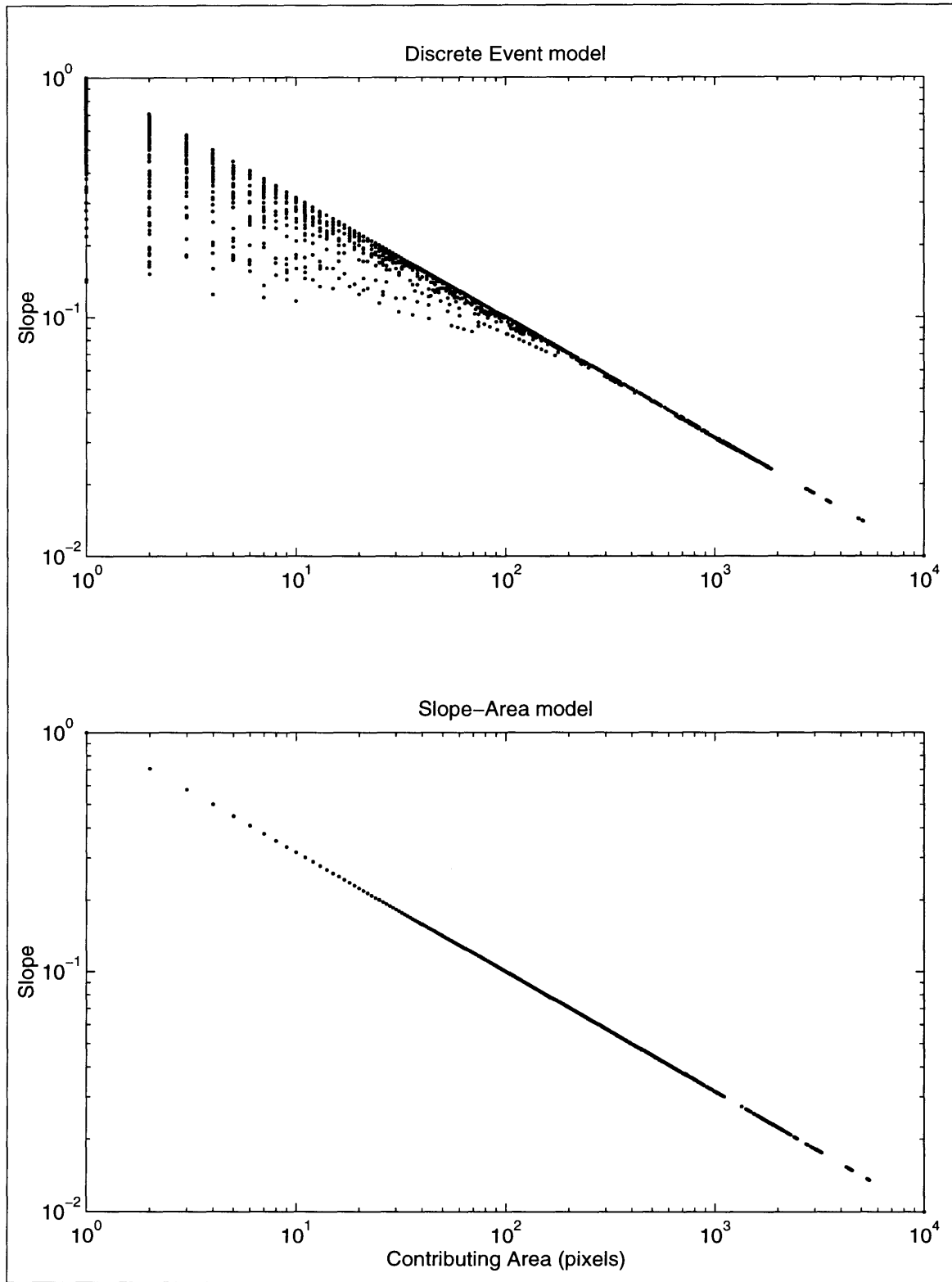


Figure 3-3: Comparison of slope-area relationships for (a) the Discrete Event model and (b) the Slope-Area model

sented. In their view both the Slope-Area model and the Threshold model would be viewed as self-organized critical. Because this debate is not central to the rest of the work presented in this document, the arguments are merely summarized for completeness, and neither position is endorsed.

3.4.1 Characteristics of Self-Organized Criticality

To illustrate the SOC idea, consider Bak's sandpile model first in one dimension. A simulation region of length N is defined which, for example, is initially devoid of sand. The left boundary is closed, but the right boundary allows the sand to leave freely. The sandpile is characterized by height differences (or slopes since the grid is regularly spaced) h where $h_i \equiv z_i - z_{i+1}$ and z is the height at a point i . Over time, grains of sand are dropped at random locations in the domain. If a grain is dropped at point i , this implies:

$$\begin{aligned} h_i &\longrightarrow h_i + 1 \\ h_{i-1} &\longrightarrow h_{i-1} - 1 \end{aligned} \tag{3.20}$$

which is simply an increase of z_i by one. When the slope at a point exceeds a critical value h_{cr} , an avalanche occurs which redistributes the mass as:

$$\begin{aligned} h_i &\longrightarrow h_i - 2 \\ h_{i\pm 1} &\longrightarrow h_{i\pm 1} + 1. \end{aligned} \tag{3.21}$$

This simply moves the excess material down the slope to the right. The adjacent right point may now exceed its critical slope; if so, it would be readjusted in the same manner. Such avalanching occurs until all points are stable. h_{cr} should not be considered a parameter since the SOC behavior does not arise under any tuning of this value.

As time progresses, the sandpile will increase to the state where all locations are at their critical slopes. This is the minimally stable state since sand added to any point will be unstable and fall straight out of the pile at the right boundary. Thus, the scale of the avalanches is infinite, and the dynamics are trivial.

Now consider a 2-D case. The addition of a sand grain in the i, j domain is defined as:

$$\begin{aligned}
 h_{i-1,j} &\longrightarrow h_{i-1,j} - 1 \\
 h_{i,j-1} &\longrightarrow h_{i,j-1} - 1 \\
 h_{i,j} &\longrightarrow h_{i,j} + 2
 \end{aligned}
 \tag{3.22}$$

In this case, h represents the slope in the $(+i, +j)$ direction. When h_{cr} is exceeded, avalanching occurs:

$$\begin{aligned}
 h_{i,j} &\longrightarrow h_{i,j} - 4 \\
 h_{i\pm 1,j} &\longrightarrow h_{i\pm 1,j} + 1 \\
 h_{i,j\pm 1} &\longrightarrow h_{i,j\pm 1} + 1
 \end{aligned}
 \tag{3.23}$$

which represents the shifting of material in the $i + 1, j$ and $i, j + 1$ directions if the smaller effects on $h_{i+1,j-1}$ and $h_{i-1,j+1}$ are neglected. The model can also be viewed as two dimensional nonlinear diffusion.

This model also reaches a stationary state but one with more interesting dynamics (viz. SOC). Here, not all points are at their critical slope; instead, the system is attracted to a condition where only a fraction of the points are minimally stable with the the rest more-than-stable. Since the more-than-stable points dampen perturbations, avalanches can therefore be of varying sizes and durations. The size of an avalanche is measured as the number of points where mass is redistributed from a single perturbation, and the lifetime is the number of iterations over which such redistribution occurs. At the critical state, the avalanches are observed to be distributed as a power law in size and lifetime (Figure 3-4).

Variations on this model have also been investigated by Bak and others [5]. Some cases include: initial conditions well above or below the threshold h_{cr} and closed or open boundaries. Under a broad set of conditions, the model will self-organize to a critical state.

So what characteristics of this model are required to develop SOC? This is not known exactly and represents an area of active research, but clear examples of SOC share the following characteristics: extended spatial degrees of freedom in which the system operates, two or more dimensions, and a process which is active up to a

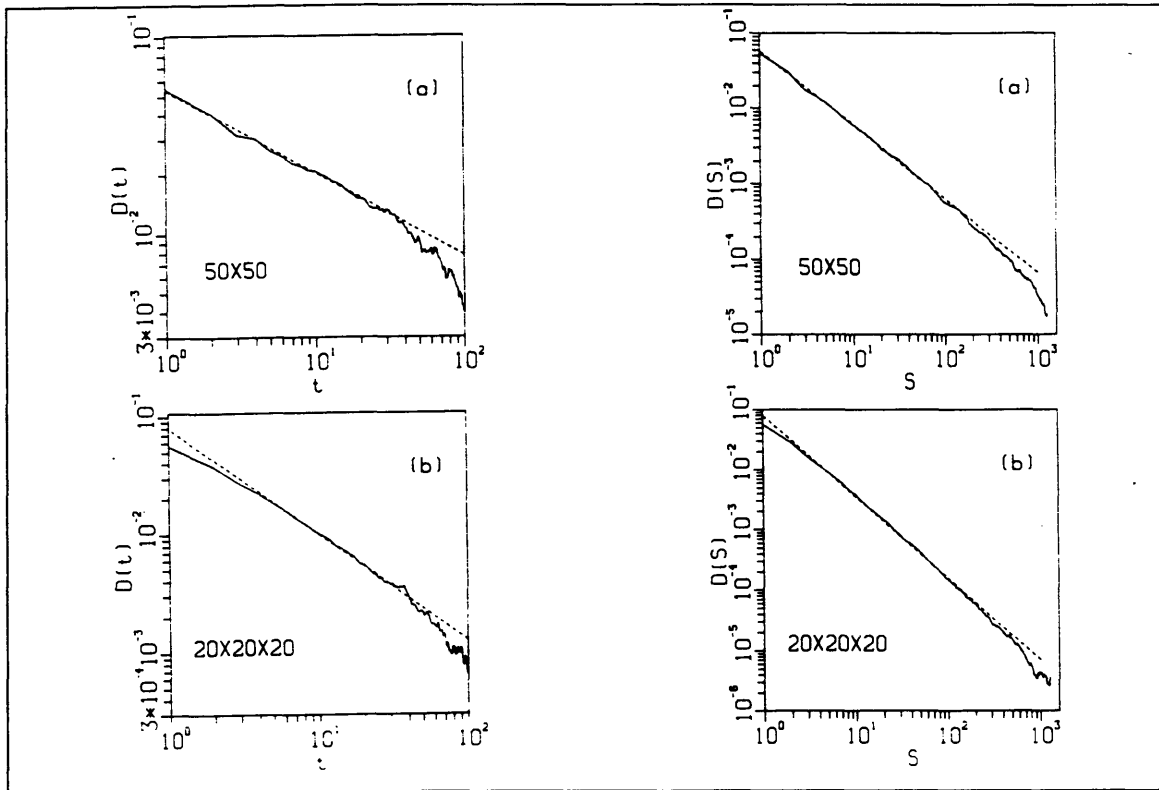


Figure 3-4: Distribution of avalanche sizes and lifetimes from Bak et al. [4] for (a) a 50x50 array, averaged over 200 samples, and (b) a 20x20x20 array, averaged over 200 samples

threshold.

Since the purpose here is to examine whether existing landscape evolution models display SOC states, the section only attempts to define the characteristics that mark the behavior of an SOC system. The principal characteristics fall directly out of the terminology.

- The SOC state is an attractor over a broad range of parameter values and initial and boundary conditions. It follows that once reaching SOC, a system never leaves this state (which implies that the state is stationary). Bak et al. [5] confirm this characteristics, “By self-organized we mean without detailed specification of initial conditions and robust with respect to variation in parameters.”
- SOC also requires criticality, implying that perturbations can propagate over all length and time scales. Alternatively, in the words of Bak et al. [5], “The dynamical process creates a stationary state where transport takes place through events on all length scales and time scales.”
- The SOC state does not correspond to the minimally stable state, and more-than-stable points play a key role in the system’s behavior. These points limit the extent of avalanches and help develop the “punctuated equilibrium” of SOC where catastrophic events of varying size pull the system away from criticality while the noise slowly pushes the system back to this state.

Using this rough definition, the geomorphic models described above can be evaluated to determine whether the ensuing power laws might derive from SOC. The next section summarizes an analysis of Sapozhnikov and Foufoula-Georgiou [34] that investigates whether the perturbation approach of the Rinaldo et al. [30] model is truly SOC.

3.4.2 Does the Threshold Model Exhibit SOC?

Many authors have claimed that they observe SOC in their geomorphic models [41, 17, 43, 30], however, none have presented a definitive demonstration of canonical SOC behavior. Upon first glance the Rinaldo et al. [30] model is clearly worth examining as

a possible example of SOC in a geomorphological context. In particular, it includes a process which operates up to a threshold, creating a system with a collection of points at barely stable and more than stable states. Furthermore, it demonstrates many of the power laws that are observed in natural basins.

Sapozhnikov and Foufoula-Georgiou [34] have examined whether the Threshold model exhibits SOC behavior. They adopt a similar description of SOC as that described above. Specifically, they observe that the SOC state is (1) critical and demonstrates power law scaling in the impacts of perturbations in space and time and (2) attracted to the critical state. The state they examine for SOC is the state after the initial growth of the model where all points lie below the critical shear stress. According the approach of Rinaldo et al. [30], this state is perturbed by adding elevation to a node and then allowing the system to re-adjust the elevations to enforce the critical shear stress condition.

Two important differences can be observed between this model and canonical SOC. First, power law scalings do not always hold in this state. Specifically, Rinaldo et al. [30] begin a simulation with a comb-like river network in which all points are stable, but the system does not display power law scaling until the final state when perturbations no longer affect the state of the system. Second, the system is not in a stationary state. As the perturbation/relaxation process advances, the power laws develop indicating a statistical change in the system. These two differences are important since they contradict the observed characteristics of SOC given above.

Additionally, Sapozhnikov and Foufoula-Georgiou [34] argue that the final configuration (once fractal scaling has developed) cannot be considered SOC as it violates the condition of a punctuated equilibrium. In this state, the elevations remain unchanged. Although this is a specific case of stationarity, there can obviously be no scaling in the lifetime or size of the impacts of perturbations. Thus, Sapozhnikov and Foufoula-Georgiou [34] conclude that no state of the system corresponds to the SOC state demonstrated by the sandpile model.

3.4.3 SOC and Cluster Growth

Other work, by Ijjasz-Vasquez et al. [17, 18], investigates the SOC behavior of the Slope-Area model from a perspective that is not considered by Sapozhnikov and Fofoula-Georgiou. This section summarizes this alternative view which relies on the self-organized critical behavior of cluster growth and branching processes.

Alstrom [2, 1] suggested that branching or cluster growth processes also exhibit SOC. Consider the tip of a single branch. This “generation” can be replaced by zero, one, or two descendants with probabilities P_0 , P_1 , and P_2 . At criticality, the process barely survives through the generations which implies $P_2 = P_0$. This stationarity holds until the cluster reaches a boundary condition. At criticality, the structure of the branches becomes scale invariant [13]. Thus, a branching process that self-organizes to reach this critical state is an SOC process (see Alstrom [2, 1] for further details). One can see several analogies between cluster growth and the sandpile model. The branching is similar to the addition of grains to the sandpile since they are perturbations on the main aggregate. The extinct branches can be considered as the completed avalanches in the sandpile model, where “extinct” limits consideration to the branches that are no longer growing. These branches as expected are characterized by power laws both in size and time of growth.

One difference exists between this view of SOC and the sandpile model. For Alstrom, the domain SOC lies right at the interface of growth. Inside the cluster lies the history of the activity, and outside the cluster lies “the future.” This implies that over a limited spatial domain of simulation, the process will eventually become inactive and stationarity will break down. In the experiments of Bak et al., the boundary conditions seem to play a much different role.

As will be described in detail in Chapter 4, the Threshold, Discrete Event, and Slope-Area models all inherently contain a cluster growth process. Specifically, one assumes a cluster growth model in deciding the order in which points with excess shear are adjusted to be stable. For example, consider applying the Threshold model to a rectangular domain with an outlet in the corner and white noise for initial elevation

throughout the rest of the region. Initially, only points adjacent the outlet will have excess shear. Once the elevations of these point are reduced, other more distant points will have excess shear. Over time, the network or cluster grows to fill the domain until limited by the domain edge or by the height of the initial surface.

Figure 3-5 presents the distributions of size and lifetimes of the extinct branches of the network for the Slope-Area model (from Ijjasz-Vasquez et al. [18]). As the figure shows, both distributions obey power laws as described by Alstrom [2, 1].

3.4.4 Summary

The previous sections have presented an overview of the debate regarding the possibility SOC in geomorphic models. Although this is an ongoing discussion in the literature, to a large extent the question is beside the point of geomorphic modeling. Although the Threshold model of Rinaldo et al. eventually reaches a stable configuration which does not radically change under perturbations, no field evidence suggests natural basins radically change their form under minor perturbations either.

Rather than attempting to develop a model that strictly obeys SOC, it seems preferential to direct efforts towards modeling characteristics and behavior observed in the field. The following chapters attempt to do just that. Several variations of the Discrete Event model algorithm, its initial conditions, and climatic forcing will be presented and the resulting basins compared with well known geomorphic indicators. By doing so, it is hoped to better understand the link between the dynamics of growth and basin form and to identify possible sensitivities of basin evolution to initial conditions and climatic forcing.

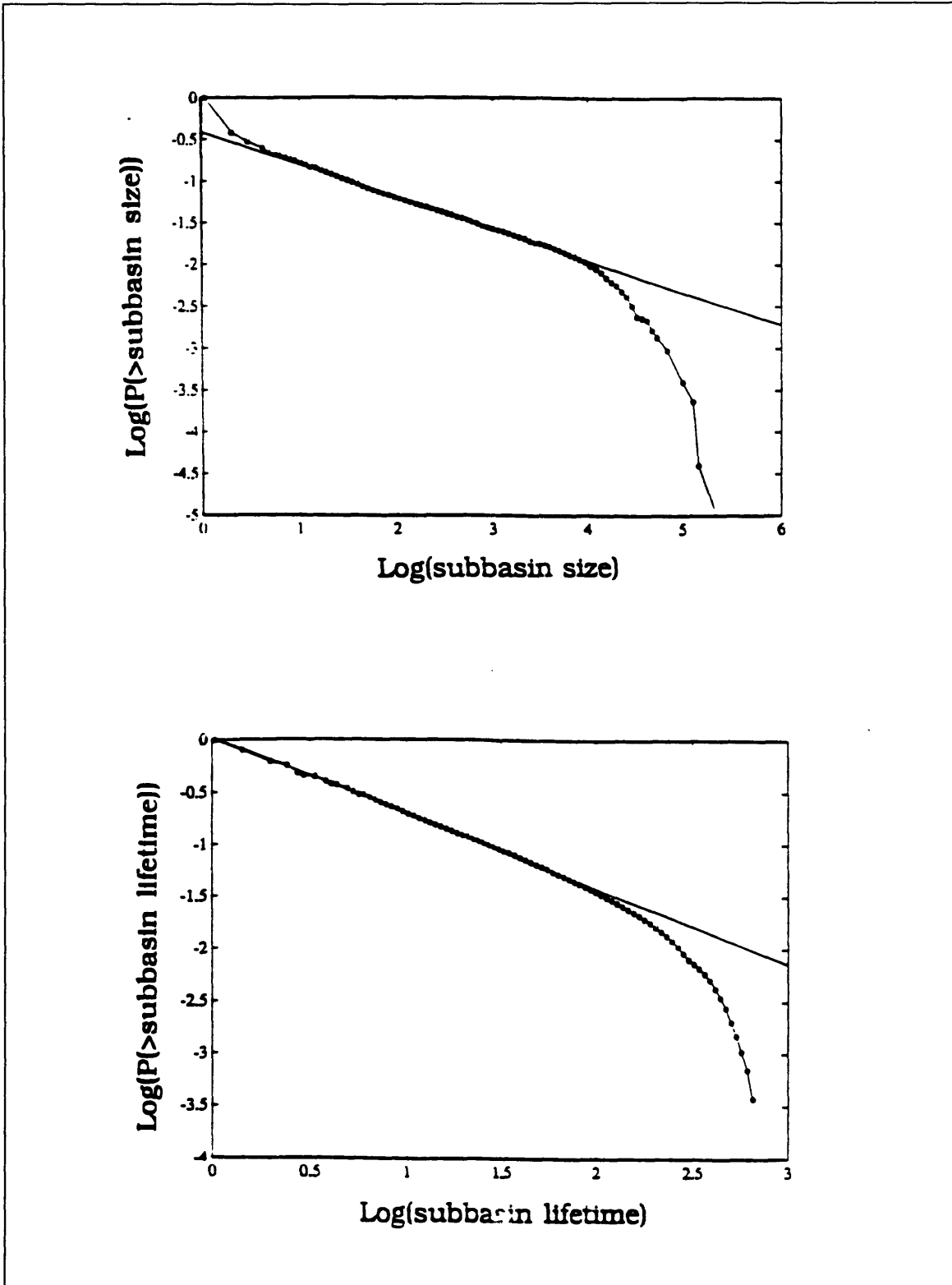


Figure 3-5: Distribution of avalanche (a) sizes and (b) lifetimes in the Slope-Area model (from Ijjasz-Vasquez et al. [18])

Chapter 4

Sequencing of Erosion Events

The organization of channel networks plays a key role in determining the overall characteristics of topography. The river network determines the orientation, sizes, and junctions of valleys and therefore influences the locations and configuration of ridges. Drainage density controls the horizontal dimensions of hillslopes and therefore influences the relief. Even the elevation of the ridge summits depends on the network organization because the hillslope baselevels correspond to river reaches whose elevations depend on the basin structure.

Because of this important role, considerable attention has been focused on the formation of channel networks. At least three different conceptual models have been proposed to describe the network development (see Chapter 2 for thorough descriptions). These models essentially differ in their emphasis on either network expansion or internal changes of structure. In addition, they ascribe different relative behavior to major and minor tributaries. Specifically, Horton [14] favors a view where reorganization plays the key role in drainage network development. He proposed that parallel rills immediately develop over a surface. Then, the channel network structure forms as one rill begins to dominate redirecting and capturing the others through cross-grading and micropiracy. Alternatively, Howard [15] proposed that channel networks grow headward in an intense “wave of dissection” where channels lengthen and bifurcate as they cut into an initially undissected region. As this wave passes, it leaves behind the mature channel network. Finally, Glock [10] proposed a similar view to

Howard's except that the main channels first *elongate* to capture the region, then the minor tributaries are added in a period of *elaboration*. He also envisaged a period of *integration* which involves a reduction in the number of tributaries near the main trunk as it migrates laterally.

Several studies have attempted to observe network growth in the field to assess which of these models best applies. Unfortunately, the diversity of boundary conditions and substrate properties as well as the long time scales for network growth has hindered any clear conclusions. Morisawa [28] observed network development on a lake shore in Montana after an earthquake tilted the region, exposing small new sections for dissection. She concluded that Glock's phases of extension (including both elongation and elaboration) occur simultaneously with integration, but her results do not particularly support either perspective on the relative growth of major and minor tributaries. Schumm [36] observed the growth of networks on a clay-sand fill at Perth Amboy, New Jersey. His observations generally support Howard's notion of headward growth, however, integration was also simultaneously observed.

Schumm et al. [37] describe a set of experiments that were performed in an attempt to investigate the role that initial conditions play in determining which of the above models best describes network growth. In an experiment with a relatively flat initial condition coupled with baselevel lowering, the wave of intense dissection was observed. However, for an experiment with a steeply graded initial surface and baselevel lowering only in the later stages of growth, Glock's phases of elongation and elaboration could be identified.

This chapter examines the network growth implied by several variants of the Discrete Event model and the impacts that the mode of growth has on the resulting basin morphology. In the model, network growth can be controlled by the sequencing of the erosion events. Particular choices of the sequencing will also be shown to closely resemble other published models of landscape evolution.

The outline of the chapter is as follows. First, the various possibilities of sequencing are discussed in terms of their physical meaning and relationship to the above hypotheses of network growth (and other models described in the literature). Then,

a series of basins generated by these model variants are examined using various geomorphic measures. Finally, the implications and conclusions from the results are discussed in the last section.

4.1 Sequencing Variants

As described in the previous chapter, the Discrete Event model can be summarized in a simple, five-step algorithm. The third step is to determine which points are to be adjusted at any given iteration. The order in which points are adjusted is important since the new elevations depend on a downstream elevation z^{down} and a contributing area A —both characteristics of the existing network structure. If carefully selected, this step provides the opportunity to investigate the role of various feedbacks in the network growth in determining the basin geometry. The following subsections describe the four alternatives considered for the sequencing of erosion events.

4.1.1 Headward Growth

In the *Headward Growth* variant of the model, points are eroded in a strictly headward fashion. This is accomplished by beginning a cycle of erosion events (or an iteration in the algorithm described in Chapter 3) from any pits and outlets in the current elevation field. First, the points immediately upstream of the pits and outlets are evaluated for excess shear. If any of these points are unstable, their elevation is reduced to make them stable. Then the points draining immediately into the previous set are evaluated and eroded as necessary. This process is continued until the channel sources are reached.

Notice that in this algorithm, the z^{down} values used upstream are the newly updated downstream elevations. The contributing areas and drainage directions used are updated only after each complete pass (a model iteration). By decoupling these, the erosion events are, in effect, instantaneous events that span many pixels before the network structure redevelops in the area.

Figure 4-1 shows some schematic slopes to demonstrate the behavior of the model

variants in one dimension. Each row of diagrams exhibits the behavior of a given model variant on two different slopes. Initially, both slopes have two unstable points (points 3 and 4), and the point on the far right (point 6) does not drain toward the rest of the slope. The two slopes differ in the curvature of the unstable section: the lefthand example is concave and the righthand one is convex. Neither slope has tributaries, and the concavity of stable river profiles is ignored for simplicity. The solid lines in the plot show the slope profiles between iterations; the dashed lines show the profiles as they change during given model iterations (i.e. intermediate stages).

The top row displays the Headward Growth variant. During the first iteration, the elevations of the two initially unstable points are reduced which creates a newly unstable point upstream from these two points which is also reduced. The erosion of the first iteration continues until reaching the initial divide, since the final point still drains in the opposite direction. After the first erosion event, the final point adds its contributing area to the channel, thus requiring a reduction in all slopes for stability. Again, a wave of dissection moves upstream to bring the slope to stability. After only two iterations, this slope has reached its final form.

Three observations can be made from this simple experiment which will prove useful in interpreting the behavior of more complicated two dimensional growth. First, the erosion event is always triggered at the downstream edge of any unstable sections, and it is the propagation of this removal of material that dictates the size of each erosion event. Second, much of the total erosion occurs before the additional drainage area is captured. In fact, if no additional contributing area is captured during an erosion event, no further erosion is needed to achieve stability throughout the basin. Third, the initial shape of the slope only affects the erosion through locations of unstable points and the placement of the divide.

Figure 4-2 shows a snapshot during the growth of a river basin for each of the model variants. In this figure a very large escarpment is initially specified to accentuate the differences between the model variants. The top portion of this figure shows Headward Growth in progress. Behind a clearly defined escarpment, a well formed basin has already developed. As mentioned for the one-dimensional example, all

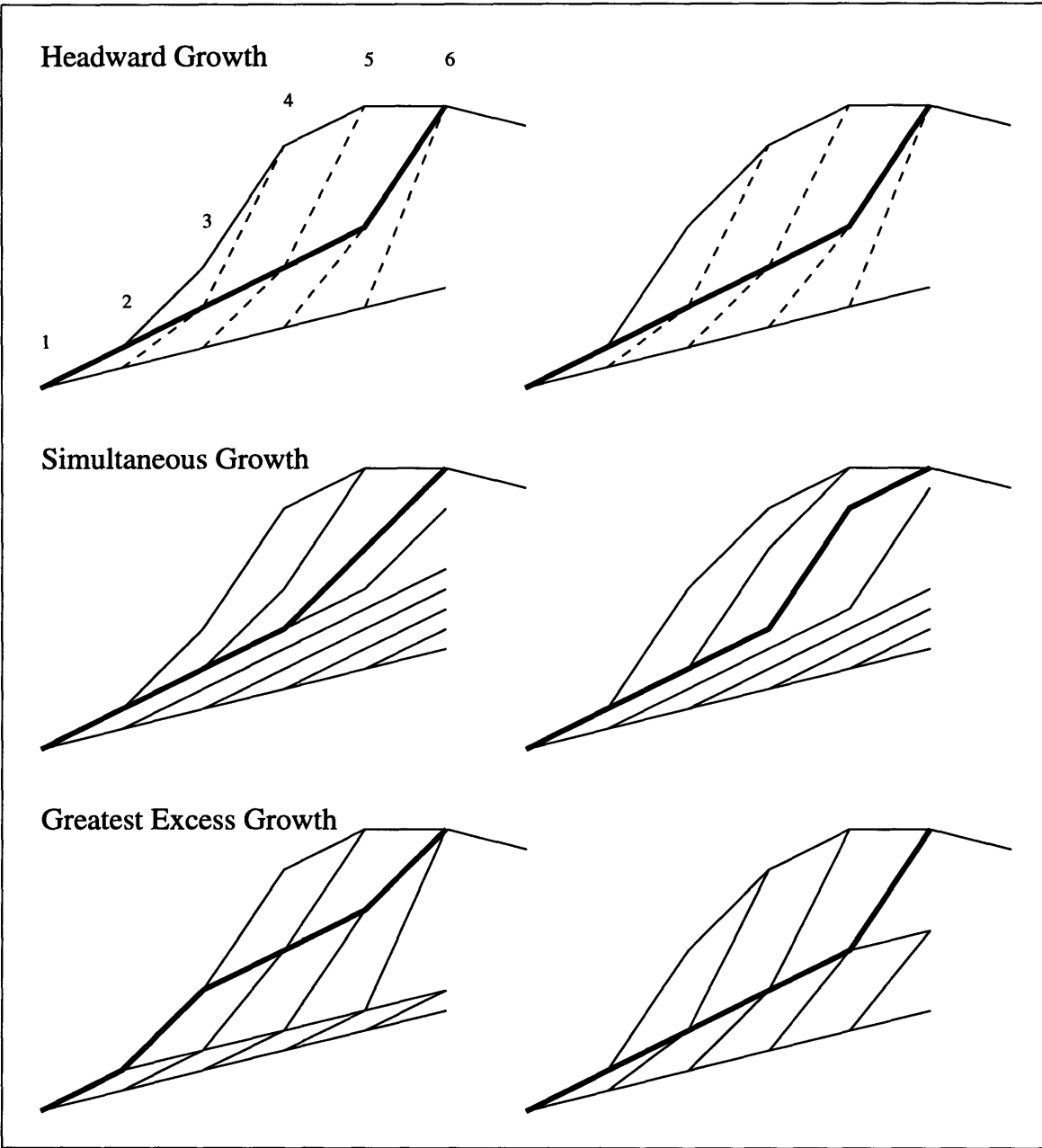


Figure 4-1: Schematic diagram of three different erosion algorithms at work on two example slopes. Solid lines indicate slope profiles in between model iterations, whereas dashed lines indicate the changing profile shape during a single iteration. The bold line shows the profile when point 6 is captured

points in this basin are stable with the exception of those which were captured at the previous iteration. This type of erosion sequencing is considered to be the most strict example of headward growth since no readjustment occurs after the initial capture and erosion of points. As Howard [15] describes it, erosion occurs as an intense “wave of dissection” that propagates headward. Additional area is captured only after much of the excess material within the basin has already been removed. Note that this model is not the numerical model proposed by Howard; rather it simply embodies the concept of strictly headward growth.

4.1.2 Simultaneous Growth

Another alternative of erosion sequencing is termed *Simultaneous Growth*. In this model, no preference is given to any point in the basin. Rather, all points with excess shear are simultaneously reduced in elevation in order to achieve stability under the current network configuration. This implies that at each iteration, every point in the domain is simultaneously evaluated for stability. If a given point is unstable, its elevation is reduced assuming the drainage directions, contributing areas, and downstream elevations that are present at the beginning of the iteration. Such a simultaneous approach is the same *sequencing* of erosion that would be used in a finite difference simulation of a differential equation.

Unlike the other erosion sequencing variants, in this case the elevation of unstable points are not immediately reduced to reach stability. Instead, a more general form of Equation 3.16 is used:

$$z_{i,j}^{new} = W_{i,j} \left(z_{i,j}^{down} + \Delta l_{i,j} \left(\frac{\tau_{cr}}{K} \right)^{1/n} A_{i,j}^{-m/n} \right) + (1 - W_{i,j}) z_{i,j} \quad (4.1)$$

where $W_{i,j}$ is a weighting function, $z_{i,j}$ is the elevation of the point at the beginning of the iteration, and $z_{i,j}^{new}$ is the new elevation. If $W = 1$, then this equation reduces to the standard form of Equation 3.16. However, for this variant $n = 1$ is assumed which follows from the relationship between hydraulic radius and discharge employed

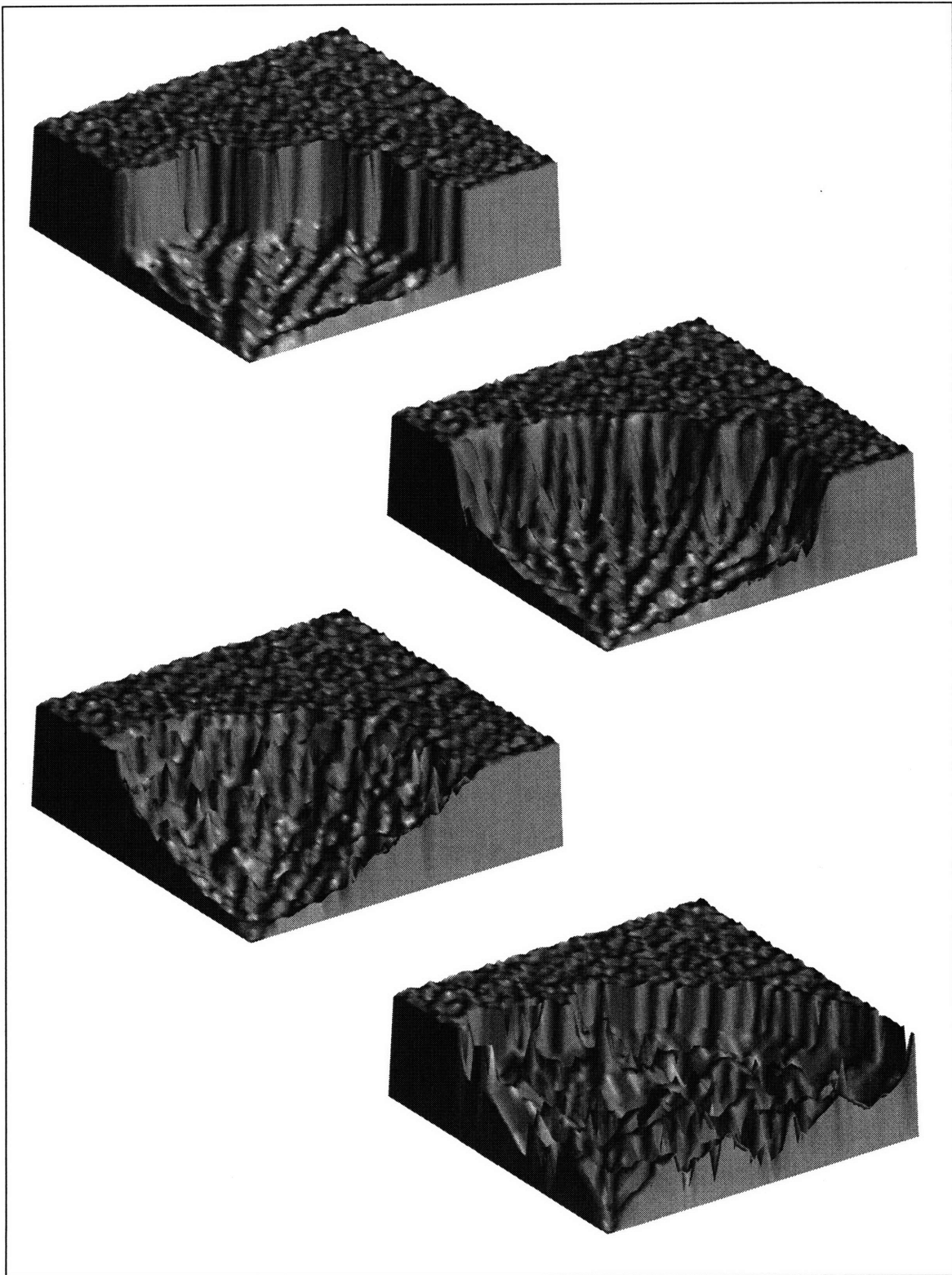


Figure 4-2: Snapshots during the erosion of a basin using (a) Headward Growth, (b) Simultaneous Growth, (c) Random Growth, and (d) Greatest Excess Growth

by Rinaldo et al. [30] (see Chapter 3). In addition, W is selected as:

$$W_{i,j} = \frac{K k_1 \Delta t}{\Delta l_{i,j}} A_{i,j}^m \quad (4.2)$$

where $k_1 \Delta t$ is a parameter whose meaning will become clear shortly. Substituting the weighting function into Equation 4.1 and rearranging, one finds:

$$\frac{z_{i,j}^{new} - z_{i,j}}{\Delta t} = k_1 \left(\tau_{cr} - K A_{i,j}^m \frac{z_{i,j} - z_{i,j}^{down}}{\Delta l_{i,j}} \right) \quad (4.3)$$

which is the (forward) finite difference version of the equation:

$$\frac{\partial z}{\partial t} = k_1 (\tau_{cr} - K A^m S). \quad (4.4)$$

Equation 4.4 is simply Equation 3.1 if $\alpha = 1$ and $n = 1$. Thus, the Simultaneous Growth variant is equivalent to a finite difference model where erosion occurs in proportion to shear stress.

Figure 4-1 shows the behavior of this sequencing variant for the example one-dimensional slopes. In the first iteration, the two points with excess shear are eroded, but the upper point (point 4) is only reduced to an elevation above the previous elevation of the downstream point (point 3). In addition, the point at the top of the slope is not yet eroded. In the second iteration, the top part of the profile is eroded because these points are now unstable, which leads to the capture of the far right point. Over the next several iterations, thin layers of material are eroded until none of the points are unstable.

This model behaves quite differently than the Headward Growth model. In particular, rather than removing a large amount of material before capturing upstream points, only thin slices of rock are eroded before expansion. This approach tends to form a transient stream profile in which all points are about equally unstable. Then, the stream profile is slowly degraded until reaching stability. Also, in this variant, the form of the slope is roughly maintained as it shifts upstream during the early stages of growth.

Figure 4-2 shows the operation of the model variant on a two-dimensional domain. The figure shows that slopes further from the escarpment are much closer to stability than those near the escarpment. This indicates that basin configuration gradually becomes better developed through time.

4.1.3 Random Growth

The third sequencing variant considered is called *Random Growth*. In this variant a single, randomly chosen point is eroded at each iteration. This point is chosen among all points in the domain with equal probability. If the selected point is unstable, then it is eroded and the drainage directions and contributing areas are immediately recalculated for the next iteration. If the selected point is stable, then no erosion occurs and another point can be immediately selected.

Because of the random nature of this algorithm, any sequence of erosion is possible in the one-dimensional profiles of Figure 4-1, and hence none is shown. However, the erosion will certainly differ from both of the above variants because only a single point is eroded in each iteration. This implies that the flow paths are immediately updated, and considered relevant to the erosion of all points. Thus, rather than the joint erosion of several adjacent unstable points as allowed by the above two models, points now behave more individually.

It can be shown by a simple consideration of probability that this erosion algorithm is equivalent to Eden Growth. Eden Growth is a simple cluster growth model that has been used to describe the development of, among other things, tumors and river basins (see below). The algorithm for Eden Growth is quite simple, and here we consider only one of the simplest versions of Eden Growth. A domain of simulation is specified on a square grid, and an initial seed (or more than one) is placed at some location on the grid. At each iteration, one of the adjacent neighbors is selected randomly to be added to the cluster. Each adjacent neighbor has probability $1/N_p$ of being selected where N_p is the number of perimeter sites [47].

In the Discrete Event model, the channel network can be considered to be a growing cluster. Consider the simple case where an outlet is specified in the corner

and the rest of the initial elevations include just enough noise to uniquely define drainage directions. Initially, all points must have elevations well above the outlet. In fact, if the basin growing around the outlet is to capture the entire domain, the initial elevations of all points must be greater than their final elevations in the network. Thus, we can define the cluster in terms of elevation: all points with elevations below the range of initial elevations (excluding the outlet) are part of the cluster.

In order to be equivalent to Eden Growth, however, the adjacent neighbors must have equal probability of being added to the cluster. In the Random Growth variant, three types of points may be selected for possible erosion: adjacent neighbors, non-adjacent neighbors, and cluster points. By definition, non-adjacent neighbors always have downstream neighbors with elevations in the initial range. So if one of these points is selected for possible erosion, it will be determined to be stable and left uneroded. Cluster points may also be selected for erosion and may be unstable. However, since these points already lie inside the cluster, their adjustment does not affect the cluster size and has no relevance to the selection of adjacent neighbors. This leaves only adjacent neighbors which, when selected must be added to the cluster since they are always unstable (see Figure 4-2). Consequently, all adjacent neighbors have equal probability of being added to the cluster, and the Random Growth variant is concluded to be a form of Eden Growth.

Howard's model [15] is also essentially Eden Growth, although he presents several variations which depart slightly from Eden Growth. Consequently, the Random Growth variant is an extension of his model where the role of elevation is also included. The addition of elevation results in much more rich behavior including internal adjustments of the channel network and the potential (depending on initial conditions) for the termination of channels due to stability.

Eden Growth has also been incorporated into a model of plateau erosion by Stark [42]. In this model, Stark does not consider elevations, rather he considers the scarp to be the frontier of a growing cluster (following an argument very similar to the one given above). Eden Growth represents the "background erosion and weathering" which includes those processes that do not depend on either groundwater

flow or substrate strength.

Figure 4-2 shows a snapshot during the development of a basin with the Random Growth variant. The basin frontier has a more irregular form than either of the previous two variants and much less refinement has been performed on the elevations inside the basin.

4.1.4 Greatest Excess Growth

The fourth and final variant considered is called *Greatest Excess Growth*. Like the Random Growth variant, only one point is selected for erosion at a given iteration. However, rather than being selected randomly, the point with the greatest excess shear stress is selected for erosion. This model implies that points which are more unstable will erode first. This is the algorithm employed by Rinaldo et al. [30].

Figure 4-1 shows this algorithm operating on the same two schematic one-dimensional profiles. Considering the concave profile on the left, the first iteration reduces the elevation of the point near the top of the slope since it had the greatest excess shear stress. This creates a small concave section in the upper part of the slope which then erodes in the next iteration to capture the additional area. In the following several iterations, the knickpoint formed in the lower portion of the profile moves upstream until all of the points are about equally unstable. Finally a long series of iterations slowly grade the river profile until stability is achieved everywhere.

Examining the convex profile, one sees different behavior. In this case, the greatest excess shear occurs at the toe of the slope, so that the erosion begins at the base and propagates up the slope until it captures the additional area. Eventually, the profile reaches a state where all points are nearly equally unstable, and readjustment occurs steadily until stability is achieved.

This algorithm is distinct from the others. First, there is greater dependence on the profile shape. When the steepest section occurs high in the profile, a second knickpoint can be created which moves individually upstream. Also, this approach has the capability of capturing the additional area very quickly or slowly, depending on the profile form. In the case of the concave profile, the algorithm quickly moves to

capture the additional contributing area, then over time adjusts its profile to reach stability.

Figure 4-2 shows a snapshot during the growth of the Greatest Excess variant on a two dimensional domain. From this picture, one can see that the Greatest Excess algorithm shares some similarities with Glock's conceptual model of network growth. He envisioned that the main channels would extend first to capture the bulk of the available area. Then, over time, the smaller tributaries would fill out to properly drain the basin. This is essentially the behavior shown in this figure. A very irregular escarpment forms as the main channels extend to capture area before the smaller channels are fully developed.

This variant also appears quite similar to the Invasion Percolation cluster growth model [47]. Invasion Percolation is similar to Eden Growth, but leads to very different scaling characteristics. In Invasion Percolation, one specifies one or more initial seeds and assigns a random number to every other point in the simulation domain. At each iteration, the largest (or smallest) adjacent number is added to the cluster. Eventually, the cluster will fill the entire region, but before this point in time, when it first reaches the boundaries, it displays fractal characteristics (unlike Eden Growth which displays self-affinity along its frontier) [47]. Invasion Percolation has been used to simulate the growth of drainage networks by Stark [41] when the effects of elevation are not included.

Similar to Invasion Percolation, the Greatest Excess variant adds the adjacent neighbor with the greatest excess shear to the basin. However, unlike Invasion Percolation, the shear stresses of points along the boundary can change over iterations. For instance, the shear stress depends on the downstream elevation which may change if the point inside the cluster is eroded, the drainage direction is altered, or contributing area is lost or gained. Consequently, this model is not exactly Invasion Percolation.

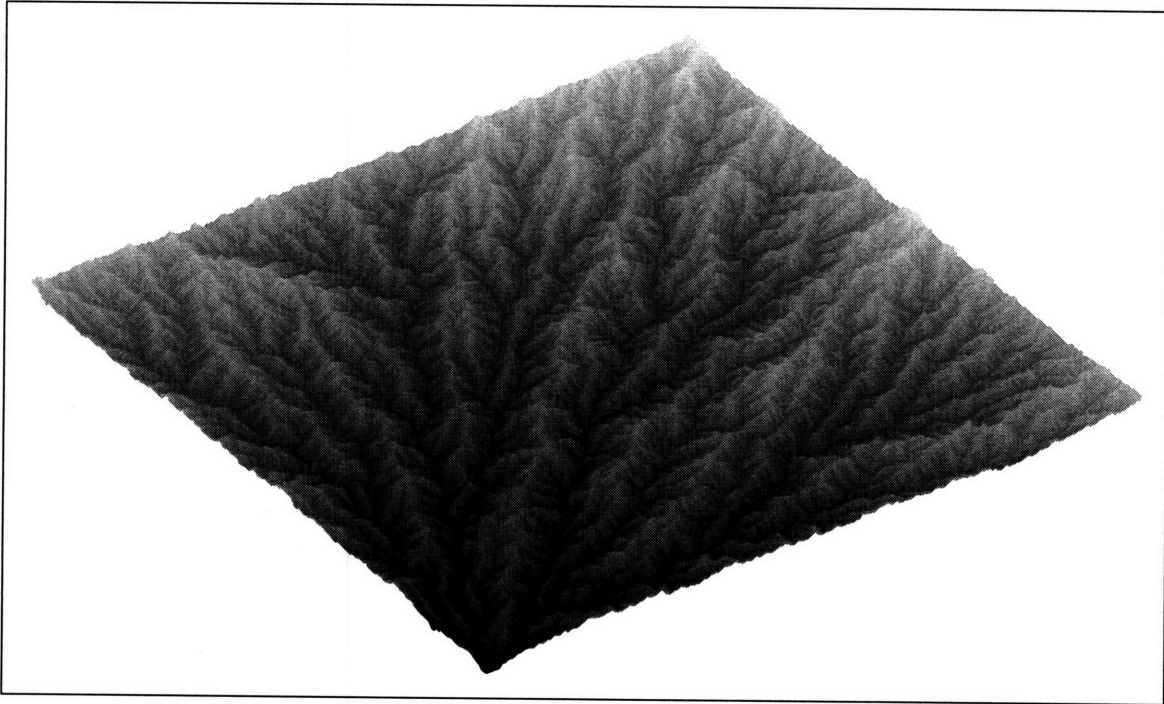


Figure 4-3: A basin developed by the Headward Growth variant

4.2 Basin Morphology Implications

Figures 4-3, 4-4, 4-5, and 4-6 shows four river basins developed using the Discrete Event model. All of these basins share the same initial and boundary conditions, including an outlet specified in the front corner. Each of these were eroded using one of the four different model variants as described above. If the model variants behaved exactly the same, the results should be identical. Small differences in the model algorithm will introduce changes in the resulting network even if the variants are nearly identical. However, no systematic changes in the network structure should be introduced if these variants do not affect the resulting topography.

As the figures show, some significant differences are clearly visible between the simulations. The most obvious result is the distinctive form of the basin developed by Greatest Excess Growth variant. Its ridge lines and channels are clearly much more irregular and complex in form than the other three cases. The ridge lines follow a tortuous path and the ridges branching off the main divides have a variety of lengths and orientation. In this basin, large irregular regions maintain consistently high or

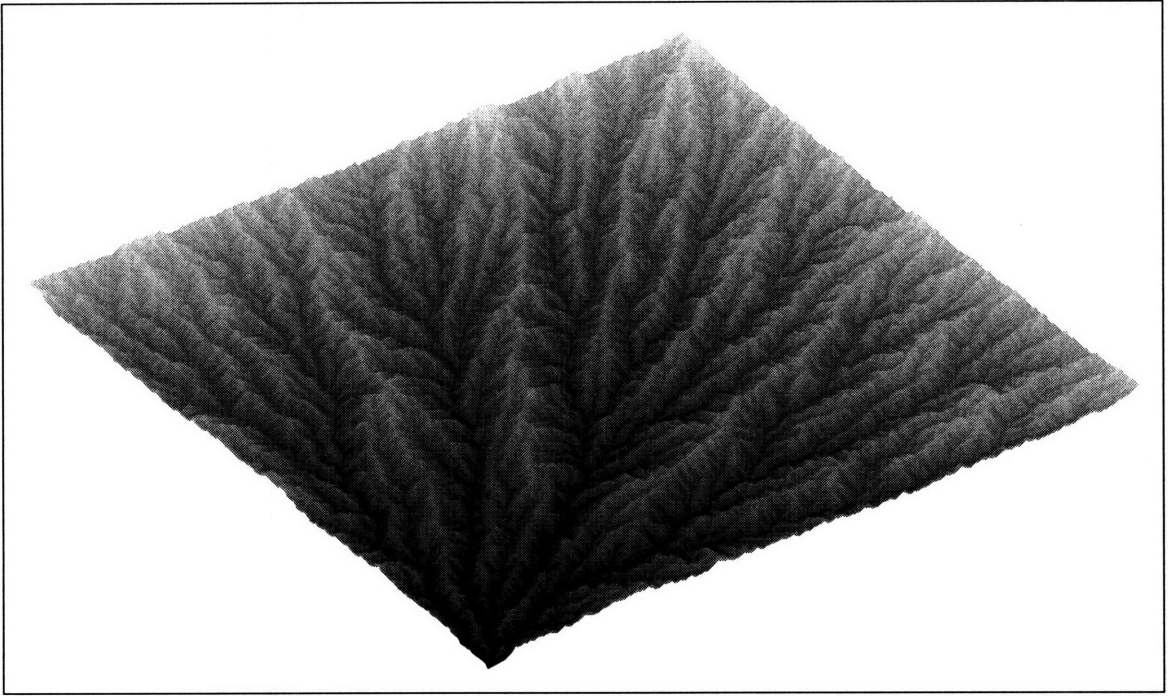


Figure 4-4: A basin developed by the Simultaneous Growth variant

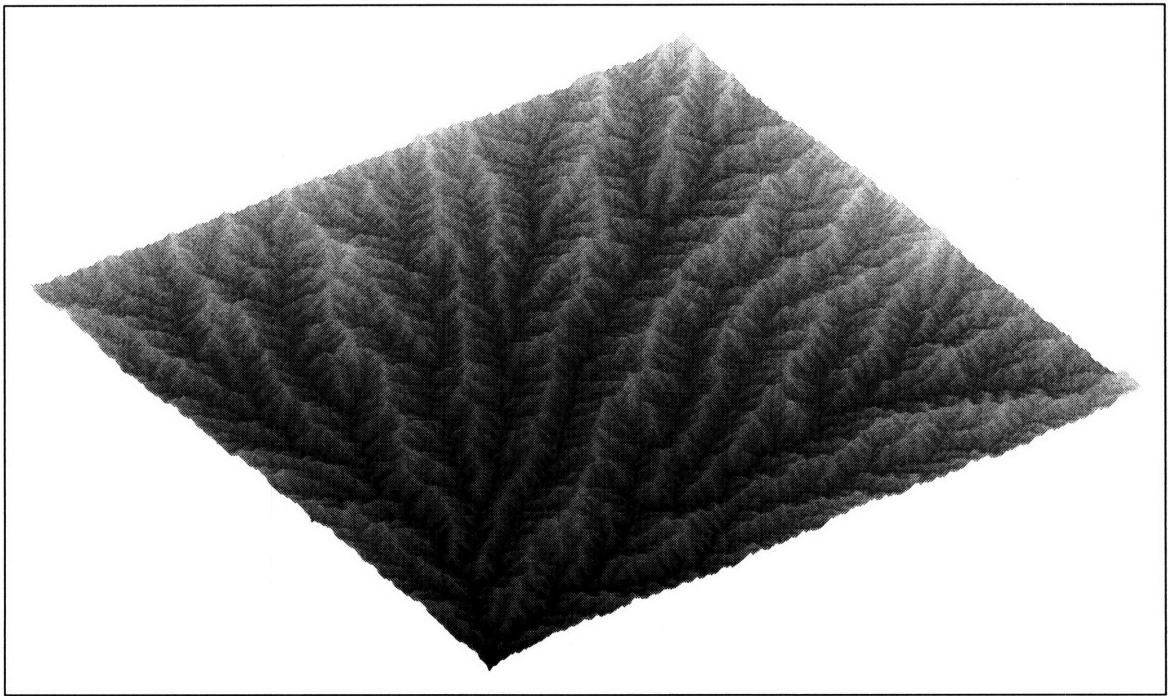


Figure 4-5: A basin developed by the Random Growth variant

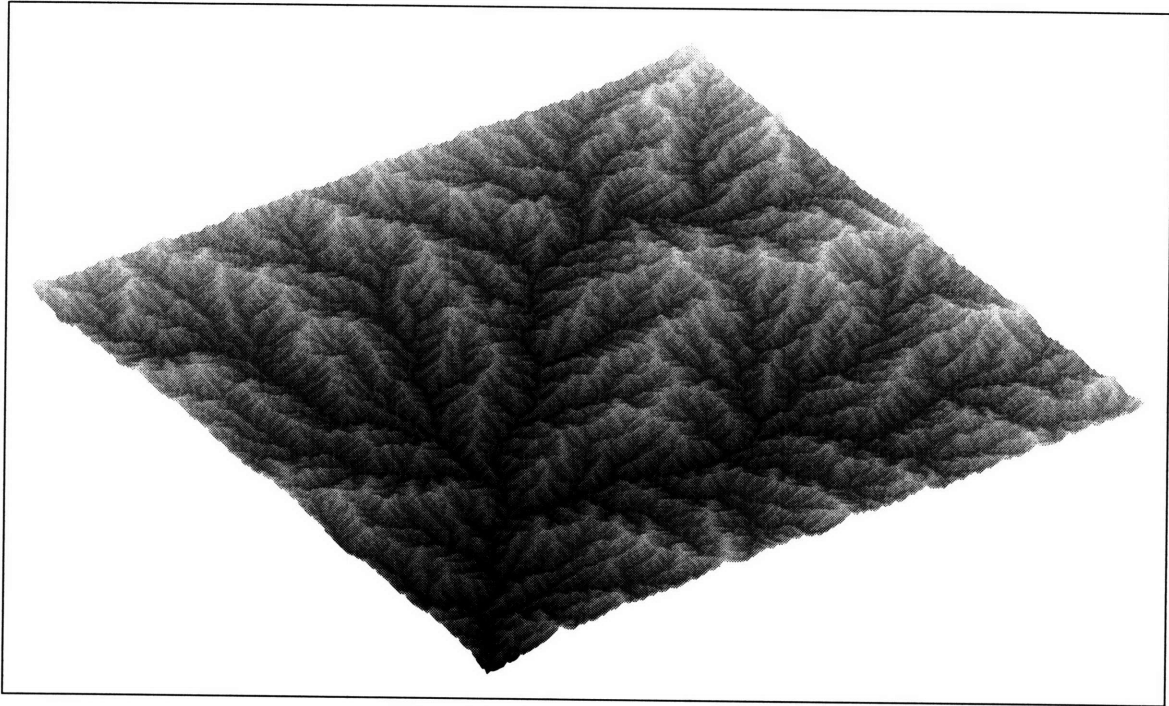


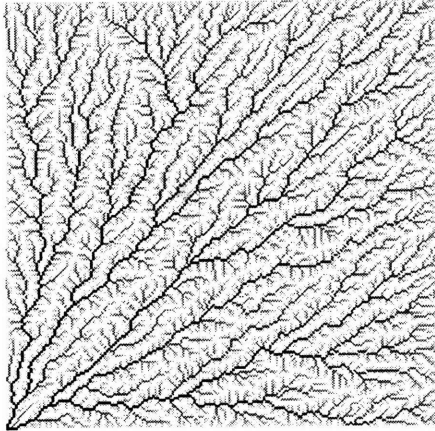
Figure 4-6: A basin developed by the Greatest Excess Growth variant

low elevations relative to the rest of the basin.

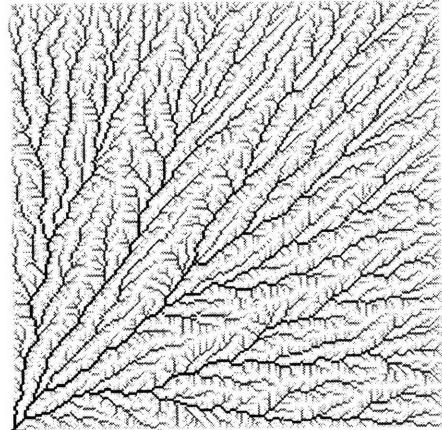
Even among the other three basins small differences can be seen in the texture. The Simultaneous Growth algorithm develops smoothly varying and nearly radial channels and ridges. The basin from the Random Growth algorithm also develops relatively smooth ridges with regularly spaced side valleys, giving the impression that the ridges have ribs.

Figure 4-7 shows the river networks associated with the four basins by shading each pixel according to its contributing area. The Simultaneous Growth variant tends to develop a large number of channels that are oriented directly towards the specified outlet. These channels also remain very straight. Relatively more irregular main channels are visible in the Headward Growth and Random Growth variants. The Random Growth algorithm in particular appears to develop very few truly straight sections along the channels. However, all three of these basins seem clearly controlled at larger scales by the outlet location. The fourth variant, from the Greatest Excess Growth, has channels with some relatively straight sections but their orientations have much less dependence on the outlet location.

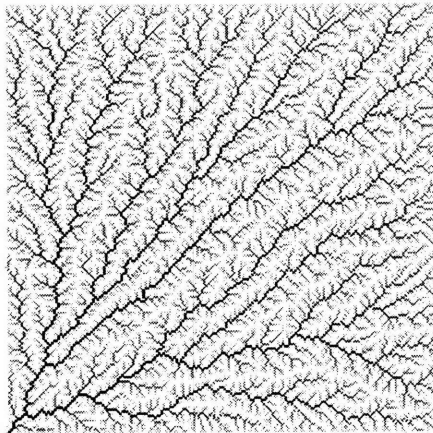
Headward Growth



Simultaneous Growth



Random Growth



Greatest Excess Growth

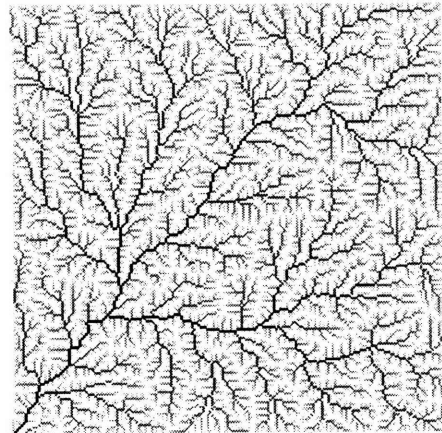


Figure 4-7: Networks developed by the Discrete Event model variants

This observation is confirmed by Figure 4-8 which shows the distribution of drainage directions for points with areas larger than 10 pixels. In this figure, the distance away from the origin indicates the relative number of points with the given drainage direction. The drainage directions are normalized so that 0 degrees always represents a drainage direction pointing directly towards the outlet and 180 degrees indicates a drainage direction pointing directly away from the outlet. Each of the four plots includes the results from several basins developed with the same boundary conditions, but different initial conditions. Clearly, the outlet has a strong influence in determining the orientation of the main channels in the Headward Growth and Simultaneous Growth algorithms. Slightly more variability is observed for the basins eroded by the Random Growth algorithm, and significantly more variability is observed for the Greatest Excess Growth basins.

For comparison, the distribution of drainage directions has been computed for real basins from DEMs (the bottom two plots in Figure 4-8). It is clear that in both cases, the real drainage networks exhibit more variability in the normalized drainage directions than all of the model variants. Real data are most similar to the Greatest Excess Growth variant. Thus, in this regard, the Greatest Excess variant appears to better reflect observations.

Another way to examine the spatial organization of the river network is through the distribution of contributing areas. Figure 4-9 shows the exceedance probabilities of contributing area for the four model variants. As required by observations from real basins, all of the model variants develop distributions which obey a power law although some deviation is exhibited by the Random Growth case. This measure also shows the difference in the role of the boundary conditions. In Headward, Simultaneous, and Random Growth, the boundary conditions exert a strong influence on the distribution. Scaling is certainly not found in the distribution above $A = 1000$. Whereas for Greatest Excess Growth, the scaling continues at larger areas and ends more abruptly.

The scaling exponent also varies among the model variants but the exact values are sensitive to the range used for the regression. Headward Growth gives exponents

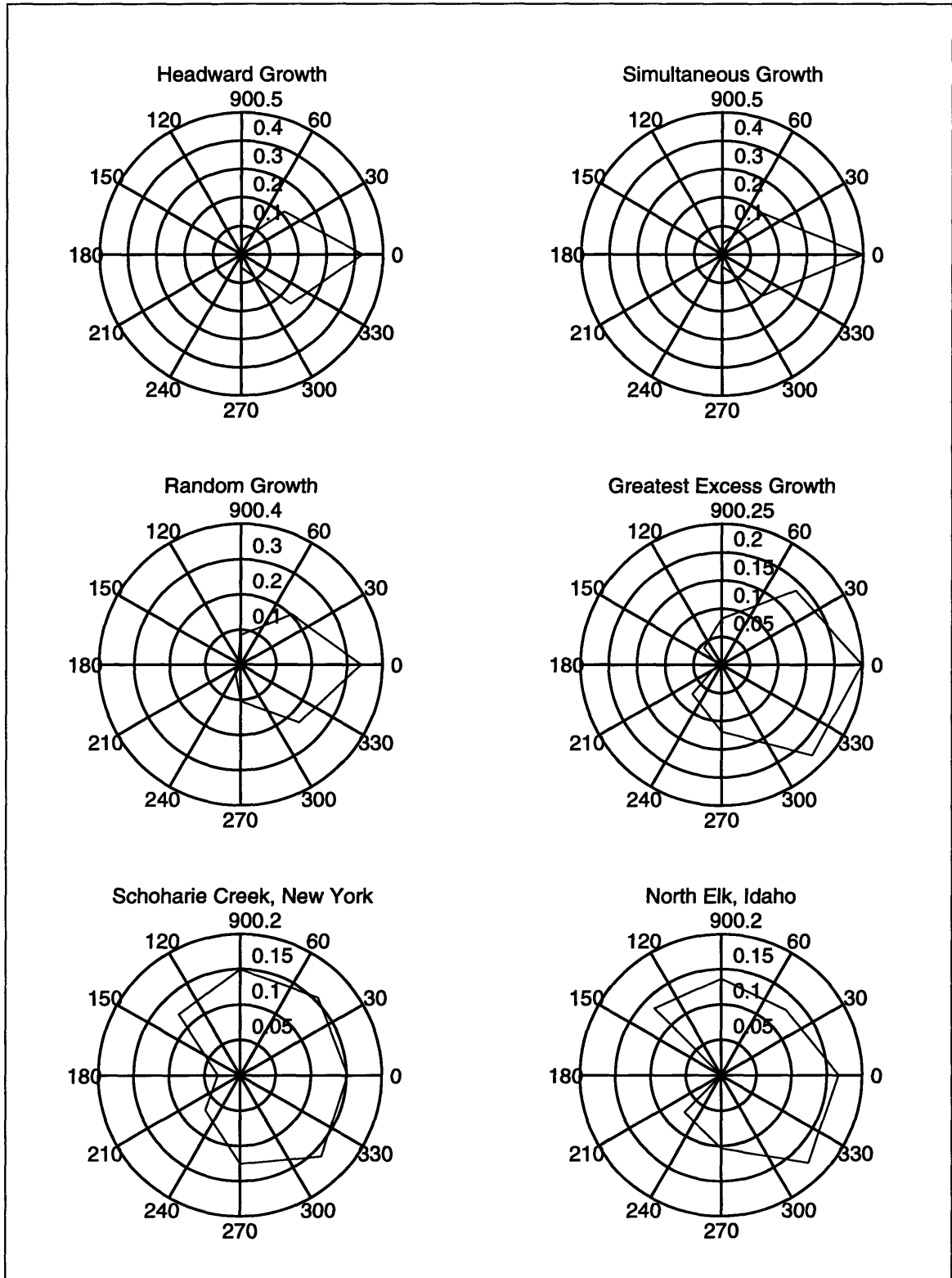


Figure 4-8: Distribution of drainage directions normalized by the outlet direction for a collection of runs of the four model variants

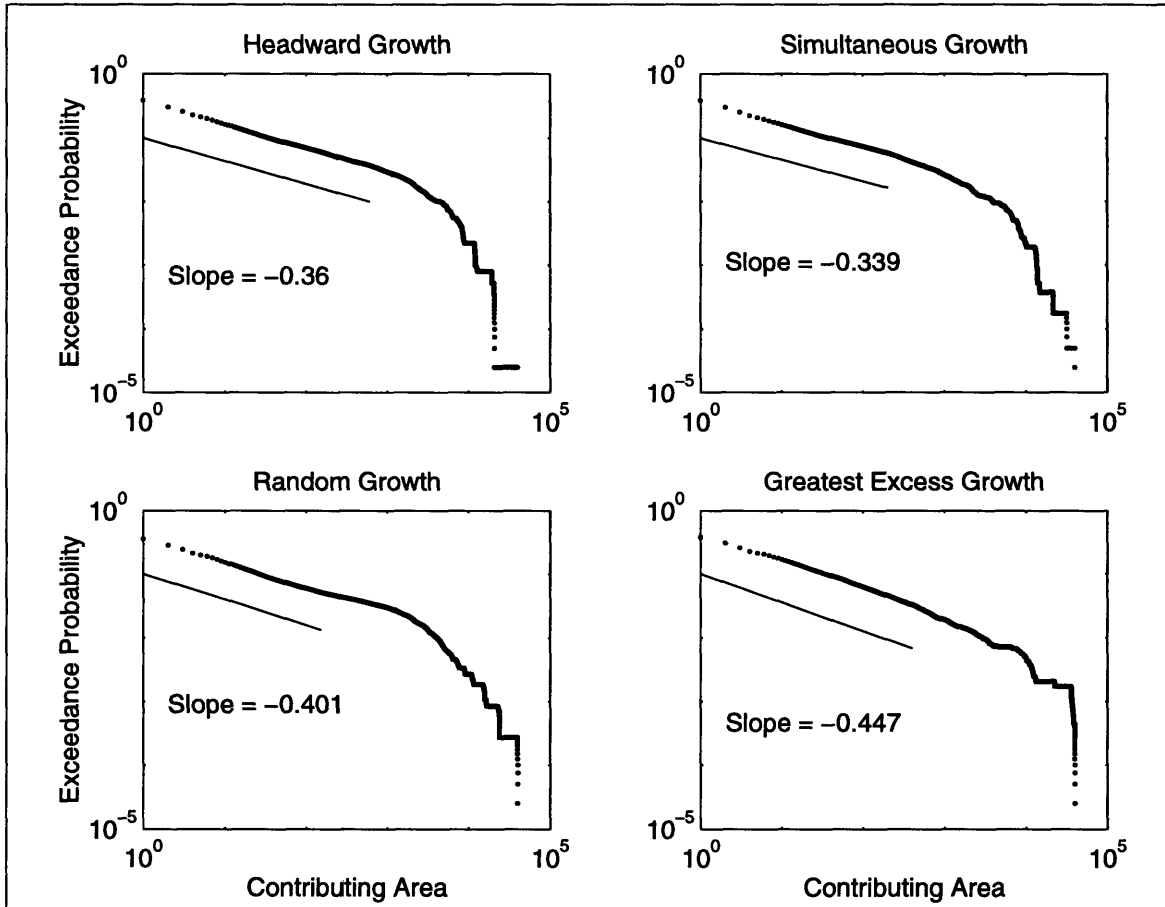


Figure 4-9: Distributions of contributing area for basins developed by the Discrete Event model variants

with values ranging around -0.36 to -0.39 while the Simultaneous Growth gives the lowest values (around -0.33 to -0.37). With Random Growth, a wide range of slopes are observed depending upon the range for the regression. Calculated values can range from -0.33 to -0.41. For Greatest Excess Growth the steepest slopes are consistently observed with values ranging from -0.43 to -0.46. Different values for the exponent indicate different distributions of pixels across the range of contributing areas or alternatively different “rates” of aggregation as one moves down the network towards the outlet. Observations from DEM’s support a slope of -0.43 according to Rodriguez-Iturbe et al. [31]. This gives a second indication of the superiority of the Greatest Excess Growth variant.

Moglen and Bras [27] performed an analysis which provides useful context for the interpretation of Figures 4-8 and 4-9. They investigated the effects of adding spatial heterogeneity into the coefficient of erodability (essentially K in the notation used here). When the degree of variability of K is increased, they observed more tortuous channels which would imply more variability in the distribution of drainage directions. In addition, they found that the slope on the distribution of contributing area becomes more negative when the heterogeneity increased. Since they employed a finite difference approach, their model is quite similar to the Simultaneous Growth variant. So one can safely assume that the introduction of heterogeneity will have similar effects on the distribution of drainage directions and contributing areas here.

Because of their results, one would expect the Greatest Excess Growth variant to display similar characteristics relative to the Simultaneous Growth variant. As shown in the earlier schematic one-dimensional slope profiles, the Greatest Excess Growth variant is more sensitive to the shape or irregularities in the initial slope profile than the other variants. Thus, it is not surprising that it displays characteristics similar to Simultaneous Growth if heterogeneity were introduced.

The width functions also demonstrate differences between the basins developed by the four model variants (see Figure 4-10). In the first three cases, the basins have a similar wedge shaped width function. For the basin developed by the Greatest Excess Growth variant, the width function is much more irregularly shaped.

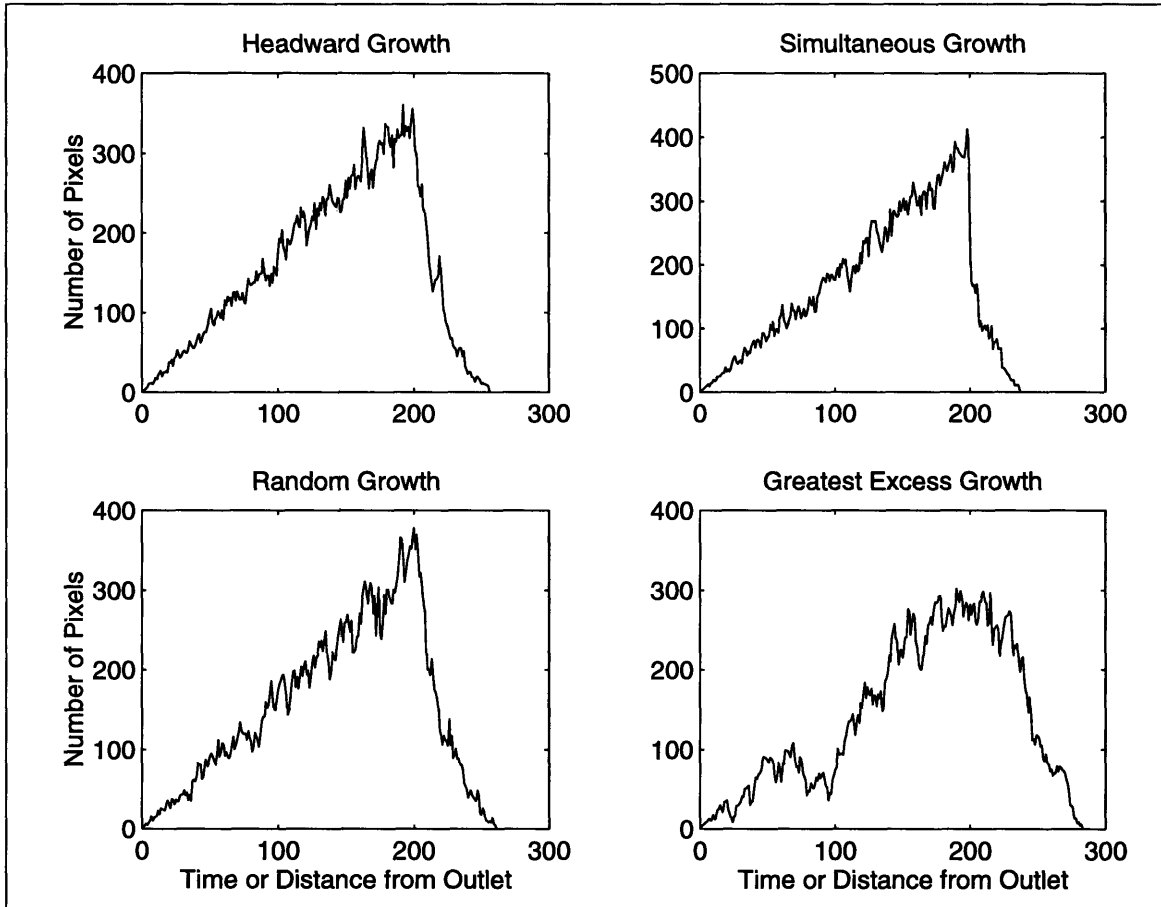


Figure 4-10: Width functions for basins developed by the Discrete Event model variants

The slope-area relationships also demonstrate important differences between the model variants (Figure 4-11). In all cases, one can recognize the upper bound on slope for each contributing area as dictated by the critical shear stress. For the basins developed by the first two variants, a sizable amount of scatter is seen at small contributing areas. In addition, one can see organization in this scatter in the form of strings of points along the same arcs. These strings occur when a long tributary which is nearly at equilibrium loses contributing area at its headwaters. Suddenly, much of the channel is well below the limit of stability. Therefore, these strings indicate the degree to which the internal organization of the basin is achieved when new contributing area is still being captured. For the second two variants, the basin is far less ordered during the extension, and therefore losses in contributing area have a much weaker effect and fewer points are left below the threshold. In reality, significant variability is expected in the threshold itself, thus blurring any such effects in natural slope-area relationships.

Hypsometric curves are also shown for the four basins in Figure 4-12. Notice that the axes are in terms of relative elevation and area, to examine only the shapes of the curves. In this plot, while some small differences can be observed, the four variants develop very similar hypsometry.

Finally, the total energy expenditure [32] is also considered for the four variants. On a 100x100 pixel grid, the energy of the first three variants falls in the range from 40,000 to 43,000, while the fourth variant always expends less energy at about 39,000. For the 200x200 simulations shown in the figures throughout this chapter, the four variants have energy expenditures of: 193000, 191000, 192000, and 176000, respectively. This again shows that the Greatest Excess Growth algorithm expends less energy. It is difficult to determine the relative efficiencies of the first three variants due to significant variability. After fifteen simulations on various sized domains with various boundary conditions, it appears likely that the Random Growth variant generally expends the most energy.

Lower energy expenditure is expected in basins which have confluences located far upstream. In such basins, a few large channels are developed in lieu of a large

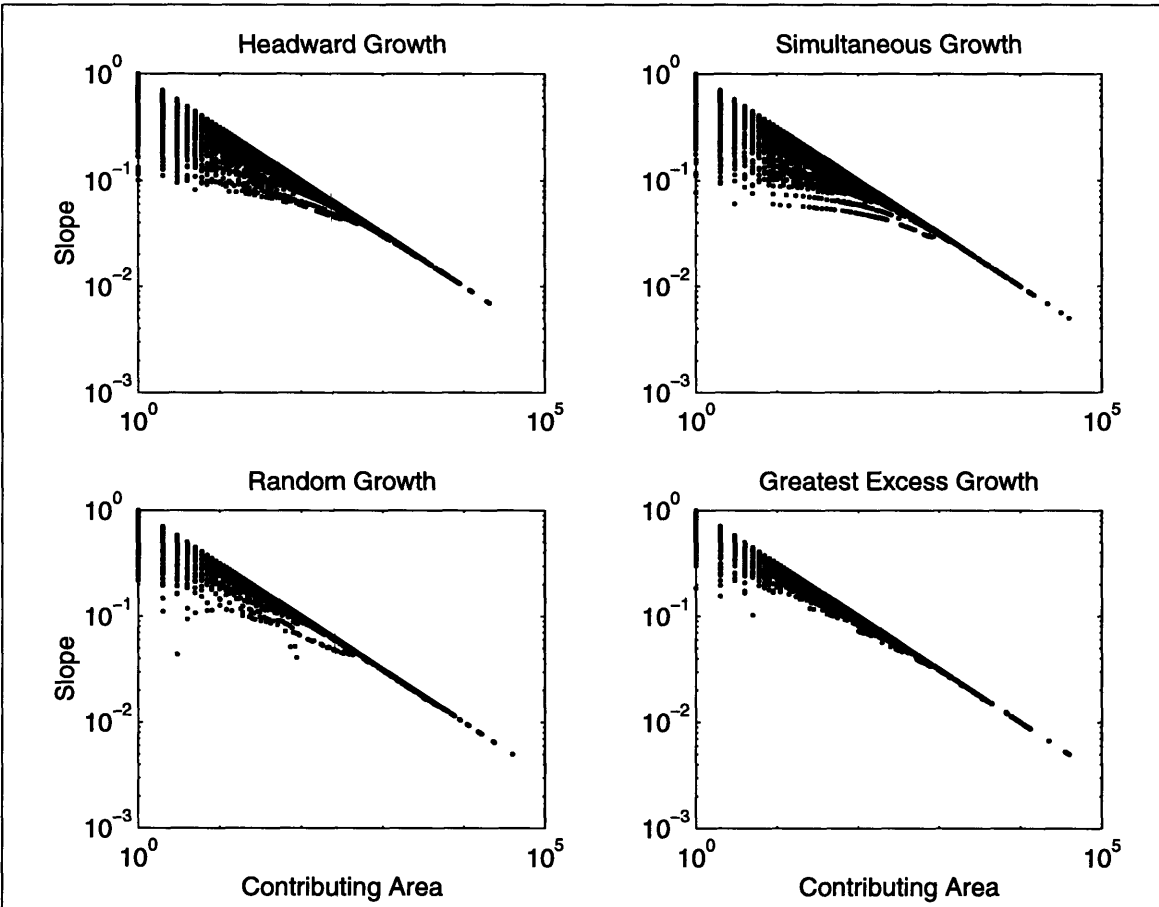


Figure 4-11: Slope-area relationships for basins developed by the Discrete Event model variants

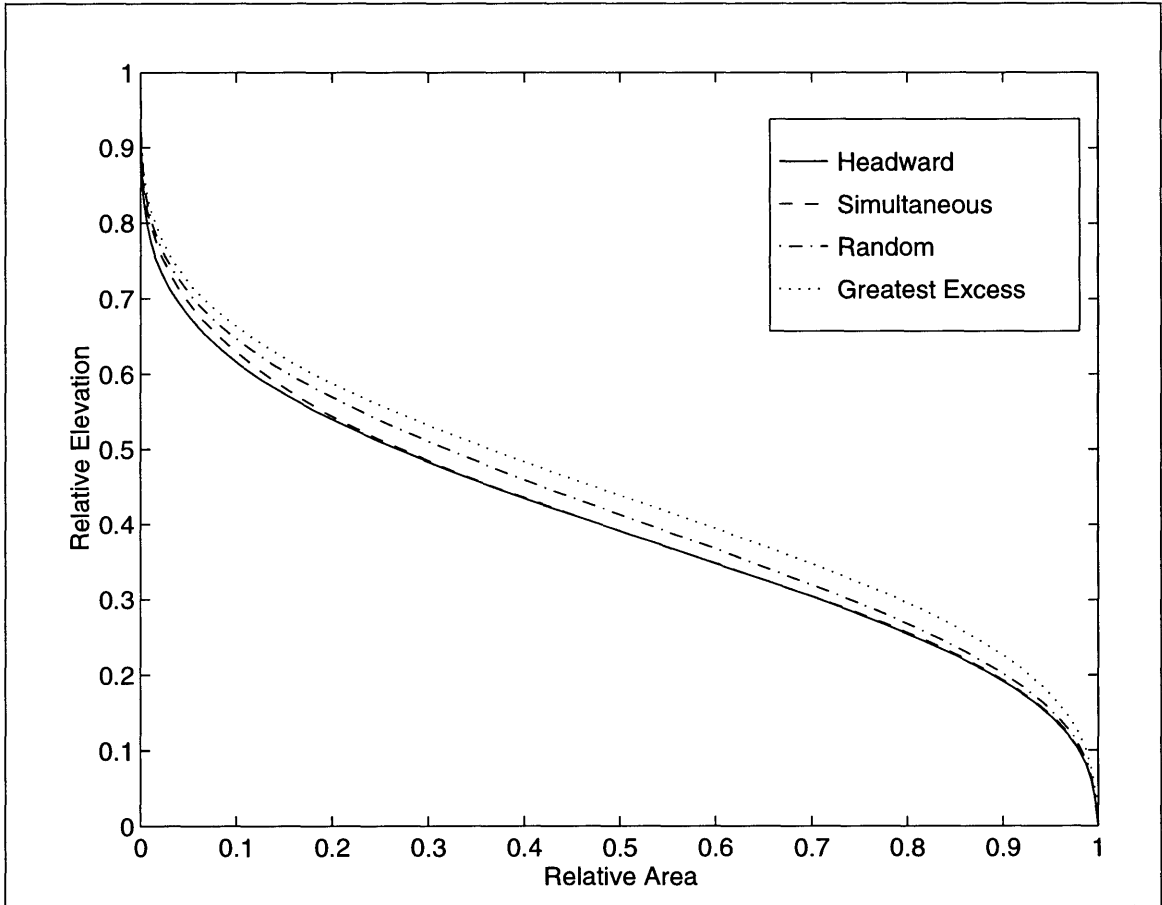


Figure 4-12: Hypsometry for basins developed by variants of the Discrete Event model

number of smaller channels. Since energy expenditure is nonlinear with respect to contributing area, this behavior is preferential. Thus, one can easily confirm the lower energy expenditure in the Greatest Excess Growth variant from the drainage networks shown in Figure 4-7.

In Chapter 3 a comparison was made between the Discrete Event model and the Slope-Area model. In that comparison, both models used the Headward Growth algorithm. It should be noted that while the Headward Growth variant of the Discrete Event Model expends about 41,500 in energy on a 100x100 pixel grid, the Slope-Area model expends about 39,700. Even with the inefficient growth variant, the Slope-Area model is able to achieve energy expenditure levels almost as low as the Greatest Excess Growth algorithm.

4.3 Conclusions

This chapter has performed a comparison between several models of landscape evolution. All of the models attempt to describe the development of a basin through the erosion by bedrock channels. To do so, each model employs a threshold of stability based on shear stress. If shear stress at a point is less than a critical value, no erosion occurs. However, if there is excess shear, the points are eroded to reach stability.

The only difference between the models is in the description of the erosional process and the implied modes of network growth. Two of the model variants, Headward Growth and Simultaneous Growth, erode parts of the basin larger than one pixel in a given iteration. In the Headward Growth variant, erosion events are always triggered at the downstream edge of the unstable region and propagate strictly headward. In the Simultaneous Growth variant, layers of rock are shaved off of the unstable sections at each iteration. Two other variants, Random Growth and Greatest Excess Growth, erode only a single point each iteration. In the Random Growth variant, a random unstable point is selected for erosion, while in the Greatest Excess Growth variant, the most unstable point is selected.

Some differences arise in the basin morphology depending on the mode of network

growth. In particular, the first three variants behave relatively similarly while the Greatest Excess Growth variant is quite unique. The first three variants all tend to develop channels oriented toward the outlet, although the degree of smaller scale irregularity differs between these variants. In contrast, the Greatest Excess Growth variant exhibits more freedom from the boundary conditions, developing more irregularly oriented channels and further upstream confluences. Such a network structure also results in lower energy expenditures.

This analysis also provides an interesting caveat to the work of Moglen and Bras [27]. Because the Simultaneous Growth variant without heterogeneity fails to reproduce the empirical distribution of drainage directions and the distribution of contributing area, one must consider how these observed characteristics arise. From the analysis of Moglen and Bras, one might interpret them as the result of naturally occurring heterogeneity. However, this analysis offers another explanation. It suggests that the discrepancies may arise from insufficient sensitivity of the model to variability in the surface elevations (i.e. inaccuracy in the mode of network growth). In order to address this question, the actual variability in erodabilities should be observed and compared with that required by a finite difference approach to achieve the observed basin characteristics. Aside from this question, both analyses emphasize the importance that variability in some form has in shaping river basins.

Chapter 5

A Comparison of Stability and Dynamic Equilibrium

A spectrum of conceptual models have been proposed in the literature to describe the process of landscape evolution under the effects of tectonic uplift and denudational processes. At one extreme, Davis [7] suggested that regions are first rapidly uplifted and then denuded by surface processes over much longer time scales. From this view, topography progresses through stages of development with young topography marked by large relief and old topography approaching a peneplain. Alternatively, Hack [12] proposed that all parts of the landscape adjust to one another forming a condition of equilibrium. His general notion has since been extended to the quantitative idea of *dynamic equilibrium* where the influx of material from tectonic uplift is balanced at all points by the removal of material by erosion. The models of Davis and Hack can be considered as end-members since in the former, uplift occurs at time scales much shorter than denudation, while in the latter the two processes share similar time scales. These conceptual models have also been investigated in a more quantitative framework by Kooi and Beaumont [21]. They have shown that the qualitative behavior of these extremes can be achieved by the same erosion model if the uplift rate is varied from a rapidly (or initially) uplifted tectonic structure to a gradual rate of tectonic uplift.

In the previous two chapters, a set of models of landscape evolution were presented

that follow the Davisian perspective. In all of these model variants, no uplift is included during the lifetime of the erosion. Instead, instability arises from an initially uplifted plane with a local baselevel supplied by specified outlets. Erosion then occurs until all points have shear stresses lower than a critical value. Eventually, the basin reaches a stationary state—henceforth termed *stability*—in which all points are stable and no erosion occurs. Clearly, this set of models is more similar to the qualitative perspective of Davis because the process of tectonic uplift is assumed to be completed before the period of erosional activity. However, a peneplain is never reached because the critical shear stress is non-zero.

This chapter examines the differences between basins evolving towards dynamic equilibrium and stability. In particular, it attempts to identify differences both in the modes of network growth and in the resulting basin structures. To accomplish this, Section 5.1 adds simple tectonic uplift to the Simultaneous Growth variant introduced in the previous chapter. In Section 5.2, a simple experiment with flat initial conditions and uniform uplift is used to examine the basin structure as critical shear and uplift rates are varied. Section 5.3 considers how sloping initial topography may affect network growth and basin characteristics for both stability and dynamic equilibrium. Finally, in Section 5.4, some general comments regarding these comparisons are made.

5.1 Uplift in the Discrete Event Model

Depending on which variant of the Discrete Event model is used, one requires different descriptions of tectonic uplift. Because the Simultaneous Growth variant departs from truly discrete erosion events and describes erosion as a rate, an uplift rate may also be incorporated directly into the model algorithm. For the other three model variants described above, uplift must take a different form. This section considers the addition of uplift in the Simultaneous Growth variant.

In Chapter 4, the Simultaneous Growth variant of the Discrete Event model was

shown to be the finite difference approximation to the equation:

$$\frac{\partial z}{\partial t} = \begin{cases} k_1 (\tau_{cr} - KA^m S), & \text{if } KA^m S > \tau_{cr} \\ 0 & \text{otherwise} \end{cases} \quad (5.1)$$

In this framework, the addition of a tectonic uplift rate U is quite simple since one can write directly that:

$$\frac{\partial z}{\partial t} = \begin{cases} U + k_1 (\tau_{cr} - KA^m S) & \text{if } KA^m S > \tau_{cr} \\ U & \text{otherwise} \end{cases} \quad (5.2)$$

For simplicity, all of the following simulations will assume that uplift is spatially uniform throughout the region and temporally invariant. In addition, no flexural isostasy is considered. Algorithmically, the above equations imply that the elevation of all points (except those of outlets or other specified baselevels) are affected by the uplift term in this equation, whereas only those points with excess shear are eroded. Thus, at any given iteration the elevations of points are set by one of the following two expressions:

$$z_{i,j}^{new} = \begin{cases} \Delta t U + W_{i,j} \left(z_{i,j}^{down} + \frac{\Delta l_{i,j} \tau_{cr}}{K} A_{i,j}^{-m} \right) + (1 - W_{i,j}) z_{i,j} & \text{if } \tau_{i,j} > \tau_{cr} \\ z_{i,j} + \Delta t U & \text{otherwise} \end{cases} \quad (5.3)$$

where:

$$\tau_{i,j} = KA_{i,j}^m \frac{z_{i,j} - z_{i,j}^{down}}{\Delta l_{i,j}}, \quad (5.4)$$

and:

$$W_{i,j} = \frac{K k_1 \Delta t}{\Delta l_{i,j}} A_{i,j}^m. \quad (5.5)$$

Note that the time step Δt was already introduced through the selection of W in Chapter 3 so that no additional parameters have been introduced here. However, as τ_{cr} becomes small, smaller time steps are required for stable numerical simulations. This simple model will be used throughout the remainder of this chapter.

Aside from the Simultaneous Growth variant described above, the Discrete Event

model cannot be written in terms of an erosion rate. Instead, erosion is the culmination of many discrete events which makes the introduction of a continuously acting uplift rate problematic.

One possibility for the introduction of uplift in the other variants is to consider it as arriving in discrete events as well. Beginning with Equation 3.1 and following a similar derivation as the one presented in Chapter 3, one can arrive at the Slope-Area model where the “uplift” parameter presented earlier includes both the critical shear stress and the actual uplift rate. However, this description of uplift is not pursued here, because its dynamics seem unrealistic. While rapid or even discrete erosion events may approximate processes such as plucking, the abrupt uplifting of locations seems a poor representation of the natural processes.

5.2 Flat Initial Conditions

Consider the following experiment. Three regions begin with a flat surface that includes enough variability in elevation to define drainage directions. The material of the first region has substantial cohesive strength, implying a significant critical shear stress, and this region has initially been uplifted above the local baselevel. The second region has weaker substrate, and experiences a gentle uplift rate through time. In the third region, there is no critical shear stress, but a significant tectonic uplift rate occurs. Will the morphology of the basins developed under these three conditions differ?

Each of these three cases may achieve a stationary condition where $\partial z/\partial t = 0$. In the first case, this state is stability and implies that all points have shear stresses below the critical value. From Equation 5.2, a slope-area relationship can be written from this condition:

$$S = \frac{\tau_{cr}}{K} A^{-m} \quad (5.6)$$

In this case, as was shown in Chapter 3, some locations may lie well below this upper bound on slope due to reorganizations of the network. At the other extreme is the third region where stationarity occurs when the uplift at every point exactly balances

the erosion. The corresponding slope-area relationship is:

$$S = \frac{U}{k_1 K} A^{-m} \quad (5.7)$$

which must be enforced exactly. In the second case, points must exceed the critical shear to balance the uplift rate which implies:

$$S = \frac{U/k_1 + \tau_{cr}}{K} A^{-m}. \quad (5.8)$$

As is obvious from the three slope-area relationships above, the values of τ_{cr} , U , K , and k_1 will all influence the vertical scale of the topography. However, if one selects parameters such as $\tau_{cr} = 0.01$ and $U = 0$, $\tau_{cr} = 0.005$ and $U = 0.005$, and $\tau_{cr} = 0$ and $U = 0.01$ for the three regions, respectively (with $k_1 = 1$ and $K = 0.01$ in all cases), one would expect the same slope-area relationship to be enforced but for different reasons. This is the case examined here.

Figure 5-1 shows the topography developed under these three conditions. At first glance, these three cases appear quite similar. In all the cases, one observes a strong tendency for the channels to be oriented towards the outlet. However, as the uplift rate becomes larger, there is a tendency for the topography to develop larger ridges. This observation stems from the fact that these river networks tend to develop fewer but larger main channels. This also translates into lower energy expenditures for these basins. For these three examples, energy expenditures are 42,100, 40,900, and 40,100, respectively, and basin magnitudes are 6246, 6196, and 6149, respectively.

One may intuitively understand the lower energy achieved for the dynamic equilibrium case by the following argument. In the case where the region is initially uplifted, the escarpment is enormous, especially when near the outlet. With such steep slopes, the growing network is immediately able to dominate the existing drainage directions to capture all of the nearby area. This allows the initiation of a large number of channels with their orientations towards the outlet. As the escarpment proceeds further upstream, it decreases in size since the elevation of its base increases. In the second case, the escarpment begins relatively small, implying much smaller slopes. In this

case, the variability of contributing areas among the adjacent points will have more influence in determining where the channels begin to grow. As time passes, the uplift rate continues feeding the growth of these channels. Thus, the initial variability plays a stronger role in determining the aggregation pattern which allows confluences to occur further upstream.

The slope-area relationships for each of the three cases are shown in Figure 5-2. As this figure shows, both the second and third cases exactly enforce their slope-area relationships. For the second case, which includes a non-zero critical shear, this implies that any point which lies below its critical slope is slowly raised relative to its neighbors (because only its neighbors are experiencing erosion). Only when the shear stress exceeds the critical value does this initially stable point begin to erode, and only when their erosion rate matches the uplift does it maintain its elevation.

Hack's Law also differs among the three cases. Figure 5-3 shows Hack's Law as measured with a constant ruler length for the three basins shown in Figure 5-1. While all values are above 0.5, lower values of Hack's exponent are observed for basins with lower critical shear and stronger uplift rates. This indicates either lower sinuosity or less elongated basins at large scales for these cases. Although it is unclear exactly how these different values arise, the higher values may indicate a departure from self-similarity brought upon by the form of the retreating escarpment. As this escarpment retreats towards portions of the basin with smaller contributing areas (i.e. smaller scales), it becomes substantially smaller. Since scale independence implies identical behavior at all scales, one may hypothesize that the retreat of this escarpment causes differing conditions of evolution at different scales.

In addition, the distribution of drainage directions indicates a systematic change in the basin structure (Figure 5-4). For the case without uplift, over 45 percent of the channels with contributing area greater than 10 pixels are oriented directly towards the outlet. For the case with zero critical shear, about 36 percent are oriented towards the outlet. This result is expected given the interpretation of the previous figures (i.e. a less dominant escarpment in the latter case).

Overall, one sees fairly similar basins for these three cases, but small, consistent

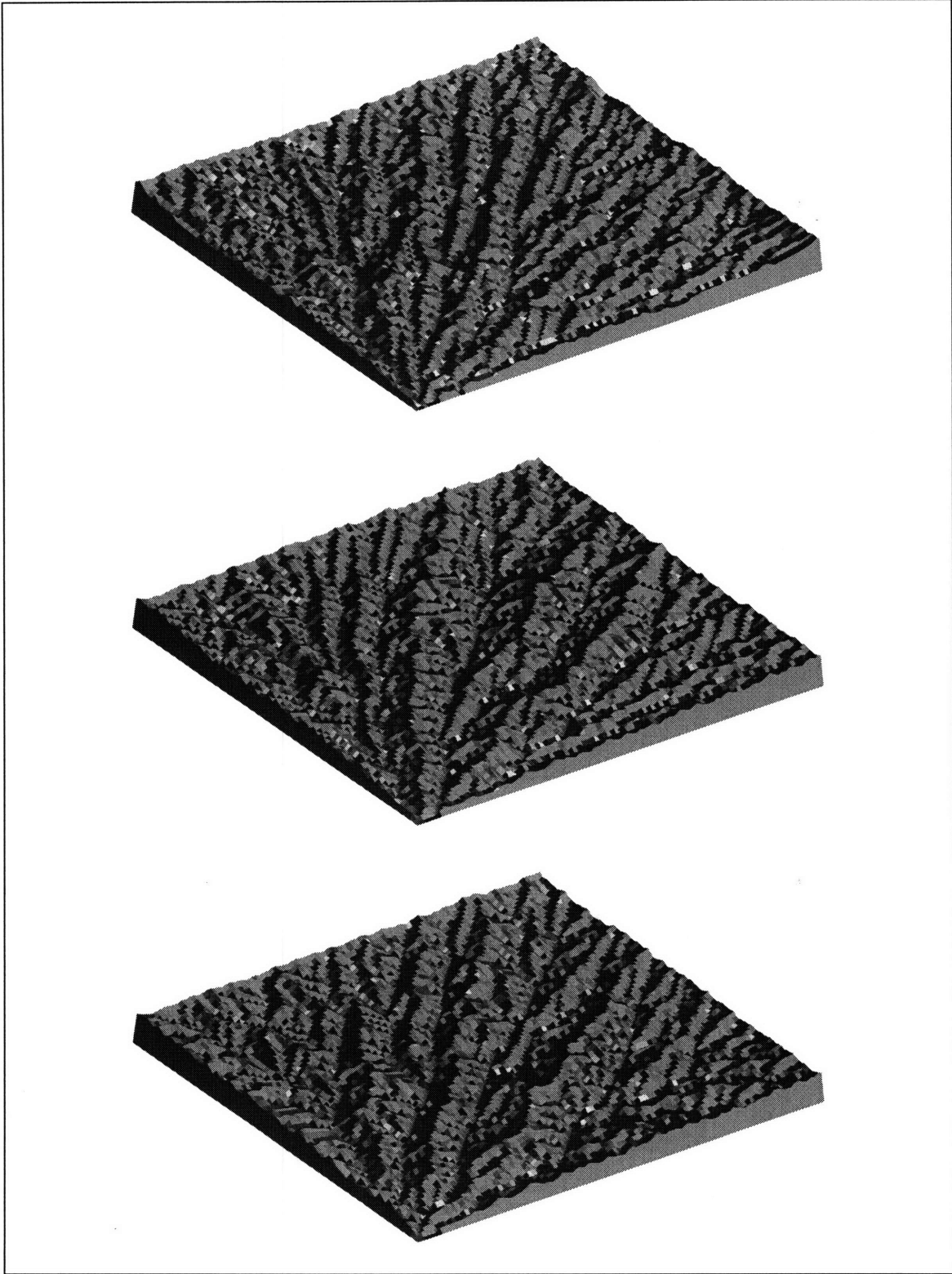


Figure 5-1: Topography generated by the Discrete Event model with (a) $\tau_{cr} = 0.01$, $U = 0$, and $K = 0.01$, (b) $\tau_{cr} = 0.005$, $U = 0.005$, and $K = 0.01$, and (c) $\tau_{cr} = 0$, $U = 0.01$, and $K = 0.01$.

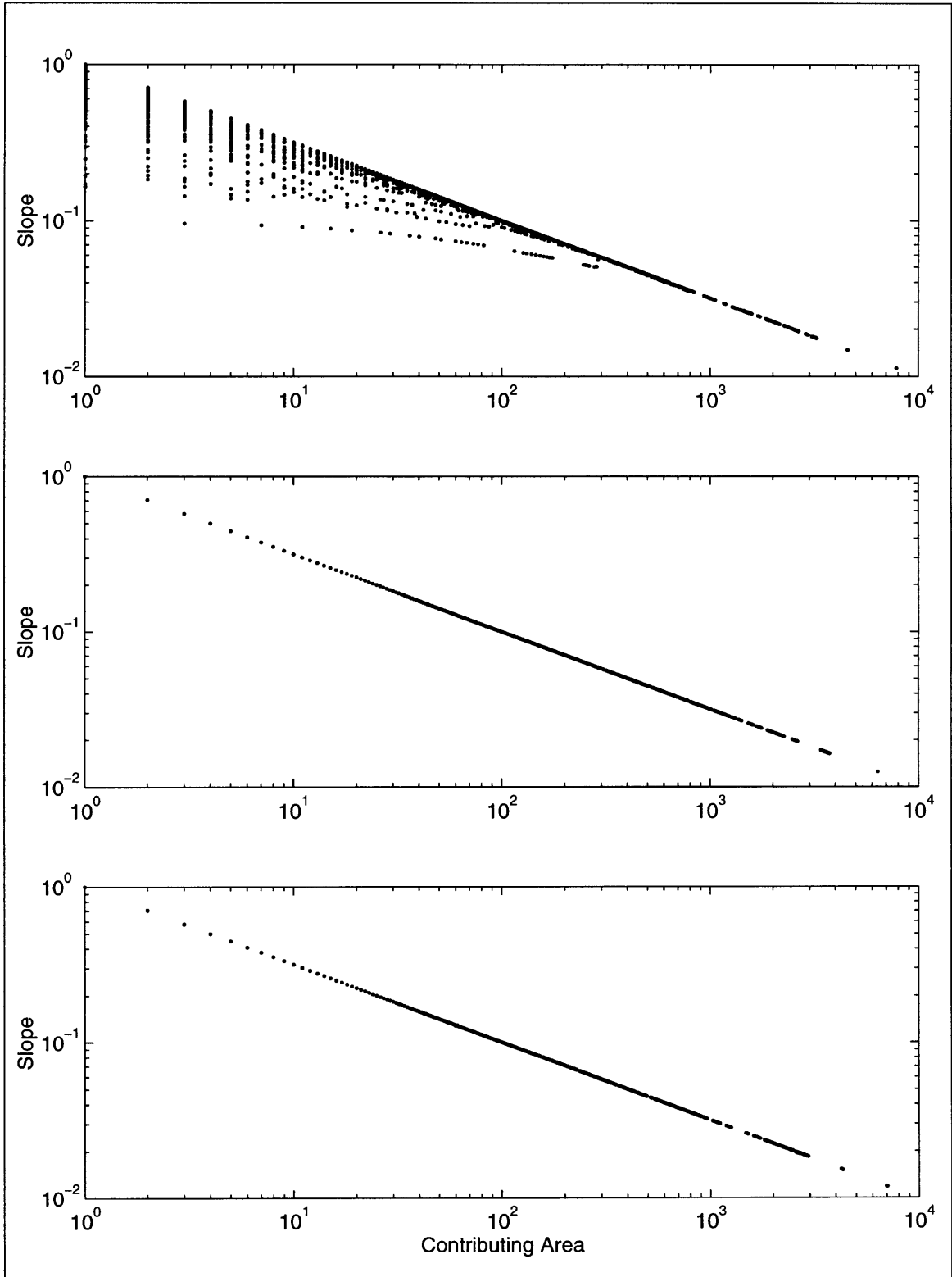


Figure 5-2: Slope Area relations for stationary topographies generated with (a) $\tau_{cr} = 0.01$, $U = 0$, and $K = 0.01$, (b) $\tau_{cr} = 0.005$, $U = 0.005$, and $K = 0.01$, and (c) $\tau_{cr} = 0$, $U = 0.01$, and $K = 0.01$.

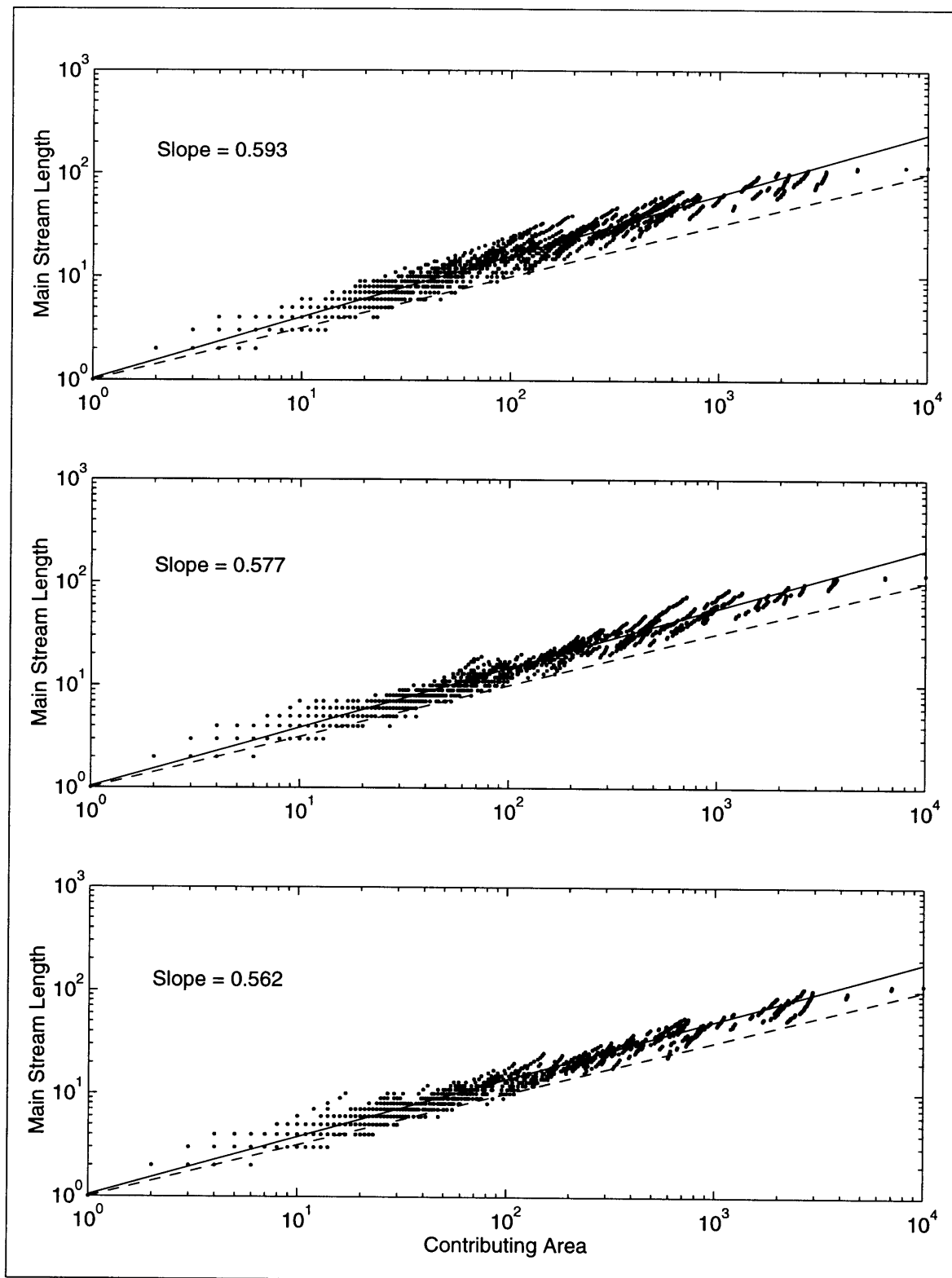


Figure 5-3: Hack's Law for stationary topographies generated with (a) $\tau_{cr} = 0.01$, $U = 0$, and $K = 0.01$, (b) $\tau_{cr} = 0.005$, $U = 0.005$, and $K = 0.01$, and (c) $\tau_{cr} = 0$, $U = 0.01$, and $K = 0.01$. Solid line shows regressions, and dashed lines show slope of $1/2$.

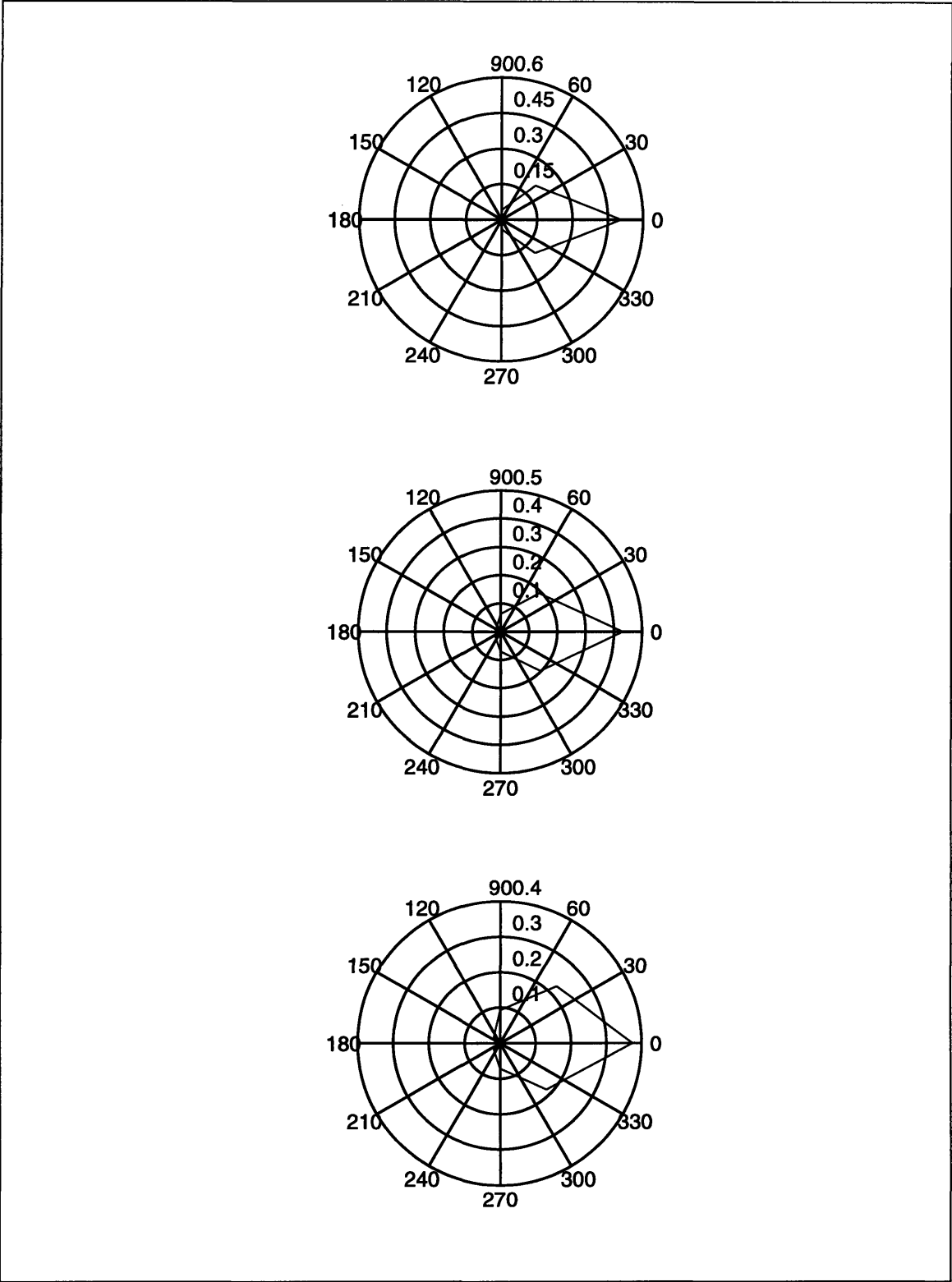


Figure 5-4: Distribution of drainage directions for basins generated with (a) $\tau_{cr} = 0.01$, $U = 0$, and $K = 0.01$, (b) $\tau_{cr} = 0.005$, $U = 0.005$, and $K = 0.01$, and (c) $\tau_{cr} = 0$, $U = 0.01$, and $K = 0.01$.

trends in the basin morphology can be identified which demonstrate differences in the evolutionary dynamics. In the next section, experiments are conducted that test the behavior of landscapes with either non-zero critical shear or non-zero uplift with sloping initial conditions.

5.3 Escarpment Retreat and Sloping Antecedent Conditions

This section examines the behavior of basins approaching stability and dynamic equilibrium under two initial conditions. In one case, the initial topography slopes gently towards one edge of the simulation domain which is held at baselevel. In the other case, the initial topography slopes gently away from the baselevel.

These experiments have particular relevance to escarpment retreat. Numerous authors [35, 48, 38] have observed that escarpments take on different forms depending on the orientation of the plateau drainage. When the water flows away from the escarpment edge so that the crest forms a drainage divide, the escarpment has an abrupt elevation change across it (probably indicating backwearing). When the plateau slope is oriented towards the escarpment, the channels deeply incise across the escarpment face resulting in more downwearing than backwearing. Seidl et al. [38] refer to these forms as drainage divide and gorge-like escarpments, respectively.

Similar escarpment forms have been simulated with landscape evolution models. Kooi and Beaumont [21], for example, have shown that these two forms occur when the orientation of the initial surface is changed. However, they do not examine the network structures developed under these two conditions. This section examines the characteristics of the river networks for these two cases and investigates whether similar escarpment retreat occurs for landscapes with non-zero critical shear stress.

This experiment includes four cases. In the first two cases, uplift occurs abruptly before any denudation occurs to create an initial escarpment along one edge of the domain. In both of these cases, the critical shear is nonzero, and the topography

develops towards stability. These two differ only in the orientation of the initial topography. In the first case, it is oriented towards the escarpment, while in the latter case, it is oriented away from the edge. The initial surfaces include a small amount of noise which is sufficient to define drainage directions, but does not dominate the trend in slope.

The second two cases are the corresponding ones for erosion without a critical shear but with a non-zero uplift rate. For these simulations, no escarpment is initially specified, but over time, the domain is uplifted while the baselevel is held fixed. Here again, the orientation of the initial surface is either towards or away from the specified baselevel (for the third and fourth cases, respectively), and the randomness in the initial elevations is relatively small. In all four cases, the parameters are selected so that the final slope-area relationships have the same coefficients and exponents.

5.3.1 Modes of Escarpment Retreat and Network Growth

Figure 5-5 shows snapshots during the evolution in order to examine differences in the mode of escarpment retreat between the four cases. Without an uplift rate (Cases 1 and 2), the orientation has little effect on the mode of escarpment retreat although slightly more irregularity of the escarpment crest is exhibited when the plateau slopes downward toward the escarpment edge (Case 1). In contrast, some clear sensitivity is observed when a gradual uplift rate is occurring (Cases 3 and 4). This difference arises because the plateau elevations are stable in the first two cases due to the non-zero critical shear. Thus, no development of river networks occurs until the escarpment reaches each point. In Cases 3 and 4, these points are susceptible to erosion at all times. Thus, organized drainage networks immediately begin to form. When the surface is oriented towards the escarpment (Case 3), the channels flow over the crest and quickly begin to incise. No obvious escarpment crest is formed, instead something resembling Seild et al.'s "gorge-like" escarpment is created. Alternatively, when the channels flow in the opposite direction (Case 4), the escarpment retreats as the drainage basins at its toe capture additional area. Notice that the plateau drainage networks (i.e. those above the escarpment) have larger channel networks and

a much greater vertical scale in Case 3 than Case 4 because the networks experience the relative lowering of their baselevel only in the former case.

The modes of channel network growth in Cases 3 and 4 are distinct from one another and from those discussed in Chapter 4. Figure 5-6 shows six snapshots during the growth of a channel network on a 100x100 pixel grid corresponding to Case 3. The first plot shows the network for the initial condition. Before erosion begins, the drainage directions display a tendency to flow towards the specified baselevel, although a significant number of pits are present. There are also many cases where the flow converges into some “channels” that continue for five or ten pixels. By the second snapshot, nearly all of the discharge is carried out of the simulation domain. In addition, well formed drainage divides have been established. The uplift over this short period of time is sufficient to allow the development of a well connected drainage pattern. It should also be noted that the main channels found at this stage remain virtually unchanged for the remainder of the simulation even though the relief will continue to increase. Over the next several snapshots, substantial reorganization does occur at the smaller scales. Eventually many of the channels initially oriented towards the imposed baselevel will be replaced by the growth of small channels oriented perpendicular to the main channels.

This style of growth seems to be most similar to Horton’s conceptual model. Unlike the cases considered in the previous chapter, reorganization of the channel network plays a key role here. As Horton envisaged, almost immediately, roughly parallel channels form in the downslope direction. Then over time, a few of these channels dominate and begin to capture the others. However, unlike Horton’s idea of cross-grading of the minor channels, often several completely new channels are formed to replace a single long channel.

It must also be acknowledged that this mode of growth also resembles Glock’s conceptual model. The main channels extend first followed by the development of the minor tributaries. However, a branching pattern that completely drains the region is formed by the second snapshot. The later development of the minor tributaries therefore seems most consistent with the Hortonian model of reorganization.

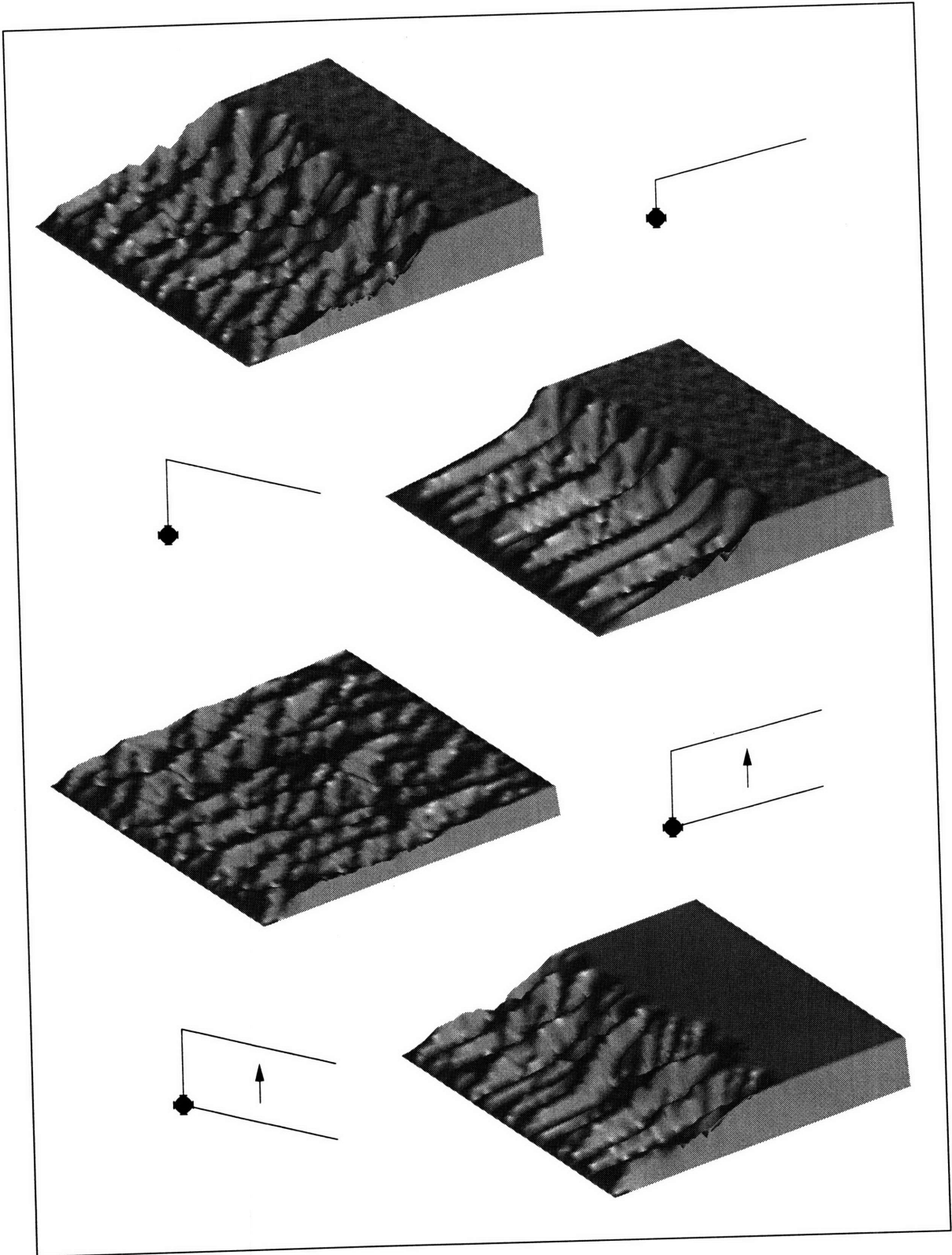


Figure 5-5: Snapshots during the evolution for the four cases where (a) and (b) include a non-zero critical shear and (c) and (d) include a positive uplift. (a) and (c) have initial surfaces sloping towards the baselevel whereas (b) and (d) have initial surfaces sloping away from the baselevel

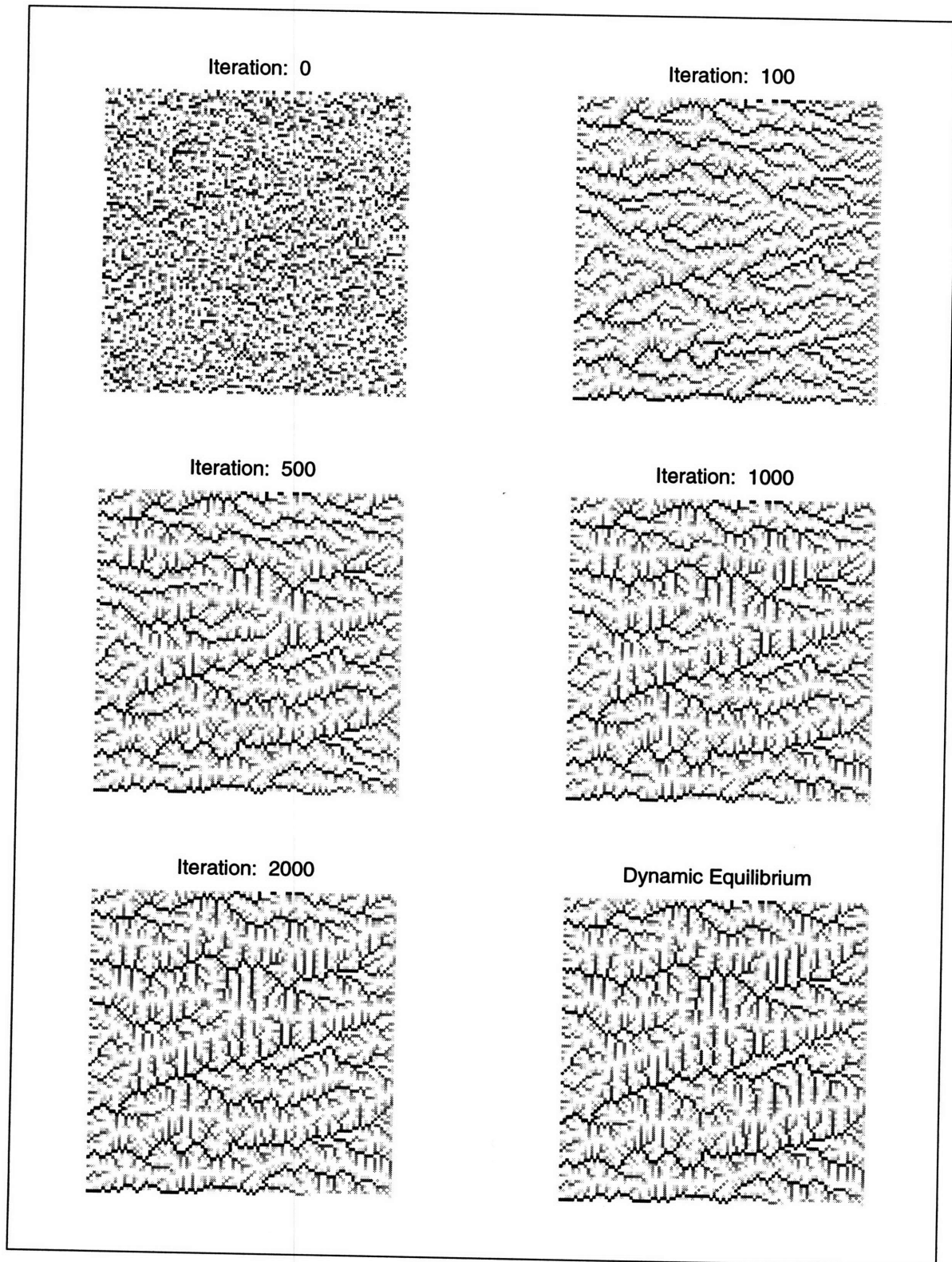


Figure 5-6: Snapshots during the growth of the channels networks for Case 3

Figure 5-7 shows the development of a channel network on a 100x100 pixel grid for Case 4. Here, reorganization of the network is less important than in Case 3. Once the region has been fully captured by the growing channel networks (Iteration 800), there is relatively little readjustment in the structure (compare with Figure 5-6). Instead, the mode of network growth is primarily headward.

The networks growing from the specified baselevel are strongly influenced by the location of the older plateau channel locations—even though they flow in opposite directions. Particularly, one can see from the snapshots that the growing main channels tend to follow pre-existing valleys whereas many of the minor tributaries cut new valleys. Notice also the change in the network structure near the specified baselevel. This change probably occurs because the plateau channel networks did not have sufficient time to develop in this location before being captured.

These results are consistent with field and laboratory data. In laboratory studies reported by Schumm [37], the mode of network growth was found to depend on the slope of the initial conditions when the basin outlet was being lowered. These modeling results additionally show that the slope of the initial surface plays a significant role in the mode of network growth when the critical shear is small relative to the initial irregularity of the surface.

5.3.2 Stationary Basin Forms

Figure 5-8 compares the drainage networks corresponding to the stationary states of each of the four cases when simulated on a 100x100 pixel grid. For both cases in which the slope is oriented towards the escarpment (Cases 1 and 3), fairly natural looking, irregular networks are formed. As expected from the previous sections, Case 1 develops small scale channels that are more oriented towards the outlets than Case 3. When the slope is oriented away from the escarpment (Cases 2 and 4), some breakdown in the scaling behavior is seen. For Case 2, very straight, regular channels progress headward only occasionally bifurcating. For comparison, fifth order streams are often achieved in Case 1, while in Case 2, streams are usually limited to third order. Some departure from scaling behavior is also observed in Case 4 near the boundary

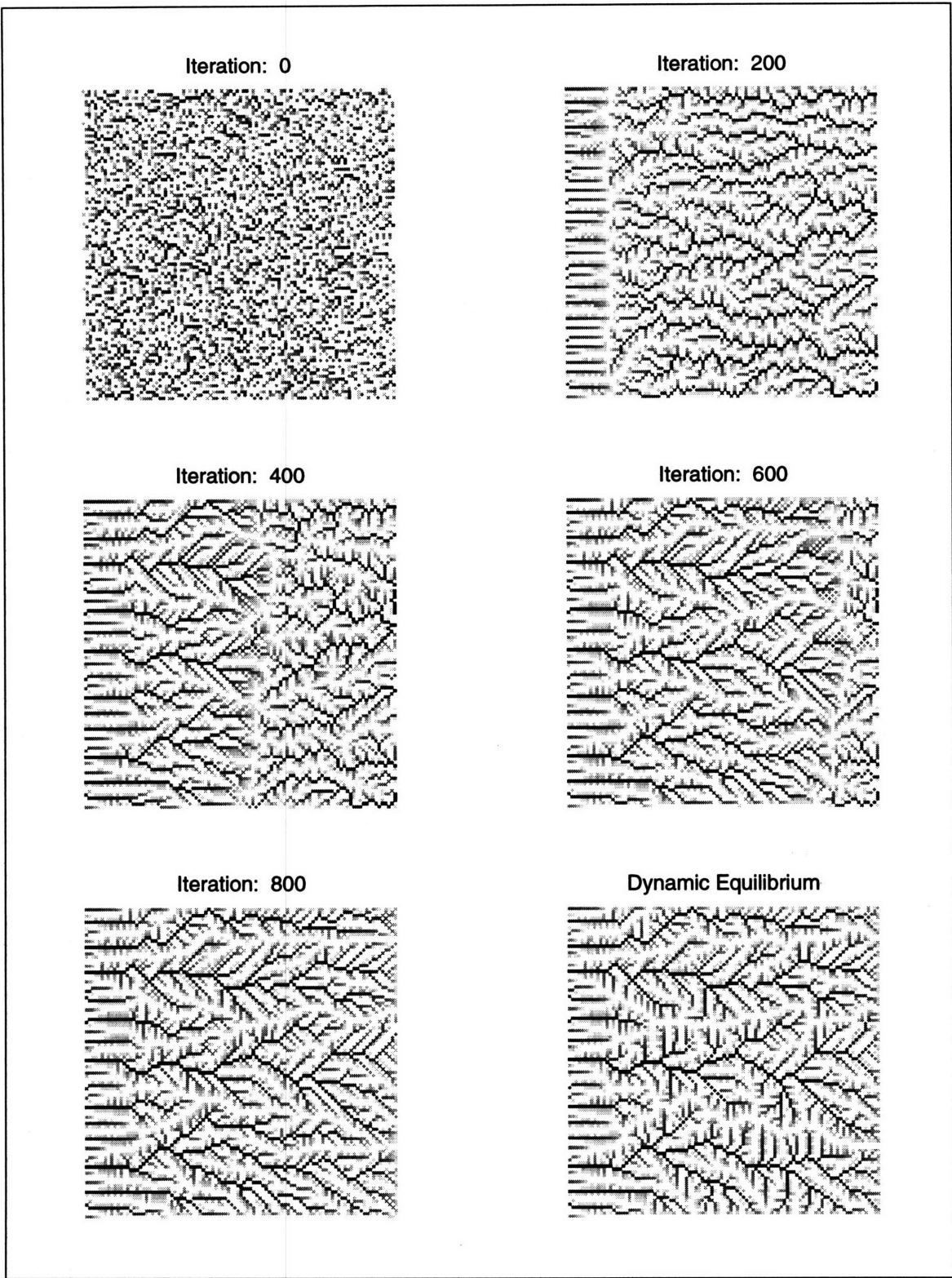


Figure 5-7: Snapshots during the growth of the channels networks for Case 4

condition. However, as shown by the snapshots of the network growth in Figure 5-7, the lack of a critical shear allows significant development of the plateau drainage networks which helps the networks growing from the baselevel to at least approach self-similarity (further examination of the scaling characteristics of the basins will be considered below).

The difference between the networks of Cases 1 and 2 can be traced to the way in which they grow. In either case, small and very disorganized drainage networks quickly form based on the randomness on the original surface (there is no erosion). Because many of the flow directions point towards the baselevel in Case 1, the points along the escarpment edge will have differing contributing areas, and therefore different erosion rates. Alternatively, when the plateau is oriented away from the escarpment crest, the flow directions are consistently oriented away from the edge causing no local convergence of flow for incision. The network growth will therefore be controlled by the internal drainage structure since the initial elevations also have very little randomness associated with them. Thus, few obstacles lie in the way of the headward progression of the channels. If, for instance, the magnitude of randomness in the initial elevations was increased, much greater irregularity would be observed in the network structure. A similar argument applies for Cases 3 and 4. In natural conditions, variability in rock type in addition to antecedent elevations will of course be present. However, these cases provide useful insight into the dependence of the morphology of river basins on the initial and boundary conditions.

In the remaining figures in this section, the largest basins developed by each of the four cases (see Figure 5-8) are analyzed. Figure 5-9 shows the distribution of contributing areas for the four basins. According to the figure, Cases 1, 3, and 4 are better able to achieve power law scaling than Case 2. Exponents determined from regression are: -0.38 to -0.43 for Case 1, -0.37 to -0.44 for Case 3, and -0.46 for Case 4 (where the ranges result from various selections for the range of the regression). In the second case, scaling is restricted to very small contributing areas (exponent of -0.43).

This difficulty in upholding the power law scaling is also visible in Hack's law

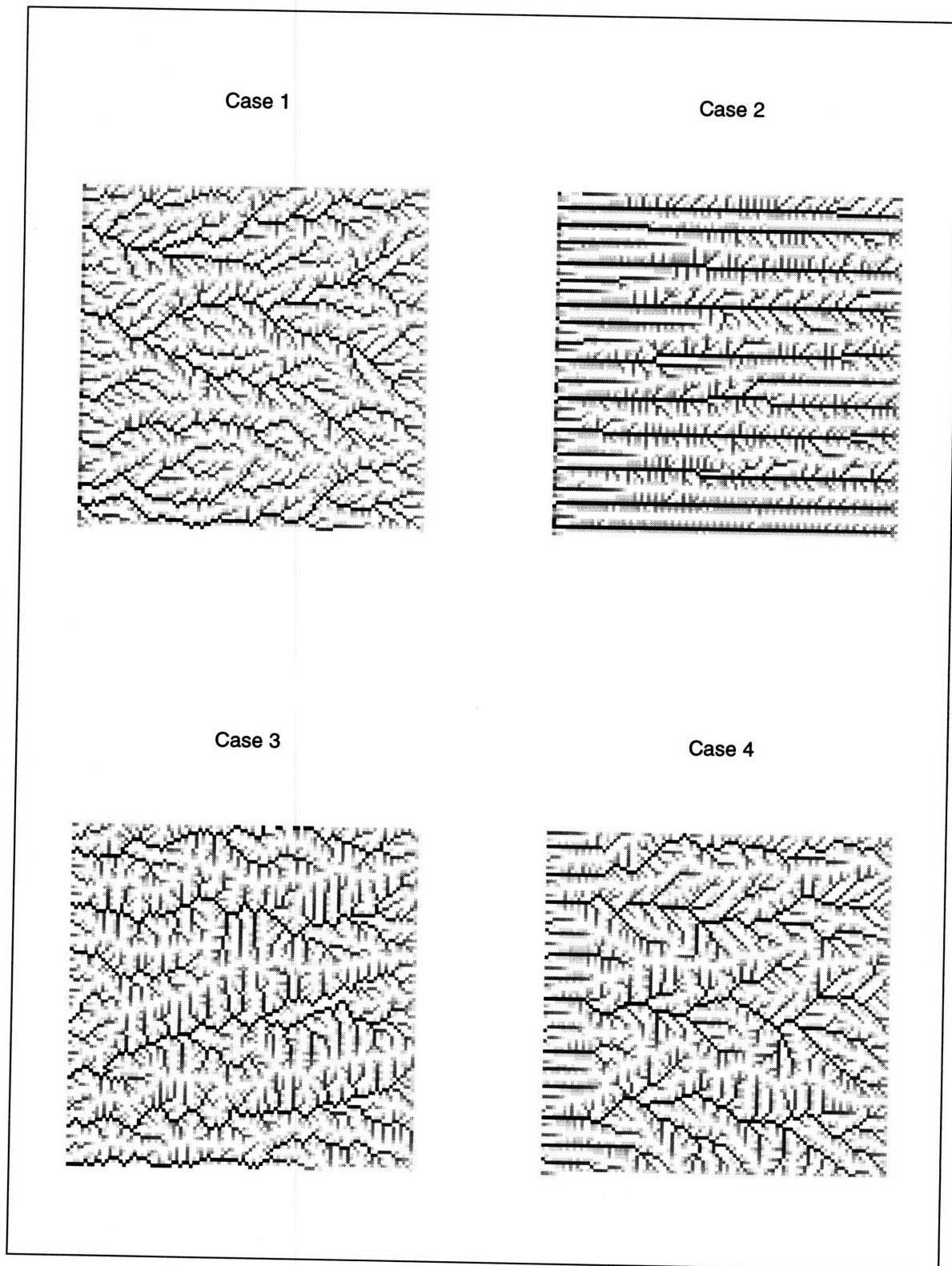


Figure 5-8: Networks developed by the Discrete Event model where (a) and (b) include a non-zero critical shear and (c) and (d) include a positive uplift. (a) and (c) have initial surfaces sloping towards the baselevel whereas (b) and (d) have initial surfaces sloping away from the baselevel

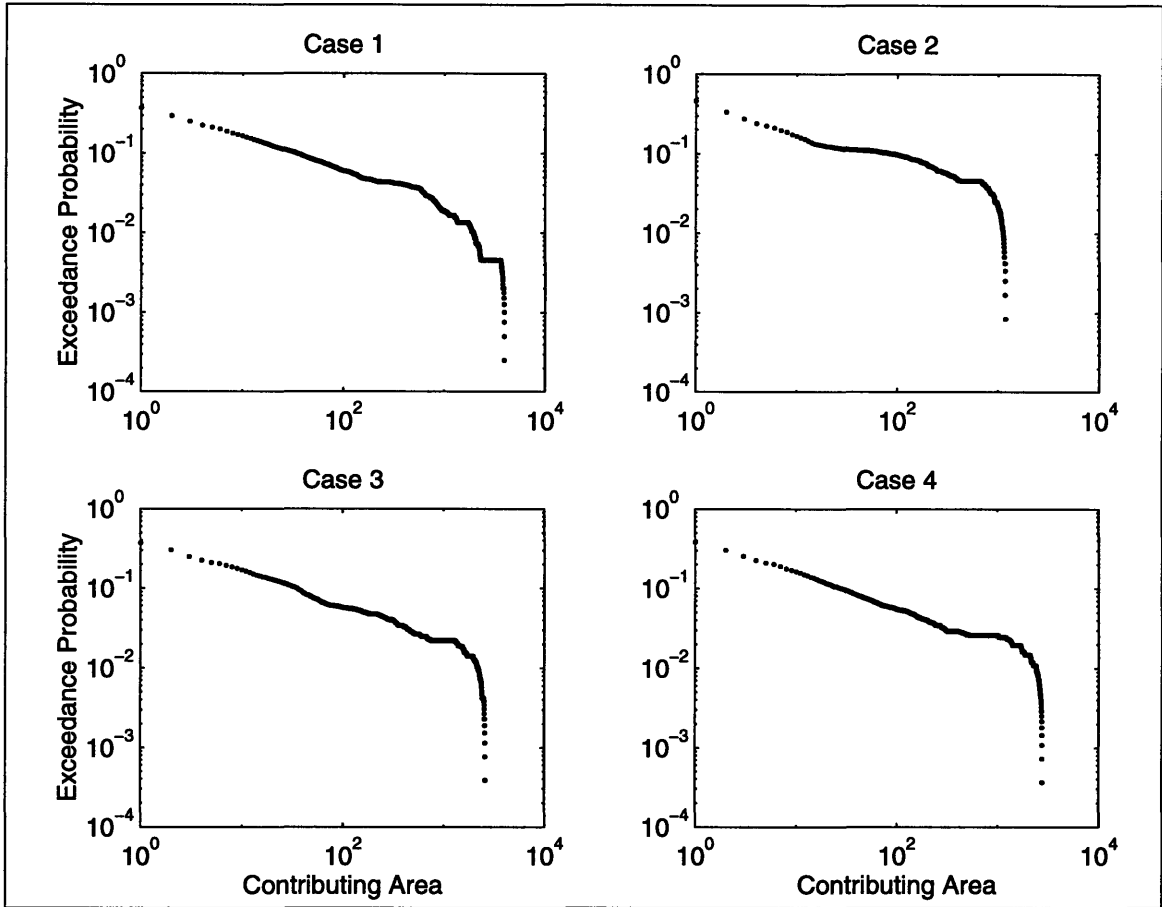


Figure 5-9: Distribution of contributing areas for the four cases

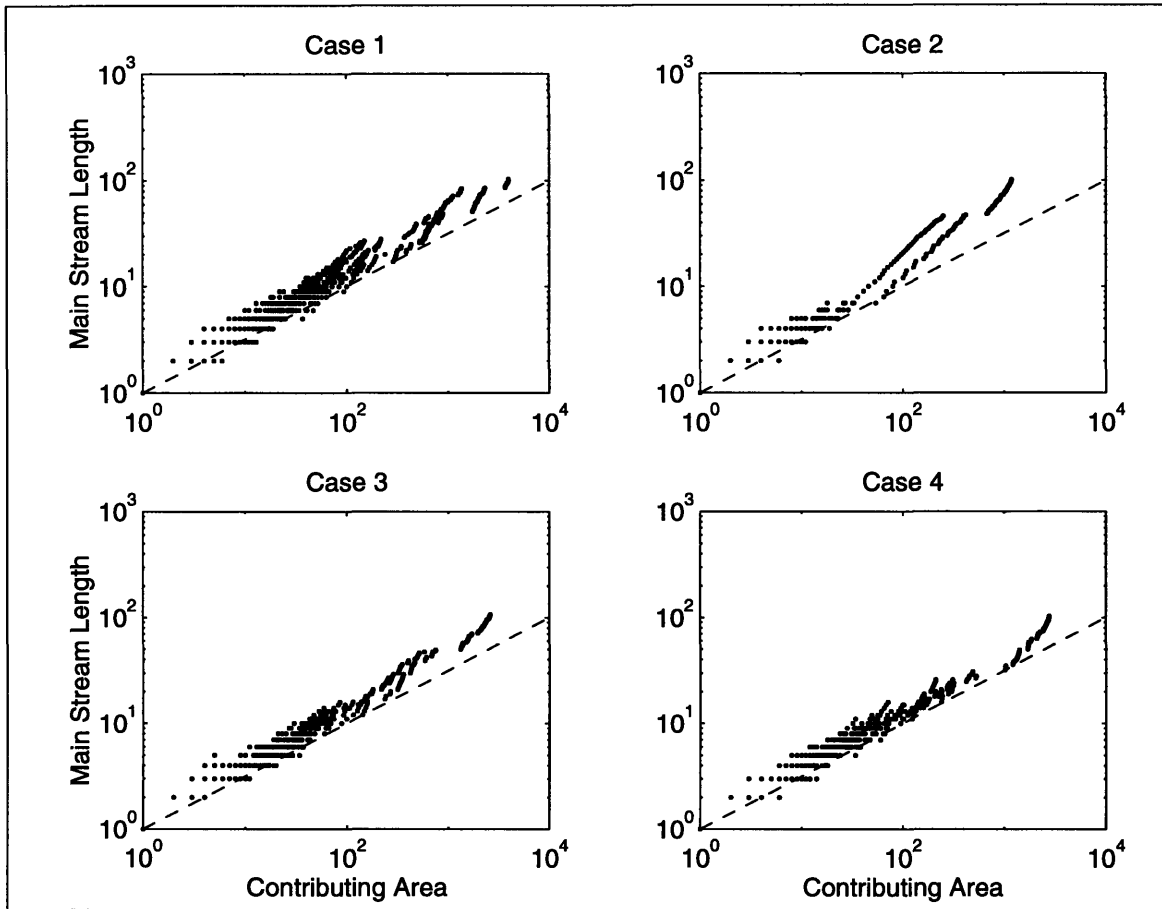


Figure 5-10: Hack's Law for the four cases

(Figure 5-10) which demonstrates some upward curvature for Case 2. The excessively steep slope at high contributing areas stems from the obvious strings of points which have slopes around one. These strings of points correspond to the long main channels shown in Figure 5-8. Cases 1 and 3 both have slopes around 0.575 whereas Case 4 has a lower slope—around 0.555. In Case 4, the breakdown in scaling shown in Figure 5-8 is also visible at high contributing areas where the slope increases noticeably.

Of course, one also sees a strong difference in the distribution of drainage directions (Figure 5-11). For Case 2, nearly 70 percent of the drainage directions point directly towards the outlet, compared to about 42 percent for Case 1. In Cases 3 and 4 one sees the greatest diversity of normalized drainage directions as well as some significant asymmetry in the distribution which is closely linked to the asymmetries of the basin shapes.

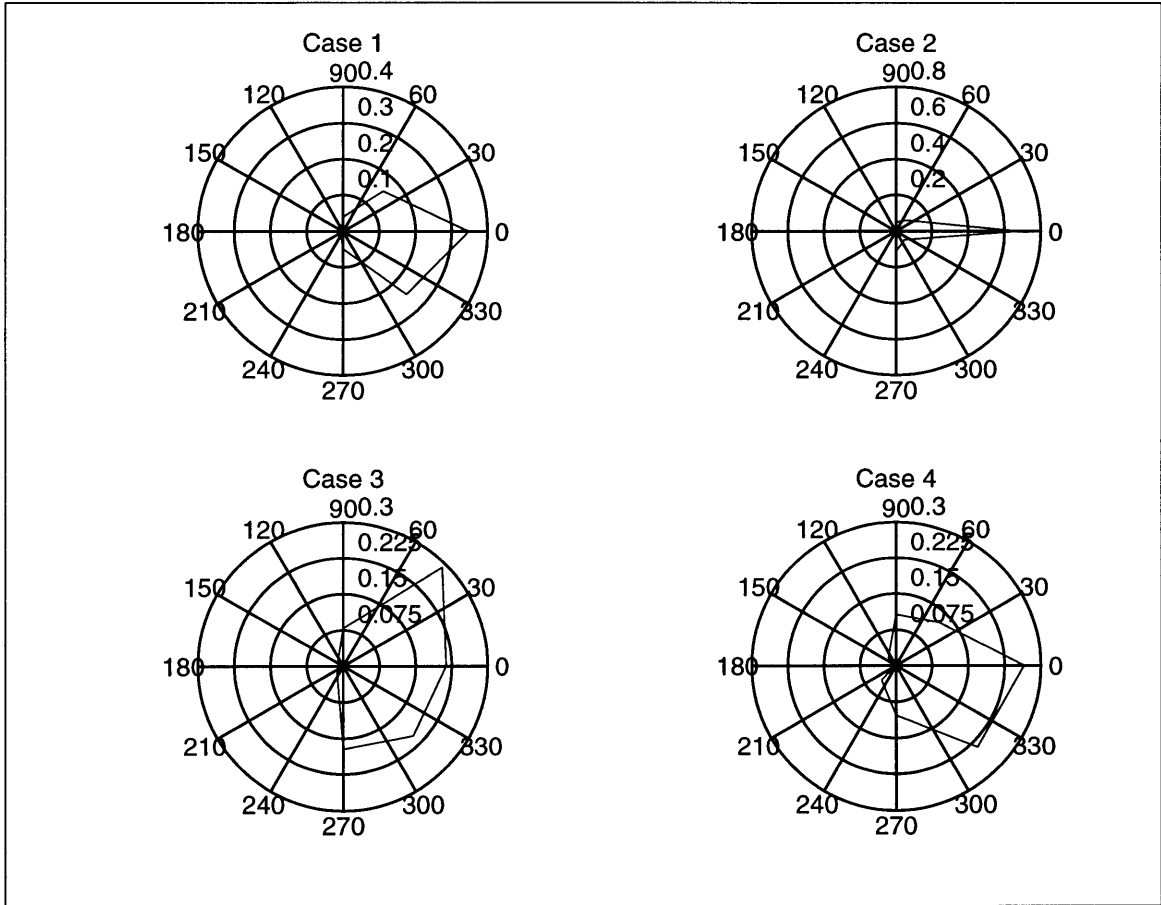


Figure 5-11: Distribution of drainage directions for the four cases

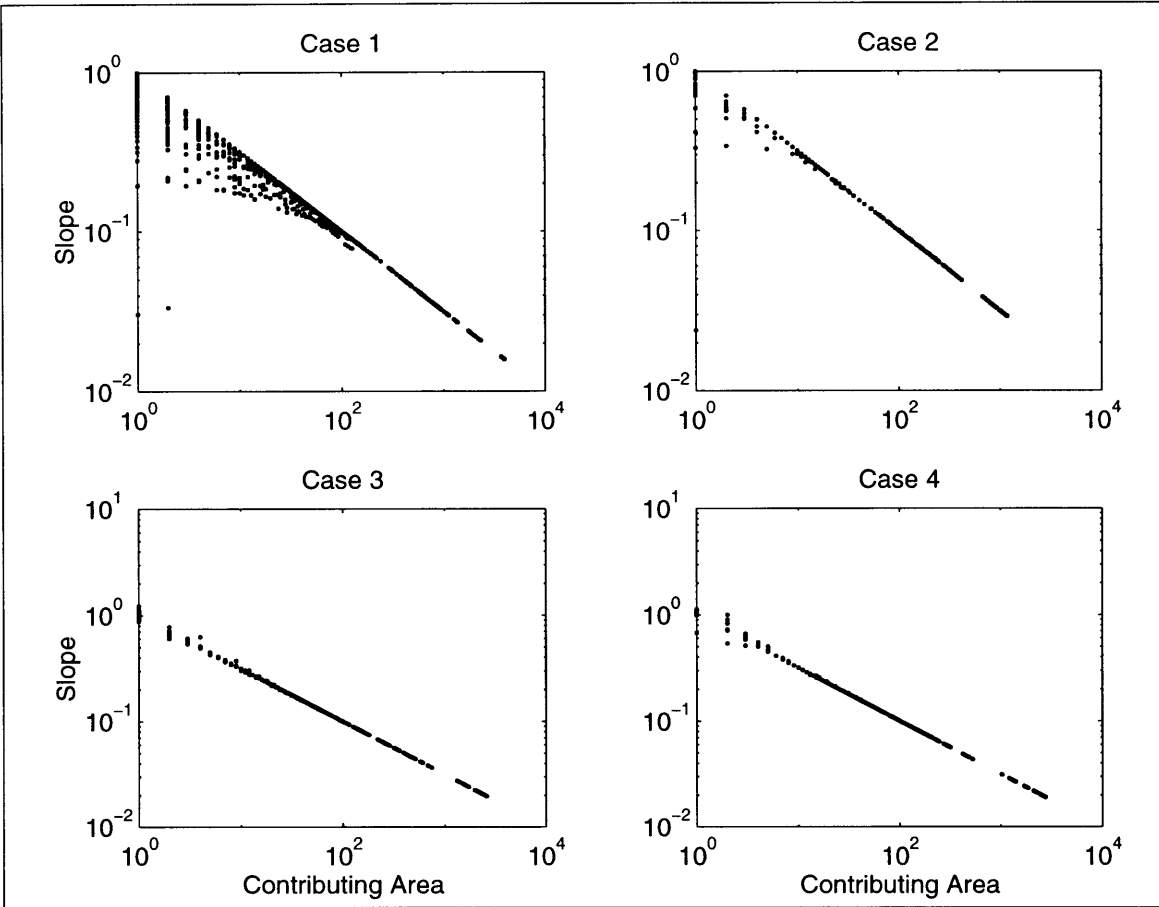


Figure 5-12: Slope-area relationships for the four cases

The slope-area relationships also differ between the four cases (Figure 5-12). In Case 2, very few points lie below the enforced slope-area relationship indicating very little readjustment in the network structure compared with Case 1. Cases 3 and 4 enforce the slope-area relationship exactly because an uplift rate is included.

5.4 Summary

This chapter has examined the differences between the condition of stability and dynamic equilibrium under sloping and flat initial conditions. For flat initial conditions with an outlet specified in the corner of the simulation domain, some small but consistent trends were identified in the equilibrium basin configurations. The results indicate that the topography with a gradual uplift rate tends to develop channel

network structures with slightly lower energy and fewer but larger main channels.

The mode of growth and equilibrium basin morphology was also analyzed for sloping initial conditions, the mode of network development was found to depend on both the direction of the slope and whether there is gradual uplift or a non-zero critical shear. When there is a non-zero critical shear, the channel networks develop mainly by a form of headward growth. However, when the initial surface slopes towards the specified baselevel and the critical shear is zero, the organization of the equilibrium network develops partly under the reorganization of an initial structure.

The scaling of the basin was also found to depend on the initial conditions. When the initial surface slopes away from the specified baselevel and the critical shear is large with respect to the initial noise in the surface, there is a break-down in the scaling of the channel networks. The scaling behavior is also affected when the critical shear is zero and the surface is gradually uplifted, but only near the baselevel boundary condition.

This chapter only considers a few special cases in an area of research which offers many directions for study. Further study could investigate more systematically the conditions under which the boundary and initial conditions affect the scaling behavior of the basin structure. In addition, the extent to which different network characteristics develop in nature depending on the boundary and initial conditions also remains an important question.

Chapter 6

Influences of Storm Duration

One of the fundamental principles of geomorphology is that the characteristics of topography reflect the processes which have shaped it. Glacial, aeolian, and fluvial action all develop identifiable traits in the landscape which allow geomorphologists to understand the history of the topography. Similarly, the intensity or character of these processes is also expected to result in differences in the evolving landscape.

Considering fluvial erosion, the effectiveness of this process is controlled in part by the total precipitation received in a region. Since deserts receive much less precipitation than humid regions, fluvial processes will be weaker in these regions. However, the surface erodability may also be higher in arid regions through the secondary effect of sparse vegetation. Thus, while the amount of precipitation may vary in a clear manner from region to region, the role of precipitation is not simple.

The character of precipitation events also varies significantly between regions and may affect the erosion process. For example, two regions may receive nearly equivalent amounts of precipitation, but one may receive it evenly throughout the year, while another may receive nearly all precipitation in a short period. Or considering shorter time scales, one region may receive most of its precipitation from short and intense convective storms, while another receives more precipitation from large frontal systems. Such differences will directly affect landscape evolution through the runoff generation mechanisms and the hydrologic response of the basin. They may also indirectly affect the geomorphology through the resulting vegetation and soil moisture

conditions.

Unfortunately, the implications of hydrologic differences are often masked by the complexity of natural topography. Very rarely can two regions be found which share the same lithology and history while varying only in their hydrology. Thus, the quantification of these impacts has yet eluded geomorphologists, and the representation of hydrology in most landscape evolution models remains very simple.

In this chapter, a standard landscape evolution model is adapted to consider two extreme cases of storm duration. In one case, precipitation events are long or even perpetual, while in the other, they are instantaneous pulses. The resulting models are examined to determine how the storm duration might affect the resulting topography. In the following section, a general framework is presented which describes discharge as the result of storm hydrographs. Then, the use of contributing area as representative of stream flow rate is shown to be appropriate for prolonged precipitation events in Section 6.2. Section 6.3 develops the other end-member case, in which precipitation events are instantaneous. The following two sections (Sections 6.4 and 6.5) discuss the implementation of these cases in the discrete event framework and the implications for basin morphology.

6.1 General Framework

Topography develops under the competition of uplift and degradational processes like fluvial erosion and diffusive hillslope processes. Unfortunately, all of these processes have high variability in both space and time which makes truly physical modeling impractical (especially over the spatial and temporal scales of landscape evolution). Despite this variability, remarkable success has been achieved in simulating landscape evolution using temporally averaged processes. Under weathering-limited conditions and neglecting hillslope processes, one can write the commonly used equation as:

$$\overline{\frac{\partial z}{\partial t}} = \bar{U} - \bar{E} \quad (6.1)$$

where z is the elevation at a point, t is time, U is uplift, E is erosion rate, and the bars indicate averaging over a period of the simulation (e.g. one time step in a numerical simulation). This equation implies that the average change in elevation during some short interval is the difference between the average uplift and average erosion during that period. Since diffusive processes have been neglected, this relation applies only where topography is fluvially dominated.

The average erosion rate in Equation 6.1 must be determined from a description of instantaneous erosion. For detachment-limited fluvial systems, instantaneous erosion rate is often described as:

$$E = \beta Q^m S^n \quad (6.2)$$

where Q is discharge rate, S is slope, and β , m , and n are parameters. As discussed in Chapter 3, Howard and Kerby [16] has shown that the above relation can be developed from consideration of bed shear stress, and Sinclair and Ball [40] have derived the same relation from more broad arguments regarding the possible influences of flow, shear stress, velocity, etc., and the scaling of hydraulic variables with slope and discharge. Depending on the arguments used to develop Equation 6.2, different values of β , m , and n are suggested. β may include the influences of material erodability, channel geometry, and other characteristics, and m and n reflect the physical description of the erosional process and the scaling of the channel dimensions.

If one considers discharge as a series of storm hydrographs, the mean erosion rate can be derived. Consider a period T during which the mean erosion rate is required (Figure 6-1). If all the storm hydrographs are assumed to have the same shape but different magnitudes and durations, then each can be characterized by a random peak flow Q_p and duration T_d . In complex records where the hydrographs of several precipitation events may or may not overlap, this assumption will clearly be violated. However, later we will further restrict the analysis to extreme cases where this issue will no longer be significant.

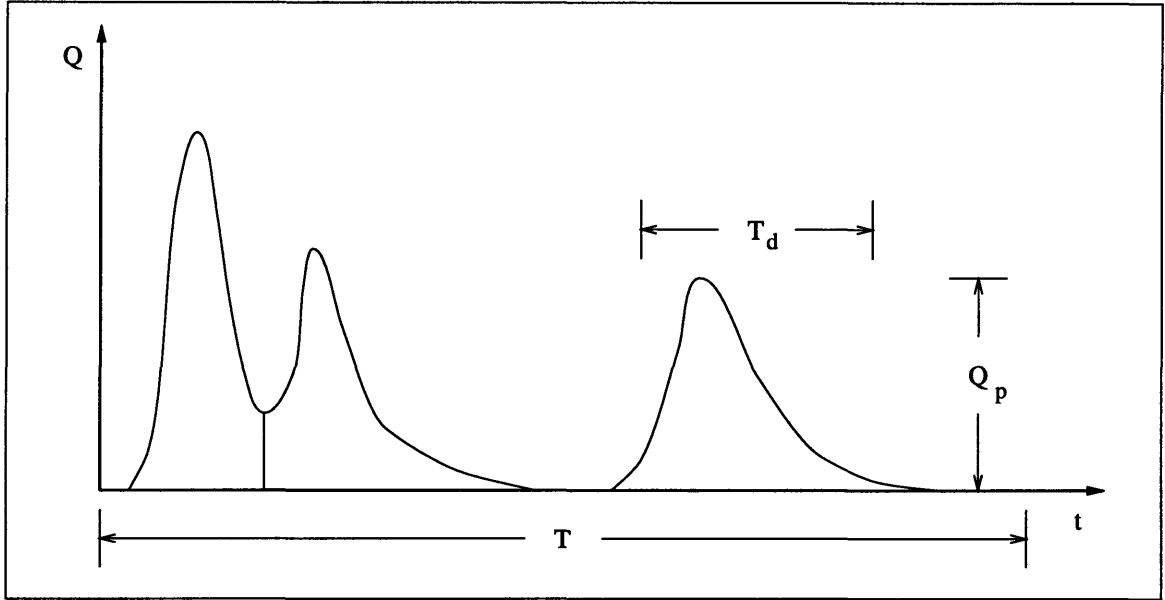


Figure 6-1: Diagram of the discharge during a period of simulation

The total material removed due to a single flood hydrograph (\hat{E}) is:

$$\hat{E} = \beta \left(\int_{-\infty}^{\infty} Q(t)^m dt \right) S^n \quad (6.3)$$

where the slope is assumed to remain essentially constant during a given storm. If a non-dimensional time and discharge are defined as:

$$t' \equiv \frac{t}{T_d} \quad (6.4)$$

$$Q'(t) \equiv \frac{Q(t)}{Q_p} \quad (6.5)$$

then the total sediment removed can be written as:

$$\hat{E} = \beta \left(\int_{-\infty}^{\infty} Q'(t')^m dt' \right) T_d Q_p^m S^n. \quad (6.6)$$

Every flood hydrograph in the period T will remove an amount of sediment defined by Equation 6.6. So if there are N floods in T (where N is a random variable), then

the average rate of sediment removal over T is:

$$\bar{E} = \frac{\beta}{T} \left(\int_{-\infty}^{\infty} Q'(t')^m dt' \right) \overline{NT_d Q_p^m} S^n. \quad (6.7)$$

In this analysis, we are interested in the erosion rate due to the hydrologic response to storms with specified characteristics. Stochastic variability in the precipitation intensities, durations, and arrival rates will be neglected. Thus, if a recurrence rate $\lambda \equiv N/t$ is defined, and the average values are replaced by their deterministic equivalents, a simplified version of Equation 6.7 can be written:

$$\bar{E} = \left(\beta \lambda \int_{-\infty}^{\infty} Q'(t')^m dt' \right) T_d Q_p^m S^n. \quad (6.8)$$

Willgoose [49] has derived a form of Equation 6.8 which includes the stochastic variability in N , T_d , and Q_p . From his results, the exact form above can be derived as a first order approximation where λ , T_d , and Q_p become average values.

Now that a long term erosion rate has been derived, it can be substituted into Equation 6.1. If uplift rate is assumed to be constant, then Equation 6.1 becomes:

$$\frac{\partial z}{\partial t} = U - \left(\beta \lambda \int_{-\infty}^{\infty} Q'(t')^m dt' \right) T_d Q_p^m S^n. \quad (6.9)$$

It is worth noting that the term in parenthesis is a constant for a given location and can therefore be considered as an adjusted β value. Thus, if T_d is constant, this equation has the same form as an instantaneous equation with Q_p replacing Q .

Q_p must still be related to the precipitation events; two cases will be developed in the following two sections. In both cases, linear dependence of streamflow on precipitation will be assumed. Because this is a unique relation, the constant Q_p assumed above implies a constant P as well. In addition, linearity amounts to assuming unit hydrograph theory. This theory, while not strictly valid, is commonly used in hydrology and is probably appropriate given the other assumptions involved in landscape evolution modeling.

6.2 Prolonged Precipitation

For the first case, consider storms that are much longer than the response time of the basin. In this simple case, the rainfall continues long enough for all points in a given subbasin to be contributing to the peak flow at the outlet (see Figure 6-2). Given the earlier assumption that the precipitation rate remains relatively constant, the peak flow becomes independent of the hydrograph shape and is proportional to the total area which contributes flow at any time through a given point. So:

$$Q_p = PA \quad (6.10)$$

where A is the contributing area and P is the effective precipitation intensity when it is raining. Substituting into Equation 6.9 the landscape evolution equation can be re-written:

$$\frac{\partial z}{\partial t} = U - \left(\beta \lambda \int_{-\infty}^{\infty} Q'(t')^m dt' T_d P^m \right) A^m S^n. \quad (6.11)$$

To summarize, the main assumptions used to reach this form are: a constant shape for all hydrographs through time, lack of any stochastic variability in the intensity, duration, and arrival rate of precipitation events, unit hydrograph theory, and prolonged precipitation events. It is acknowledged that some of these assumptions, particularly the lack of stochasticity, poorly represent reality. However, no more robust quantitative approach has been suggested in the literature that explicitly includes precipitation events in geomorphological modeling. In addition, the resulting model as expressed in Equation 6.11 (with the portion in parenthesis is constant) has been used as the basis for a variety of numerical models and simulations [27].

6.3 Instantaneous Precipitation

In some cases, the assumption of long precipitation events may not be appropriate. At large spatial scales, the response time will clearly exceed the length of the storm events. In addition, in some arid regions, short and intense convective storms are the

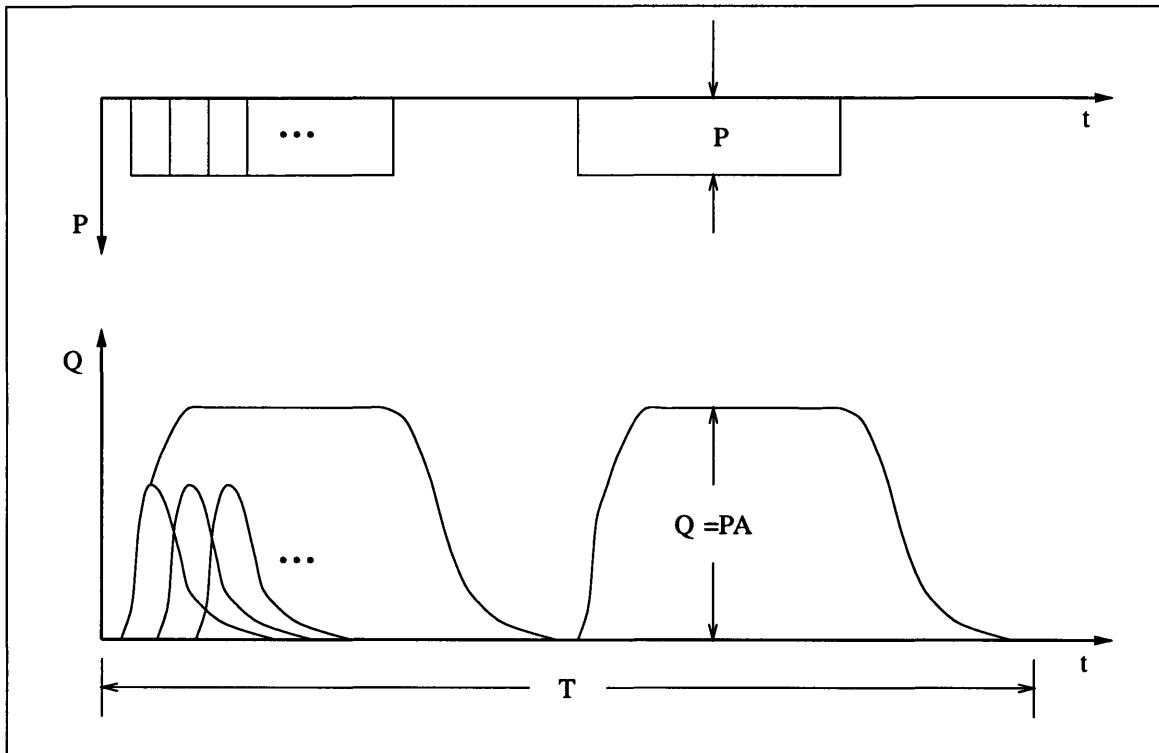


Figure 6-2: Diagram of the relationship between peak flow and contributing area for the long storm case

primary forcing of peak flows.

The problem with using contributing area with short pulses of precipitation can be seen from Figure 6-3. This figure shows two basins of the same size but with different shapes. Imagine dropping the same pulse of precipitation on each basin. In the first case, the runoff from the lower half of the basin will reach the outlet well before the runoff from the upper half, resulting in the long, flat hydrograph schematically shown below the basin. In the second case, runoff from more parts of the basin will arrive at the outlet simultaneously. In this case, the hydrograph will exhibit a more pronounced peak. Thus, two basins with the same contributing area may have much different peak flows from a short pulse of precipitation.

To consider this effect, we begin again with Equation 6.9. Instead of assuming long periods of rain, however, the other extreme case is assumed—where precipitation occurs due to instantaneous pulses that are widely spaced in time. This case implies that discharge at any point in time depends only on a single pulse of precipitation

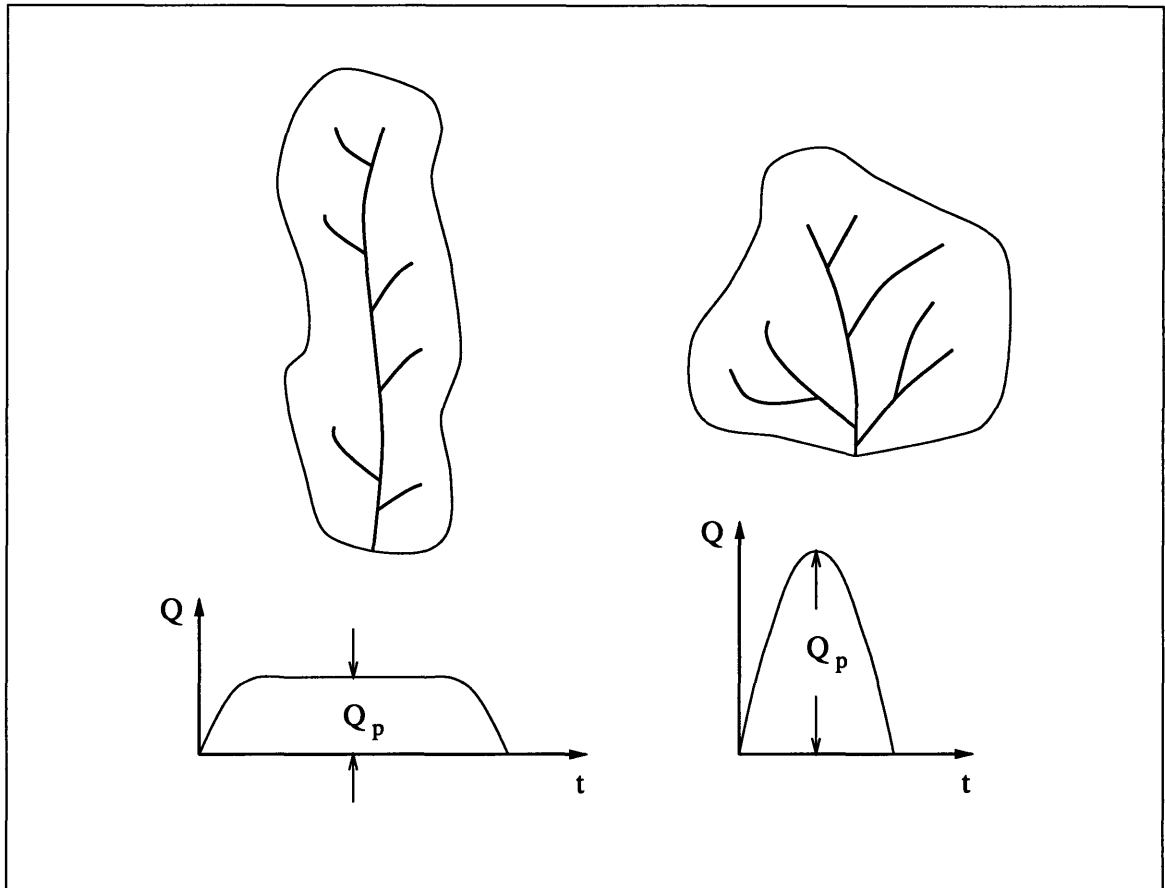


Figure 6-3: Diagram showing two basins with the same contributing area but different peak flows after an instantaneous pulse of precipitation

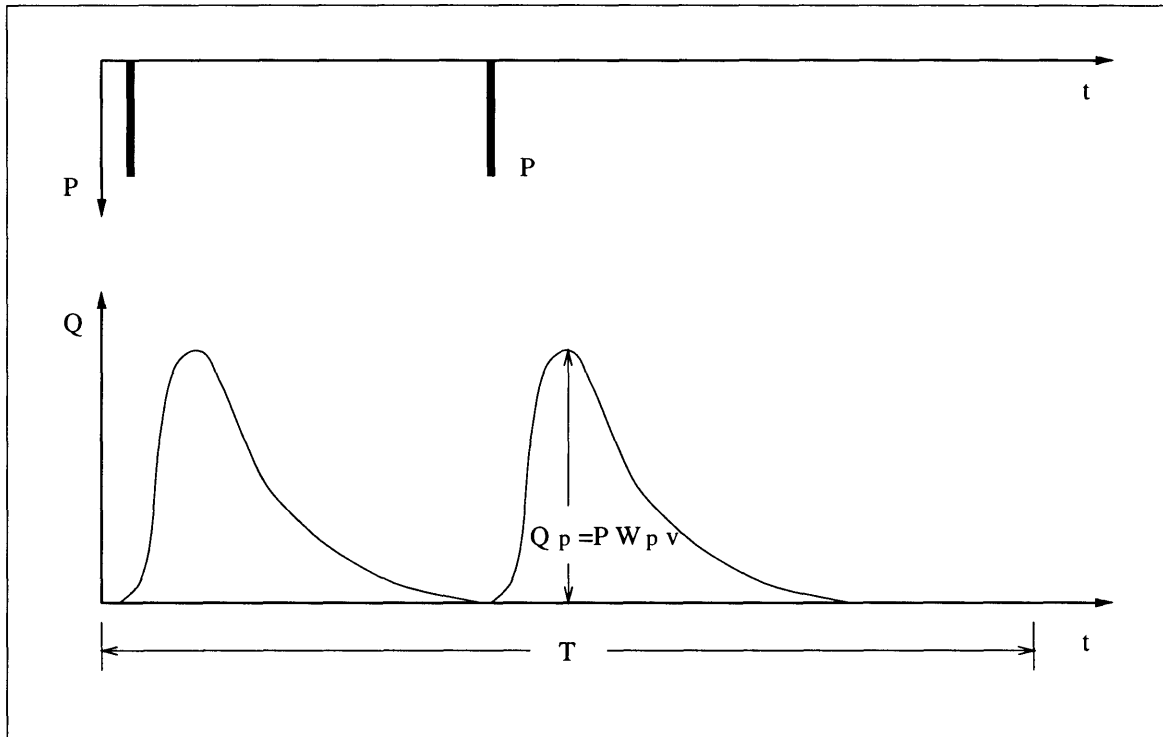


Figure 6-4: Diagram showing peak flows for the instantaneous storm case

(Figure 6-4).

In addition, for simplicity, velocity will be assumed to be constant throughout the channel network. This is the only additional assumption required to consider this extreme case. Observations by Leopold and Maddock have shown that $d \propto Q^{0.4}$, $b \propto Q^{0.5}$, and $v \propto Q^{0.1}$ where d is channel depth, b is channel width, and v is the velocity of flow [25]. Thus, while some weak dependence is observed between velocity and discharge, neglecting it is probably a reasonable working assumption in this context. Velocity may also depend on slope to a power (1/2 according to the Darcy-Weisbach equation [8]). Here we neglect this dependence as well, but inclusion of this effect represents an interesting direction for future research.

If v is constant in the network, then the width function embodies the hydrologic response of the basin and the peak value from the width function (W_p) links the storm event to the peak discharge. Thus, a simple hydrologic model can be written:

$$Q_p = P W_p v. \quad (6.12)$$

It should be noted that, in contrast to the prolonged precipitation case, P does not have units of intensity. Rather, P is the depth of a pulse of precipitation. Substituting the above equation into Equation 6.9 gives:

$$\frac{\partial z}{\partial t} = U - \left(\beta \lambda \int_{-\infty}^{\infty} Q'(t')^m dt' P^m v^m \right) T_d W_p^m S^n. \quad (6.13)$$

Upon first inspection of this equation, it appears to be simply analogous to Equation 6.11 with a constant v included in the coefficient and W_p replacing A . However, there are differences in both $Q'(t')$ and T_d . With instantaneous pulses of precipitation, $Q'(t')$ reflects the unit hydrograph or in this model the normalized width function, but with prolonged precipitation, $Q'(t')$ will reflect the fact that all points eventually are contributing to the runoff (see the difference schematically represented in Figures 6-2 and 6-4). This difference may affect the magnitude of the integral and therefore the magnitude of the coefficient. However, as will be discussed below, self-similarity indicates that $Q'(t')$ does not vary systematically with contributing area.

The more important difference comes through T_d . With long precipitation events, the duration of the hydrograph (T_d) is essentially controlled by the duration of the storm. For instantaneous precipitation events, however, T_d reflects the duration of the unit hydrograph or width function. This distinction is important since the storm duration is invariant with contributing area while the width function duration will depend on contributing area.

6.4 Application Through the Discrete Event and Slope-Area Models

Equations 6.11 and 6.13 can be simulated numerically using a finite difference approach. However, since the determination of W_p can be computationally intensive, the framework of the Discrete Event and Slope-Area models may be much more convenient.

Development of the Slope-Area model with either instantaneous or prolonged pre-

precipitation begins by considering the condition of dynamic equilibrium. When a basin reaches dynamic equilibrium, $\partial z/\partial t = 0$, and the topography remains constant. In the case of prolonged precipitation, this state implies (from Equation 6.11):

$$S = \left(\frac{U}{\beta\lambda \int_{-\infty}^{\infty} Q'(t')^m dt' T_d P^m} \right)^{1/n} A^{-m/n} \quad (6.14)$$

where the portion in parenthesis does not depend on contributing area. This equation suggests that natural basins which have developed under prolonged precipitation will exhibit slopes that scale with area to the power $-m/n$. So the Slope-Area model (see Chapter 3) retains its standard form and elevation at a grid point i, j can be set directly as:

$$z_{i,j}^{new} = z_{i,j}^{down} + \Delta l_{i,j} \left(\frac{U}{\beta\lambda \int_{-\infty}^{\infty} Q'(t')^m dt' T_d P^m} \right)^{1/n} A_{i,j}^{-m/n} \quad (6.15)$$

where z_{down} is the elevation of the downstream point and Δl is the spacing between the two points.

With either type of precipitation event, $Q'(t')^m$ will vary from pixel to pixel and could be calculated at considerable computational cost. However, such variability is not systematic with contributing area, so it can be reasonably assumed here that $Q'(t')^m$ is constant.

For basins which develop under instantaneous pulses of rain, dynamic equilibrium suggests a different condition. From Equation 6.13, dynamic equilibrium implies:

$$S = \left(\frac{U}{\beta\lambda \int_{-\infty}^{\infty} Q'(t')^m dt' P^m v^m} \right)^{1/n} T_d^{-1/n} W_p^{-m/n}. \quad (6.16)$$

Unlike the previous case, the equilibrium slope does not directly depend on contributing area. However, both W_p and T_d are characteristics which are easily determined from a given topography. Therefore, a new version of the Slope-Area model can be

written as:

$$z_{i,j}^{new} = z_{i,j}^{down} + \Delta l_{i,j} \left(\frac{U}{\beta \lambda \int_{-\infty}^{\infty} Q'(t')^m dt' P^{m_v m}} \right)^{1/n} T_{d,i,j}^{-1/n} W_{p,i,j}^{-m/n}. \quad (6.17)$$

Notice that the ‘‘Slope-Area model’’ name is now a misnomer since the model does not enforce a slope-area relation. Instead, the above relation is enforced in the manner described in earlier chapters.

Alternatively, one can use the physical arguments of the discrete event approach. A general form of shear stress can be written as $\tau = K Q^m S^n$ where K is a constant of proportionality, and m and n are parameters (see Chapter 3). In order to determine a large time scale relation (i.e. for $\bar{\tau}$), one can follow the approach in Section 6.2 and:

$$\bar{\tau} = \left(K \lambda \int_{-\infty}^{\infty} Q'(t')^m dt' \right) T_d Q_p^m S^n. \quad (6.18)$$

For prolonged precipitation, long term shear stress can then be written as:

$$\bar{\tau} = \left(K \lambda \int_{-\infty}^{\infty} Q'(t')^m dt' T_d P^m \right) A^m S^n \quad (6.19)$$

where T_d is independent of area. Similarly, for instantaneous precipitation:

$$\bar{\tau} = \left(K \lambda \int_{-\infty}^{\infty} Q'(t')^m dt' P^{m_v m} \right) T_d W_p^m S^n \quad (6.20)$$

where T_d depends on area. It should be noted that one cannot include a non-zero critical shear stress τ_{cr} or an exponent $\alpha \neq 1$ in Equation 3.1 without introducing additional nonlinearity into the derivation. These effects are not considered here, so use of the Discrete Event model is essentially restricted to the Simultaneous Growth variant with the critical shear stress equal to zero (i.e. a model similar to the one proposed by Howard and Kerby [16]).

6.5 Implications for Basin Form

The significance of storm duration to basin morphology can be illustrated by considering the cases of prolonged and instantaneous precipitation at dynamic equilibrium. From Equation 6.14, one observes that the equilibrium condition for basins with prolonged precipitation implies that slopes depend on area to the power $-m/n$. While m and n depend on the physics of erosion, their exact values are not known. If θ is defined to be the observed slope from a plot of $\log(\text{area})$ versus $\log(\text{slope})$ then:

$$\theta = -\frac{m}{n} \quad (6.21)$$

provides one equation for determining the two parameters m and n .

A different relation holds for regions with short pulses of precipitation. While the slopes do not depend directly on contributing area, both T_d and W_p will vary with contributing area since contributing area is the integral of the width function. If the dependence of these variables on A is known, then the dependence of slope on contributing area can also be determined. Because of the assumption of constant flow velocity, T_d corresponds directly to the length of the main stream. Therefore, by Hack's Law, $T_d \propto A^\gamma$ (γ is Hack's exponent) which means that $W_p \propto A^{1-\gamma}$ since A is the integral of the width function.

Self-similarity implies that $\gamma = 1/2$. If the width functions developed by Equation 6.13 are self-similar, then their proportions are constant at all scales which directly implies that $Q'(t)^m$ does not vary systematically with contributing area. In addition, because contributing area is the integral of the width function, then constant proportions implies that $T_d \propto A^{1/2}$ and $W_p \propto A^{1/2}$.

Upon first inspection, this idea of self-similarity seems to contradict Hack's observations that $\gamma \approx 0.6$. However, Veneziano et al. [46] argue that the difference arises from how one measures the length of the main channel. Hack and others have utilized a ruler length that remains constant throughout the network. However, such a method includes greater relative detail for the larger scale channels than the smaller ones giving the appearance of longer main stream length in larger basins (hence $\gamma > 1/2$).

Instead, Veneziano et al. [46] argue that the ruler length should increase when moving downstream on the channel network in order to measure the same amount of relative detail.

Such self-similarity is confirmed by simulations of Equation 6.13 with the Discrete Event model. Figure 6-5 shows data taken from two simulations: one where grid resolution (or ruler length) is constant and one where the grid resolution varies with contributing area. The figure confirms that $\gamma > 1/2$ for a constant ruler and $\gamma = 1/2$ for one that varies appropriately with contributing area (see Veneziano et al. [46] for further details).

With self-similarity, Equation 6.16 implies:

$$S \propto A^{-(1+m)/2n}. \quad (6.22)$$

Defining ϕ as the observed slope on a plot $\log(\text{area})$ versus $\log(\text{slope})$ then the above relation suggests that:

$$\phi = -\frac{1+m}{2n}. \quad (6.23)$$

Here the dependence of slope on contributing area is different than the previous case. In general, given the same values of m and n , the prolonged and instantaneous precipitation models will develop different slope-area exponents.

The difference between the two precipitation cases depends on the values of m and n . Figure 6-6 shows four simulated basins. The first three basins were all developed under instantaneous precipitation but with $m = 1/2, 1, 2$ and $n = 1, 2, 4$, respectively. Since the ratio of m/n is the same for all cases, the equilibrium basin for prolonged precipitation is the same in all three cases and is shown as the fourth plot.

For the first case, the resulting topography has very shallow slopes at large contributing areas, giving the impression of a river network incised in a flat plane. This case corresponds to the specific values of m and n used by Rinaldo et al. [30] for the Threshold model. With increasing values of m and n , steeper slopes characterize large contributing areas and the basins appear increasingly bowl-shaped. For the case with $m = 1$ and $n = 2$, little change is observed between the basins with prolonged

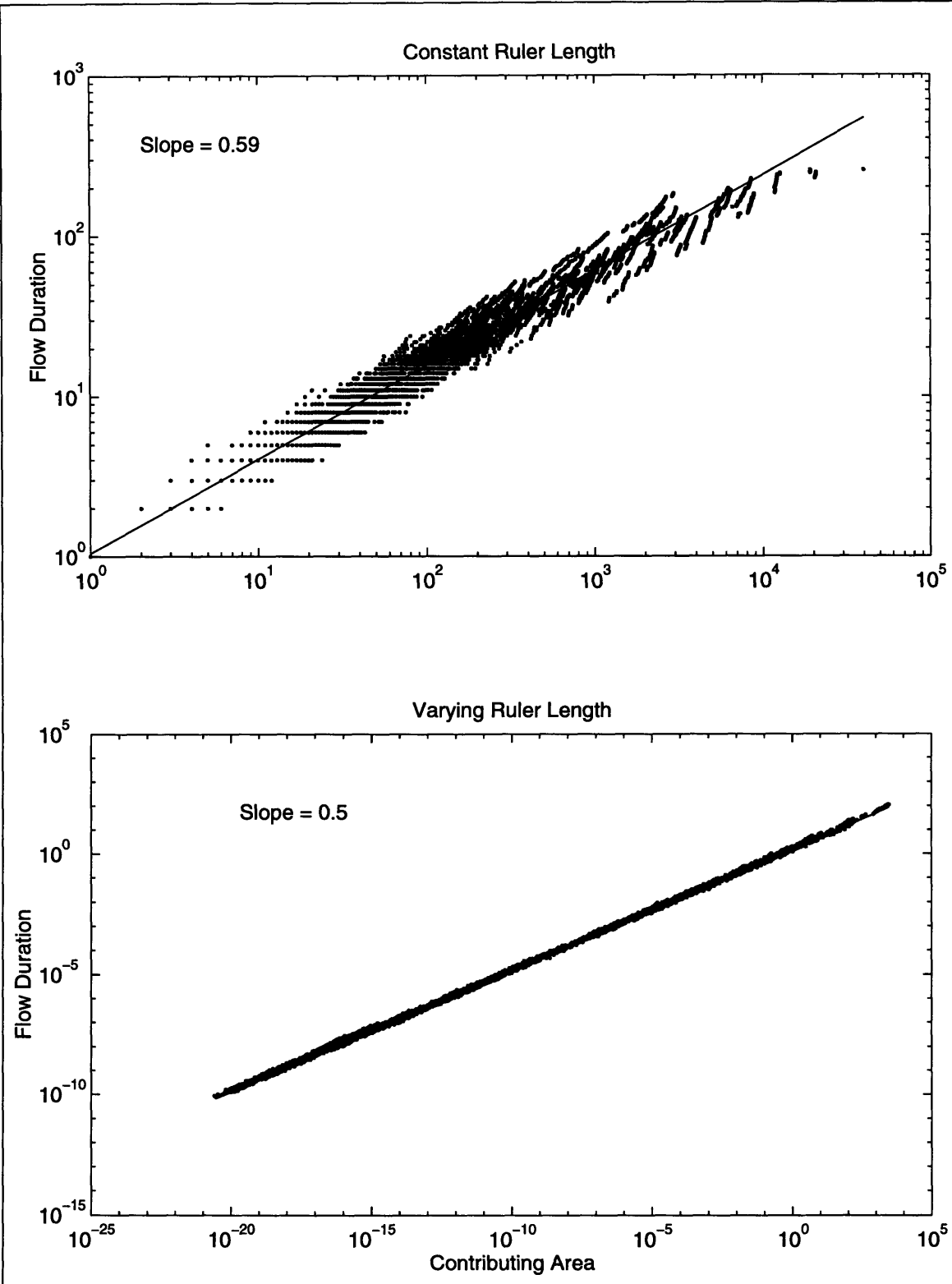


Figure 6-5: Correlation between contributing area and flow duration (or main stream length) using (a) a constant ruler length and (b) a ruler length that varies according to contributing area (solid lines show regressions)

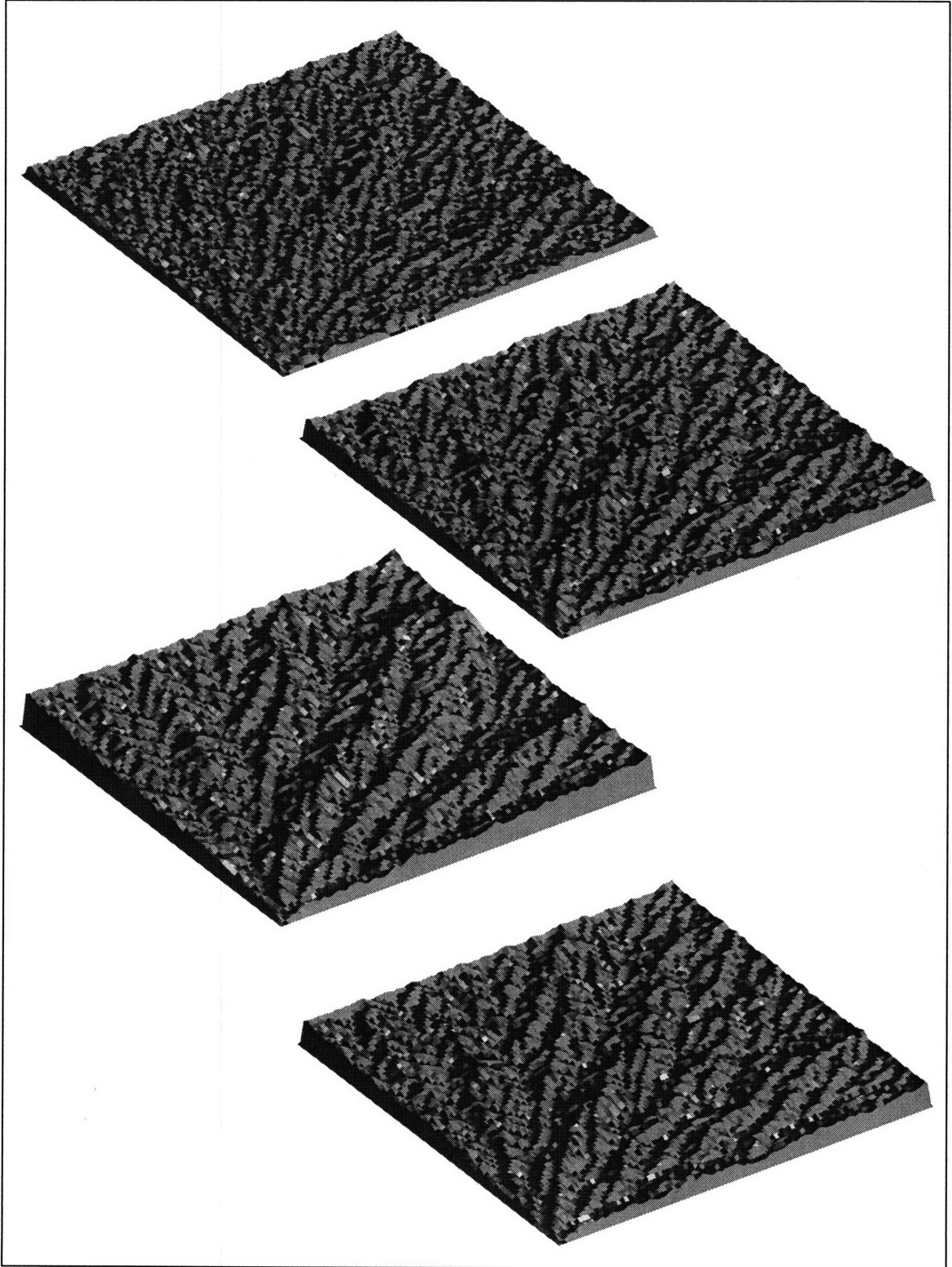


Figure 6-6: Simulated basins where (a)-(c) have instantaneous precipitation and (d) has prolonged precipitation. Parameters are: (a) $m = 1/2$, $n = 1$, (b) $m = 1$, $n = 2$, (c) $m = 2$, $n = 4$, (d) $m/n = 1/2$

and instantaneous precipitation.

The relationship between the parameter m and the observed slope-area exponents θ and ϕ is shown in Figure 6-7. This figure shows that m only depends on the observed ratio of $\alpha \equiv \phi/\theta$. If observations of natural basins that evolved under instantaneous and prolonged precipitation support that $\theta = \phi$, for example, then $\alpha = 1$ and Equations 6.21 and 6.23 give the result that $m = 1$. This is intuitively satisfying since $m = 1$ implies that erosion is linearly dependent on discharge. Under these conditions, the distribution in time of a given amount of discharge no longer matters, and landscape evolution can probably be described adequately by either model.

Even when $\theta = \phi$, however, the scatter in the slope-area relationship will vary between the two cases. For the prolonged precipitation case, slope directly depends on area, and barring any stochastic variability, no scatter will be observed in the slope-area relationship. For the instantaneous precipitation case, however, the relationship between slope and area will include (among other possible scatter) the statistical variability in subbasin shapes as reflected in variability of the width functions.

Some observations by Tarboton (based on DEM data) have suggested that the slope-area exponent is commonly near 0.5 [44]. In that analysis, no identifiable trend with climate was observed, but the analyzed data represents a relatively narrow range of climates (particularly humid). However, if one interprets this data to mean that $\theta = \phi = 0.5$, then only $m = 1$ and $n = 2$ are consistent with the data and the above analysis (see Equations 6.21 and 6.23). In order to confirm any hypothesis, however, data for regions with short and intense pulses of precipitation must be analyzed. Systematic differences in the slope-area relationship would confirm the model and provide estimates of m and n . If $m = 1$, no differences will be observed between θ and ϕ , and the model can only be confirmed by a careful examination of the scatter in the slope-area relationship.

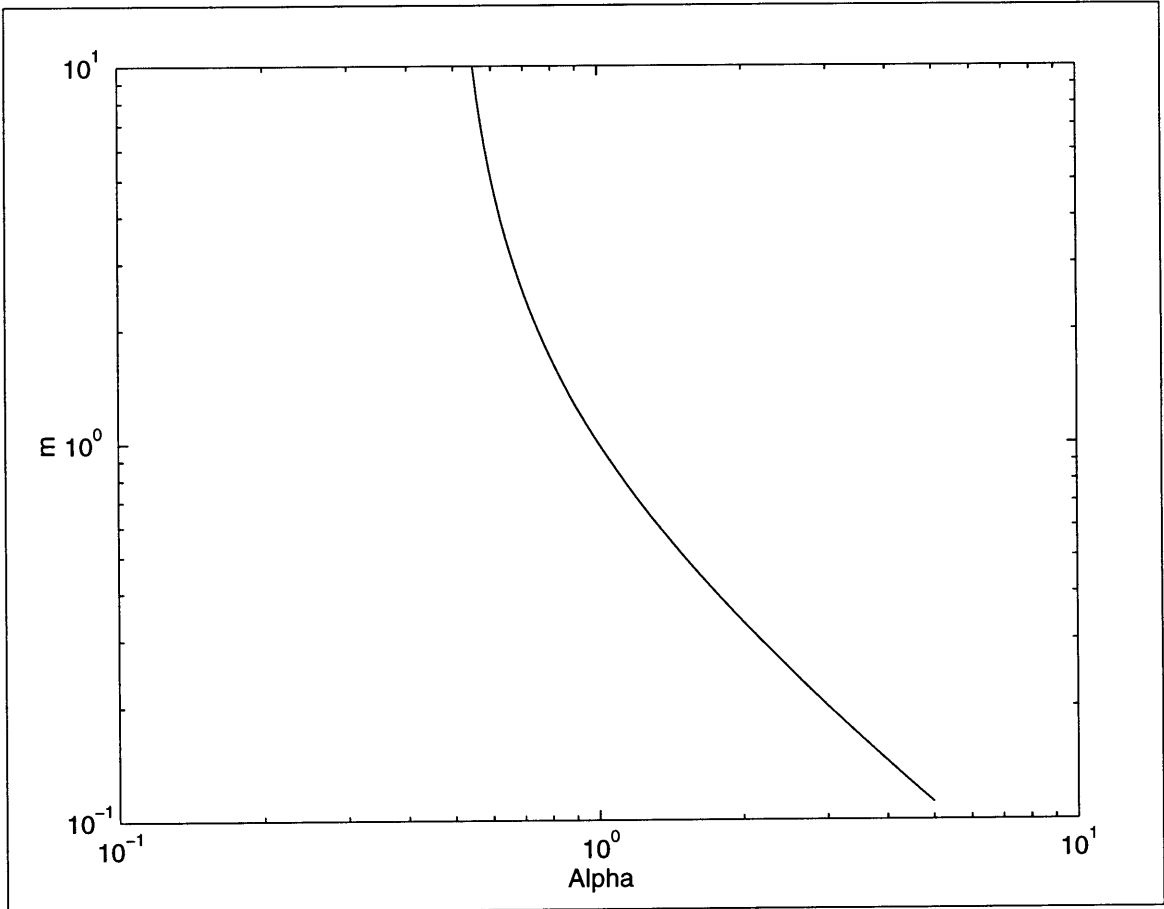


Figure 6-7: The dependence of m on $\alpha \equiv \phi/\theta$

6.6 Conclusions

This chapter has examined whether the duration of precipitation events has an identifiable impact on the resulting basin morphology. The method utilized was to consider two end-member cases—one where precipitation arrives in widely spaced instantaneous pulses and one where the precipitation results from prolonged events. The prolonged precipitation model is equivalent to employing contributing area as a surrogate for discharge rate, and the instantaneous case is equivalent to utilizing the width function as a surrogate for discharge.

Because m and n are independent of the storm characteristics, significant differences in the basin morphology may arise between the instantaneous and prolonged precipitation cases. In particular, if $m > 1$, the slope-area exponent will be less negative for basins with instantaneous pulses of rain than for those with prolonged precipitation. When $m < 1$, the opposite is true. Only when $m = 1$ will the storm characteristics not influence the scaling of slope with area. Even under these circumstances, the scatter in the slope-area relationship will depend on the storm characteristics.

Several key factors may dull the effects of storm character. First, both cases examined here are idealized extremes. No basin will fall perpetually in one of these categories. Rather precipitation records may be dominated by one extreme but will always include some stochastic variability. Second, velocity in the channel network is not constant. A departure from constant velocity toward systematic variation with either slope or area will affect the results. However, if m is far from one, then some systematic variation in the slope-area relationship may still be visible with climate. Such an investigation represents an interesting direction for further research.

Chapter 7

Conclusions

7.1 Summary of Results

The goal of this analysis was to further understand the link between the dynamics of basin evolution and the resulting morphology. Specifically, it investigated the morphological impact of channel network growth, initial conditions, and climatic and tectonic forcing. This section summarizes the main results.

In chapter 3 the Discrete Event model framework was introduced and compared with the Slope-Area model. Two important conceptual differences were identified between these two models. First, the Discrete Event model attempts to describe the physical dynamics of basin evolution, whereas the Slope-Area model basically approaches a stationary basin configuration by a series of trial solutions. Secondly, the stationary state reached by the Discrete Event model is one of *stability* where all points have shear stresses less than the specified critical value. In contrast, the Slope-Area model approaches *dynamic equilibrium* where the influx of material from tectonic uplift exactly balances the denudation of points by erosional processes. The physical configuration of basins developed by the two models (using the Headward Growth variant in each) were compared and found to differ slightly. Basins developed by the Slope-Area model tended to have confluences located further up the network and had lower energy than basins from the Discrete Event model. A comparison of the conditions of stability and dynamic equilibrium within a Discrete Event modeling

framework was performed in Chapter 5.

In Chapter 4, the influences of the mode of network growth on basin form was investigated. Four variants of the Discrete Event model were introduced. The *Headward Growth* variant always adjusts elevations beginning from pits and outlets and progresses headward. In that sense it represents Howard's conceptual model of headward growth. The *Simultaneous Growth* variant departs some from the idea of discrete erosion events and describes erosion as a continuously varying rate. It was shown to be equivalent to a finite difference model where erosion is proportional to shear stress. The *Random Growth* variant erodes points with excess shear in a random sequence. This variant is equivalent to Eden Growth. Finally the *Greatest Excess Growth* variant always erodes the point with the greatest excess shear stress. This variant is similar both to Glock's conceptual extension/elaboration model and to Invasion Percolation. Basins developed by these four variants were compared using standard geomorphic measures. Each develops basins that have unique characteristics. However, the Greatest Excess Growth variant was the most distinctive. It was observed that the irregularity of channels from this variant is much greater than ones from the other variants. In addition, it achieves slopes on the area aggregation curve nearest the field value of -0.43 and expended the least energy at stability.

In Chapter 5, the differences between the conditions of stability and dynamic equilibrium were examined. To consider dynamic equilibrium, a description of uplift was added to the Simultaneous Growth variant introduced in Chapter 4. Numerical simulations allowed comparison of basins developed with various magnitudes of uplift rate and critical shear. Using essentially flat initial conditions, some subtle differences were identified in the distribution of drainage directions and Hack's exponent. As the critical shear stress goes to zero and the uplift rate increases, Hack's exponent decreases slightly. Another set of experiments considered the role of uplift and critical shear stresses when the initial conditions either slope towards or away from a specified baselevel. When the critical shear is zero and gradual uplift occurs, the mode of network growth depends on the orientation of the initial surface. As expected from field observations, slopes oriented toward the escarpment crest tend to form escarpments

with deeply incised channels. The mode of network growth in this case is closest to Horton's conceptual model since readjustment of a quickly formed network is important. When the initial surface slopes away from the escarpment crest, the escarpment takes the traditional drainage divide form. Breakdowns in self-similarity were also observed when the initial slope was oriented away from the baselevel and escarpment crest. Especially in the case when there was no gradual uplift but a non-zero critical shear stress, the developed networks were not self-similar.

In Chapter 6, the role of precipitation events in landscape evolution models was considered. Two cases were included: one where precipitation events are prolonged so that all points in the basin contribute to the peak flow and another where precipitation arrives in short, widely spaced pulses. If the precipitation events are short, the hydrographs are essentially the width functions (see Chapter 6 for details of the assumptions). Thus, the flow duration scales with the integral of the width function which is the contributing area. If the storm duration is long enough that all points in the basin contributing to the peak flow, the flow duration is controlled externally by the precipitation event. Therefore, if the exponent on discharge in the erosion term is not unity, the scaling of the slope-area relationship depends on the storm type.

7.2 Avenues for Further Study

This analysis has traversed a wide scope, and additional study in each of the various areas is possible. Particularly, with the topics of Chapter 5 and 6 two broad and important questions are raised by the analysis. First, what is the impact of a wide range of boundary conditions and forcing on the properties of the basin? Second, what is the impact of a more accurate hydrological description on geomorphological models?

In regards to the first question, this topic has both mathematical and practical motivations. Robustness of many scaling properties between various climatic and geologic conditions has been shown in the field. However, little understanding of the role of initial conditions in mathematical models exists. For example, in order to

show that a given differential equation develops self-similar structures, one must assess the influence of the boundary and initial conditions. In addition, identification of conditions that result in deviations from self-similarity would allow increased understanding of the history and dynamics of regions where such conditions are expected.

Regarding the second question, very crude hydrology is included in virtually all existing geomorphological models. For example, most models essentially enforce the slope-area relationship at equilibrium due to their crude description of hydrology. However, such a relationship has yet to be shown to result from more detailed and realistic hydrologic descriptions of river basins. A more accurate hydrologic model where discharge does not depend simply on contributing area is expected to affect the basin form.

These are only two among the broad questions that are raised by this analysis. Clearly, much additional study in these areas would benefit our understanding of basin evolution.

Bibliography

- [1] P. Alstrom. Self-organized criticality and fractal growth. *Physical Review A*, 41(12):7049–7051, 1990.
- [2] P. Alstrom. Spatiotemporal fluctuations in growth phenomena: Dynamical phases and 1/f noise. *Physical Review A*, 41(6):3403–3406, 1990.
- [3] P. Bak, K. Chen, and M. Creutz. Self-organized criticality in the ‘game of life’. *Nature*, 342:780–782, 1989.
- [4] P. Bak, C. Tang, and K. Wiesenfeld. Self-organized criticality: An explanation of 1/f noise. *Physical Review Letters*, 59(4):381–384, 1987.
- [5] P. Bak, C. Tang, and K. Wiesenfeld. Self-organized criticality. *Physical Review A*, 38(1):364–374, 1988.
- [6] C. G. Chase. Fluvial land sculpting and the fractal dimension of topography. *Geomorphology*, 5:39–57, 1992.
- [7] W. M. Davis. The geographical cycle. *Geography Journal*, 14:481–504, 1899.
- [8] W. E. Dietrich, C. J. Wilson, D. R. Montgomery, and J. McKean. Analysis of erosion thresholds, channel networks, and landscape morphology using a digital terrain model. *Journal of Geology*, 101:259–278, 1993.
- [9] J. J. Flint. Stream gradient as a function of order, magnitude, and discharge. *Water Resources Research*, 10(5):969–973, 1974.

- [10] W. S. Glock. The development of drainage systems: A synoptic view. *Geographical Review*, 21:475–482, 1931.
- [11] J. T. Hack. Studies of longitudinal stream profiles in Virginia and Maryland. *Geological Survey Professional Papers*, 294-B:45–97, 1957.
- [12] J. T. Hack. Interpretation of erosional topography in humid temperature regions. *American Journal of Science*, 258A:80–97, 1960.
- [13] T. E. Harris. *The Theory of Branching Processes*. Springer, 1963.
- [14] R. E. Horton. Erosional development of streams and their drainage basins: Hydrophysical approach to quantitative geomorphology. *Bulletin of the Geological Society of America*, 56:275–370, 1945.
- [15] A. D. Howard. Simulation of stream networks by headward growth and branching. *Geographical Analysis*, 3(1):29–50, 1971.
- [16] A. D. Howard and G. Kerby. Channel changes in badlands. *Geological Society of America Bulletin*, 94:739–752, 1983.
- [17] E. J. Ijjasz-Vasquez, R. L. Bras, and I. Rodriguez-Iturbe. Self organized criticality in river basins. *Eos*, 72(44):202, 1991.
- [18] E. J. Ijjasz-Vasquez, R. L. Bras, and I. Rodriguez-Iturbe. Form, scales, and optimality in the basin landscape and its channel network. Technical Report 339, Massachusetts Institute of Technology, Ralph M. Parsons Laboratory, Massachusetts Institute of Technology, Cambridge, Massachusetts, 1993.
- [19] H. Schenck Jr. Simulation of the evolution of drainage-basin networks with a digital computer. *Journal of Geophysical Research*, 68(20):5739–5744, 1963.
- [20] H. Kooi and C. Beaumont. Escarpment evolution on high-elevation rifted margins: Insights derived from a surface processes model that combines diffusion, advection, and reaction. *Journal of Geophysical Research*, 99(B6):12191–12209, 1994.

- [21] H. Kooi and C. Beaumont. Large-scale geomorphology: Classical concepts reconciled and integrated with contemporary ideas via a surface processes model. *Journal of Geophysical Research*, 101(B2):3361–3386, 1996.
- [22] S. Kramer and M. Marder. Evolution of river networks. *Physical Review Letters*, 68(2):205–208, 1992.
- [23] R. L. Leheny and S. R. Nagel. Model for the evolution of river networks. *Physical Review Letters*, 71(9):1470–1473, 1993.
- [24] L. B. Leopold and W. B. Langbein. The concept of entropy in landscape evolution. *Geological Survey Professional Papers*, 500(A):1–20, 1962.
- [25] L. B. Leopold and T. Maddock. The hydraulic geometry of stream channels and some physiograph implications. *Geological Survey Professional Papers*, 252:1–57, 1953.
- [26] J. G. Masek and D. L. Turcotte. A diffusion-limited aggregation model for the evolution of drainage networks. *Earth and Planetary Science Letters*, 119:379–386, 1993.
- [27] G. E. Moglen and R. L. Bras. Simulation of observed topography using a physically-based basin evolution model. Technical Report 340, Massachusetts Institute of Technology, Ralph M. Parsons Laboratory, Massachusetts Institute of Technology, Cambridge, Massachusetts, 1994.
- [28] M. Morisawa. Development of drainage systems on an upraised lake floor. *American Journal of Science*, 262:340–354, 1964.
- [29] R. Rigon, A. Rinaldo, and I. Rodriguez-Iturbe. On landscape self-organization. *Journal of Geophysical Research*, 99(B6):11971–11993, 1994.
- [30] A. Rinaldo, I. Rodriguez-Iturbe, R. Rigon, E. J. Ijjasz-Vasquez, and R. L. Bras. Self organized fractal river networks. *Physical Review Letters*, 70(6):822–825, 1993.

- [31] I. Rodriguez-Iturbe, E. J. Ijjasz-Vasquez, R. L. Bras, and D. G. Tarboton. Power law distributions of discharge mass and energy in river basins. *Water Resources Research*, 28(4):1089–1093, 1992.
- [32] I. Rodriguez-Iturbe, A. Rinaldo, R. Rigon, R. L. Bras, A. Marani, and E. Ijjasz-Vasquez. Energy dissipation, runoff production, and the three-dimensional structure of river basins. *Water Resources Research*, 28(4):1095–1103, 1992.
- [33] D. H. Rothman and S. Zaleski. *Lattice-Gas Cellular Automata: Simple Models of Complex Hydrodynamics*. Cambridge University Press, 1997.
- [34] V. B. Sapozhnikov and E. Foufoula-Georgiou. Do the current landscape evolution models show self-organized criticality? *Water Resources Research*, 32(4), 1996.
- [35] K. H. Schmidt. Factors influencing structural landform dynamics on the Colorado Plateaus and the necessity of calibrating theoretical models by empirical data. In F. Ahnert, editor, *Geomorphological Models—Theoretical and Empirical Aspects: Catena Supplement*. 1987.
- [36] S. A. Schumm. Evolution of drainage systems and slopes in badlands at Perth Amboy, New Jersey. *Geological Society of America Bulletin*, 67:597–646, 1956.
- [37] S. A. Schumm, M. Paul Mosley, and W. E. Weaver. *Experimental Fluvial Geomorphology*. John Wiley and Sons, 1987.
- [38] M. A. Seidl, J. K. Weissel, and L. F. Pratson. The kinematics and pattern of escarpment retreat across the rifted continental margin of SE australia. *Basin Research*, 12:301–316, 1996.
- [39] R. L. Shreve. Statistical law of stream numbers. *Journal of Geology*, 74:17–37, 1966.
- [40] K. Sinclair and R. C. Ball. A mechanism for global optimization of river networks from local erosion rules. *Physical Review Letters*, 76(18), 1996.

- [41] C. P. Stark. An invasion percolation model of drainage network evolution. *Nature*, 352:423–425, 1991.
- [42] C. P. Stark. Cluster growth modeling of plateau erosion. *Journal of Geophysical Research*, 99(B7):13957–13969, 1994.
- [43] H. Takayasu and H. Inaoka. A new type of self-organized criticality in a model of erosion. *Physical Review Letters*, 68:966–969, 1992.
- [44] D. G. Tarboton, R. L. Bras, and I. Rodriguez-Iturbe. The analysis of river basins and channel networks using digital terrain data. Technical Report 326, Massachusetts Institute of Technology, Ralph M. Parsons Laboratory, Massachusetts Institute of Technology, Cambridge, Massachusetts, 1989.
- [45] G. E. Tucker. *Modeling the Large-Scale Interaction of Climate, Tectonics, and Topography*. PhD thesis, Pennsylvania State University, 1996.
- [46] D. Veneziano, J. D. Niemann, G. Tucker, R. L. Bras, F. Colaiori, and A. Flammini. Scaling laws of fluvial topography from self-similarity. 1997.
- [47] T. Vicsek. *Fractal Growth Phenomena*. World Scientific, 1992.
- [48] J. K. Weissel and D. J. Harding. Tectonics and erosion: Topographic evolution of rift flanks and rifted continental margins. 1993.
- [49] G. Willgoose, R. L. Bras, and I. Rodriguez-Iturbe. A physically based channel network and catchment evolution model. Technical Report 322, Massachusetts Institute of Technology, Ralph M. Parsons Laboratory, Massachusetts Institute of Technology, Cambridge, Massachusetts, 1989.